UNCLASSIFIED

AD 289 084

Reproduced
by the

ARMED SERVICES TECHNICAL INFORMATION AGENCY
ARLINGTON HALL STATION
ARLINGTON 12, VIRGINIA

UNCLASSIFIED

ANTENNA LABORATORY

Technical Report No. 61

THE BACKFIRE BIFILAR HELICAL ANTENNA

by

Willard Thomas Patton

Contract AF33(657)-8460
Project No. 6278, Task No. 40572

September 1962

Sponsored by:
AERONAUTICAL SYSTEMS DIVISION
WRIGHT-PATTERSON AIR FORCE BASE, OHIO

ELECTRICAL ENGINEERING RESEARCH LABORATORY
ENGINEERING EXPERIMENT STATION
UNIVERSITY OF ILLINOIS
URBANA, ILLINOIS

Antenna Laboratory

Technical Report No. 61

THE BACKFIRE BIFILAR HELICAL ANTENNA

by

Willard Thomas Patton

Contract AF33(657)-8460
Project No. 6278, Task No. 40572

September 1962

Sponsored by

AERONAUTICAL SYSTEMS DIVISION

WRIGHT-PATTERSON AIR FORCE BASE, OHIO

Electrical Engineering Research Laboratory
Engineering Experiment Station
University of Illinois
Urbana, Illinois

ACKNOWLEDGEMENT

The author wishes to thank all members of the staff of the Antenna Laboratory of the University of Illinois for their help and encouragement during this study. The guidance of his adviser, Professor G. A. Deschamps, and the suggestions of Professor P. E. Mayes are particularly appreciated.

Thanks are also due to Samuel C. Kuo who assisted in the data reduction and prepared the illustrations, and to Bradley Martin, Calvin Evans, and Edward Young, who assisted in the experimental measurements. This work was sponsored by the United States Air Force, Aeronautical Systems Division, Wright-Patterson Air Force Base, under contract number AF33(616)-6079 and AF33(657)-8460, for whose support the author is grateful.

ABSTRACT

The backfire bifilar helical antenna, consisting of two opposed helical wires fed with balanced currents at one end, is a new type of circularly polarized antenna. When operated above the cutoff frequency of the principal mode of the helical waveguide, the bifilar helix produces a beam directed along the structure toward the feed point. The term "backfire" is used to describe this direction of radiation in contrast with "endfire" which denotes radiation away from the feed point.

Radiation patterns, measured for a wide range of helix parameters, show maximum directivity slightly above the cutoff frequency. The pattern broadens with frequency, and, for pitch angles near forty-five degrees, the beam splits and scans toward the broadside direction.

Near field measurements show the current decaying rapidly to a level about twenty decibels below the input level at a rate that increases with frequency. Phase measurements in the near field show that in the feed region the direction of phase progression is toward the feed point. The oppositely directed phase progression and direction of energy flow is characteristic of a backward wave. The direction of phase progression is consistent with the backfire direction of the main beam observed in the radiation patterns and the increasing rate of current decay is consistent with the broadening of the main beam with increasing frequency.

A theoretical analysis of the bifilar helical antenna is obtained. It is based upon the semi-infinite model using thin wire assumptions. These, so-called, linearizing assumptions consist of replacing the current distribution on the surface of the wire with a line current on the center line of the

wire and of satisfying the boundary condition along one line on the conducting surface. The Fourier transform of the current distribution on the semi-infinite helix is deduced from the determinantal equation of the bifilar helical waveguide by a Wiener-Hopf technique. The relation between this Fourier transform and the radiation pattern of the backfire bifilar helical antenna is shown. The results predict the patterns of the experimental study and show the effect of wire size on antenna performance.

CONTENTS

CONTENTS (continued)

ILLUSTRATIONS

ILLUSTRATIONS (continued)

ILLUSTRATIONS (continued)

1. INTRODUCTION

1.1 Statement of the Problem

The purpose of this study is to provide a mathematical model of the backfire bifilar helical antenna which contains the essential features of the practical antenna and which is amenable to solution. This model has been solved for the far field radiation pattern of the antenna, and the results are compared with the radiation patterns that have been obtained experimentally. One outstanding characteristic of these patterns is that the principal direction of radiation is in the backfire direction. The backfire direction of a surface wave antenna is along the structure toward the feed point. Radiation in this direction can be associated with a phase progression toward the feed point, while the group velocity must be away from the feed point. This is characteristic of a backward wave of current on the structure. The term "backfire" is used for contrast with the more usual endfire surface wave antenna for which the principal direction of radiation is away from the feed point of the structure.

The backfire bifilar helical antenna, shown in Figure 1, is constructed of two helical wires wound in a right circular cylinder with a constant pitch. The corresponding points of the wires are located at the ends of a diameter of the cross section of the cylinder. The helical wires are fed with balanced currents from a source on the axis of the cylinder. A complete description of the antenna includes: the radius b, measured from the axis of the cylinder to the center line of a conductor; the pitch distance p, measured along a generator of the cylinder; the wire radius a, and the total length of the antenna.

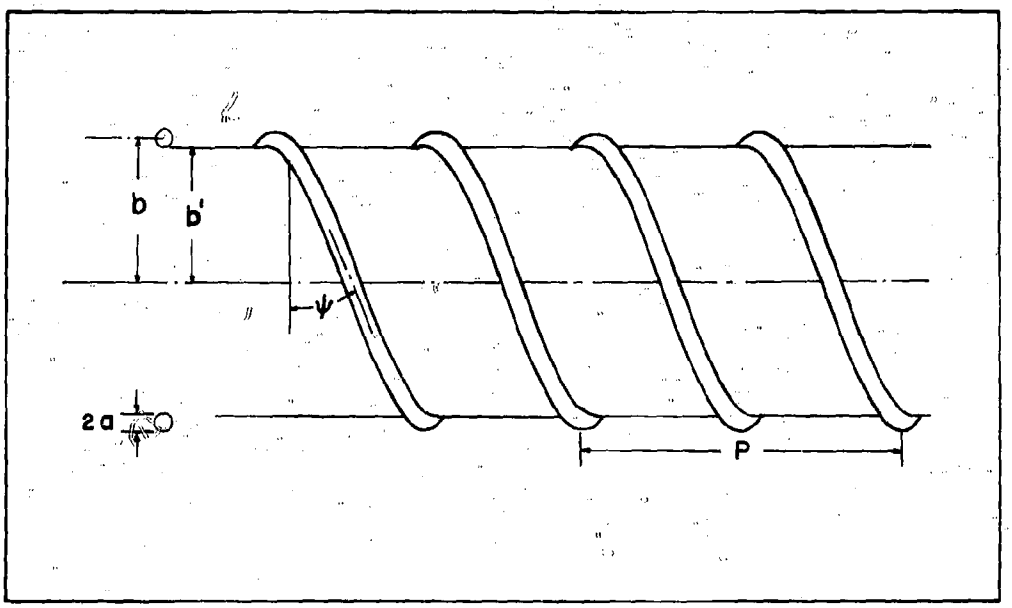

Figure 1. The Geometry of the Bifilar Helix

1.2 Method of Solution

A solution of the backfire bifilar helical antenna problem is obtained, first, by considering the basic helical geometry to be extended to infinity in both directions. This is the helical waveguide problem which already has an extensive literature. An exact account of the boundary conditions in this problem involves finding a current distribution over the surface of the conductor which makes the tangential electric intensity vanish everywhere on the surface of the conductor. An approximation used by Sensiper[1] and Kogan[2] is to require that the tangential electric intensity vanish only along some line along the surface. This approximation is good for relatively thin conductors. Sensiper, in treating the tape helix, makes a further approximation in assuming a functional dependence for the distribution of current across the width of the tape. Kogan makes a similar approximation by assuming that the surface current distribution may be replaced by a current flowing along the center line of the helical conductor. The approximations involved in replacing a surface current by a line current and in satisfying the boundary conditions along only one line of the surface have been termed linearizing approximations. A formulation of the helical waveguide problem, similar to that of Kogan, is used in this study.

Using the above approximations, the desired current distribution becomes a function of only one variable. This variable may be either distance along the helix or distance along the helical axis. In this paper the helical axis is taken to coincide with the z-axis of a cartesian coordinate system, and z is taken as the independent variable of the current distribution. The integral equation for the current on the helical waveguide now has the form of a convolution integral. This happy circumstance related

to invariance under a one dimensional Abelian congruence group, suggests a solution by Fourier transformation. The determinantal equation for the Fourier spectrum of the current distribution has three pairs of real roots at the lower frequencies. As the frequency is increased, two pairs of roots tend together and coalesce at the critical frequency, f_c. This frequency marks the lower limit of the range of frequencies of interest in this study. The critical frequency depends, in a complicated way, upon the radius of the helix, its pitch, and the conductor radius, and no simple expression is given for it.

The second step in the solution of the backfire bifilar helical antenna problem is to obtain a solution for the current distribution on a helical waveguide extending only along the positive z-axis of the coordinate system. This is accomplished by a Wiener-Hopf factorization of the transformed solution for the helical waveguide. The boundary conditions on the factorization are such that the current is identically zero for all negative z and approaches a finite non-zero limit as z approaches zero from the right. The discontinuity in the current at the origin is the source of energy in the problem, and corresponds to a pair of oscillating point charges separated by the helix diameter. The result of this calculation is the Fourier transform of the current distribution on a semi-infinite bifilar helix fed by a charge dipole in the plane $z = 0$.

The solution obtained in this way is limited by the linearizing approximations described above. The remaining approximations in the theory developed here are contained in equating this solution to the radiation pattern of a finite-length bifilar helical antenna fed from a source on its axis. The practical antenna differs from the mathematical model in the

vicinity of the feed point by the addition of a current flowing along a diameter of the cylindrical cross section. This additional current element is short in the range of helix diameters of primary interest in this study and will not contribute noticeably to the radiated field. Measurements of the current on several models of the bifilar helix above the critical frequency show that the current decays rapidly with distance from the feed point. At a level about 20 decibels below the input value, an undamped wave becomes dominant. Because of the rapid attenuation of current on the bifilar helix, the radiation pattern of the finite structure is expected to be the same except for "end-fire" radiation caused by the residual "free-mode" wave. It is well known that a finite line current distribution and its far field radiation pattern are Fourier transform pairs. This is extended here to include the semi-infinite structure, and it is shown that in this case also the radiation pattern is simply related to the transform of the current distribution as a function of z except in the vicinity of the current distribution at infinity.

The Fourier transform of the current distribution is obtained by numerical techniques using an automatic digital computer. The computed patterns based upon this Fourier transform show good agreement with measured patterns presented in this report. This confirms the validity of the approximations used in constructing the mathematical model of the antenna.

1.3 Review of Helix Analysis

The study of electromagnetic wave propagation on helical conductors through 1955 has been summarized by Sensiper[3] and his thesis[1] contains an extensive bibliography of the literature. He obtains an exact solution

of the "tape" helix by expressing its field as a sum of sheath helix modes and by requiring the tangential electric intensity to be zero on the tape. The resulting arithmetic is found to be intractable, and he quickly obtains a more manageable approximate solution by requiring only that the tangential electric intensity at the center of the tape be zero. When the resulting expression is compared with that obtained by Kogan[2] from a potential integral formulation, they are found to differ principally in the form of the convergence factor introduced by the approximation. Kogan treats the helical wire model with the null field boundary condition satisfied only at the points of tangency between the helical conductor and a cylinder with radius equal to the outer radius to the helical wire.

The work of these authors is directed toward the evaluation of the "free-mode" propagation constants for undamped traveling waves of current on the helical conductors. Although Sensiper[1] does devote some space to the source problem, his formulation of this problem is for the infinite helix. It is used to interpret the "free-mode" solutions of the source free problem.

Many authors have contributed to the literature on the helical waveguide. Since their work has been reviewed by Sensiper[1, 3], the bibliography is not reproduced here.

1.4 Helical Antennas

The helical antenna which most nearly approaches the backfire bifilar helical antenna in performance is the helical beam antenna introduced by Kraus[4] in 1947. Kraus's antenna is a monofilar helical wire fed at one end against a ground screen. The properties of this antenna have been discovered by experimental techniques. The current distribution on helical structures of this type was studied by Marsh[5]. The analysis of a helical

antenna of this type suffers the same difficulties as the analysis of the usual end-fire surface wave antenna. For both of these the feed region and the terminating region are important in determining their radiation characteristics. In contrast, the characteristics of the backfire bifilar helical antenna are controlled by the input region.

A bifilar version of the Kraus helix has been reported by Holtum[6]. This antenna is constructed of two coaxial helical wires on the diameters of the supporting cylinder. Each conductor is fed against a ground screen with the exciting currents in phase opposition. This differs from the backfire bifilar helical antenna in which the conductors are fed at one end, one against the other, without the presence of a ground screen. It is the absence of the ground screen that distinguishes the backfire helix from the Kraus-type helix. This fact is essential to the performance and analysis of the backfire helical antenna. On the other hand, the number of helical conductors is not essential to the backfire characteristic of the antenna. A backfire monofilar helix is shown to have substantially the same radiation characteristics as the backfire bifilar helix. The monofilar helix, however, is more difficult to feed in the backfire mode.

Although both the Kraus helix and the backfire bifilar helix are circularly polarized, several differences in the performance of these antennas must be noted. The beam width of the Kraus helix decreases with frequency while the backfire helix beam width increases with frequency. The gain of the Kraus helix increases with length while the gain of the backfire helix is independent of length provided the length is large enough. Finally, the Kraus helix is an end-fire antenna in contrast to the backfire helix which radiates along the helical axis toward the feed point.

1.5 Organization

In the present section, the backfire bifilar helical antenna is described and compared with other helical antennas of similar character. A description of the method used to obtain a solution for the radiation pattern of the antenna is given, and a brief review of the literature on the helical waveguide is included. In Chapter 2 the relation between the radiation pattern of a helical antenna and the Fourier spectrum of its current distribution is discussed. This motivates the work of the three following chapters in which the Fourier spectrum of the current distribution is obtained.

Chapter 3 describes the approximate determinantal equation for the helical waveguide as it is used in this study. This is derived from the potential integral with a linear current approximation. The equation describing the helical waveguide is factorized in Chapter 4 by the method of Wiener-Hopf, and the evaluation of the resulting expression by numerical techniques is described in Chapter 5. The results of the numerical computation are presented in Chapter 6 along with the experimental results. This Chapter also indicates the connection between this study and the log-spiral and other frequency-independent antennas. Chapter 7 summarizes and concludes the work.

2. THE HELICAL ANTENNA RADIATION PATTERN

2.1 Formulation of the Vector Potential

Since the purpose of this study is to develop a theory that is capable of predicting the radiation patterns of the backfire bifilar helical antenna, and since the geometry of the problem lends itself to a solution by Fourier transformation, a relation between the radiation pattern and the Fourier spectrum of the current distribution for the bifilar helix must be obtained. This section is devoted to establishing that relation.

The radiation pattern of an antenna will be taken to mean the angular distribution of electric intensity in spherical coordinates at a large distance from the antenna. When only those terms that vary inversely with distance are retained, the electric intensity is related to the magnetic vector potential by

$$\vec{E}_{xr} = -\vec{j}k\zeta\, A_{x\hat{r}} \qquad (1)$$

where r is a unit radial vector

$k = \omega\sqrt{\mu\epsilon}$ is the propagation constant of free space

$\zeta = \sqrt{\frac{\mu}{\epsilon}}$ is the intrinsic impedance of free space

Thus the radiation pattern is related to the angular distribution of the vector potential, and the vector potential is deduced from the current by the well known integral formula

$$\vec{A}(\vec{r}) = \iiint G(\vec{r}, \vec{r}\,')\, \vec{I}(\vec{r}\,')\, dv \qquad (2)$$

where

$$G(\vec{r}, \vec{r}\,') = \frac{\exp\left[-jk\left|\vec{r}-\vec{r}\,'\right|\right]}{4\pi\left|\vec{r}-\vec{r}\,'\right|}$$

is the Green's function in an unbounded homogeneous isotropic three dimensional space,

$\vec{r}$ is the radius vector to a point of observation and

$\vec{r}'$ is the radius vector to a source point.

By the method of induced sources, we may replace the conducting boundaries at the surface of the helical wires by a surface current distribution existing in homogeneous space. If this current distribution equals the surface current on the helical conductors, the fields external to the conductors are unchanged by removing the conductors from the space. If the conductors are sufficiently thin, the field produced by the surface current distribution will not differ much from that produced by a current distribution on the center line of the helical wire. This approximation limits the analysis to thin wire helices, but it has the advantage of converting the volume integral in Equation (2) to a line integral.

The bifilar helix then can be considered as two helical lines of current. A point on line one with axial coordinate z' will have cartesian coordinates

$$P_1 = (b \cos \tau z', \; b \sin \tau z', \; z')$$

where

$\tau = 2\pi/p$

p = pitch of helix

b = radius to centerline,

and the unit tangent to the helical wire at that point is given by

$$\hat{u}_1 = -\hat{x} \cos \psi \sin \tau z' + \hat{y} \cos \psi \cos \tau z' + \hat{z} \sin \psi$$

where ψ is the pitch angle of the helix given by

$$\cot \psi = \frac{2\pi b}{p} = \tau b$$

At the same value of the axial coordinate z' a point on line two will have cartesian coordinates

$$P_2 = (-b \cos \tau z', -b \sin \tau z', z')$$

with unit tangent

$$\hat{u}_2 = \hat{x} \cos \psi \sin \tau z - \hat{y} \cos \psi \cos \tau z' + \hat{z} \sin \psi$$

The distance between a remote point (r, θ, ϕ) and a point on line 1 is given by

$$|\vec{r}-\vec{r}'| = r_1 = \left[(r \sin \theta \cos \phi - b \cos \tau z')^2 + (r \sin \theta \sin \phi - b \sin \tau z')^2 + (r \cos \theta - z)^2 \right]^{1/2}$$

or

$$r_1 = \left[r^2 - 2br \sin \theta \cos (\tau z - \phi) + b^2 + z^2 \right]^{1/2}$$

Similarly, the distance between the remote point and a point on wire 2 is given by

$$r_2 = \left[r^2 + 2br \sin \theta \cos (\tau z - \phi) + b^2 + z^2 \right]^{1/2}$$

The currents on the helical line can be considered to be a function of the axial variable z' alone. If the currents in the two wires are equal and oppositely directed for the same value of z', Equation (2) may be written

$$\begin{aligned} A_x(\vec{r}) &= - \cos \psi \int_{-\infty}^{\infty} \left(\frac{e^{-jkr_1}}{4\pi r_1} + \frac{e^{-jkr_2}}{4\pi r_2} \right) \sin \tau z' \, I(z') \, dz' \\ A_x(\vec{r}) &= \cos \psi \int_{-\infty}^{\infty} \left(\frac{e^{-jkr_1}}{4\pi r_1} + \frac{e^{-jkr_2}}{4\pi r_2} \right) \cos \tau z' \, I(z') \, dz' \\ A_z(\vec{r}) &= \sin \psi \int_{-\infty}^{\infty} \left(\frac{e^{-jkr_1}}{4\pi r_1} - \frac{e^{-jkr_2}}{4\pi r_2} \right) I(z') \, dz' \end{aligned} \qquad (3)$$

2.2 Transformation by Parseval's Theorem

In Equation (3), the vector potential at the point (r, θ, ϕ) can be related

to the Fourier spectrum of the current distribution by Parseval's theorem. Parseval's theorem states: Given two functions, F(z) and I(z), of the spatial variable z with Fourier transforms, $\tilde{F}(\beta)$ and $\tilde{I}(\beta)$, in the transform variable β,

$$\int_{-\infty}^{\infty} F^*(z)\, I(z)\, dz = 2\pi \int_{-\infty}^{\infty} \tilde{F}^*(\beta)\, \tilde{I}(\beta)\, d\beta$$

where $\tilde{I}(\beta)$ is related to I(z) by

$$\tilde{I}(\beta) = \frac{1}{2\pi} \int_{-\infty}^{\infty} I(z)\, e^{j\beta z}\, dz$$

This introduces the Fourier transform of the current distribution into the calculations for the vector potential. In this paper the tilde (~) is used to denote the Fourier transform of a function of z, and the asterisk (*) is used to denote the complex conjugate of a function. It is now necessary to find the Fourier transform of the remaining factor in the integrand and to evaluate the transformed integral at a point remote from the helix. The complex conjugate of this factor in the first integral of Equation (3) can be written

$$F^*(z) = \left(\frac{e^{jkr_2}}{4\pi r_1} + \frac{e^{jkr_2}}{4\pi r_2}\right) \sin \tau z = (g_1 + g_2)\, \frac{e^{j\tau z} - e^{-j\tau z}}{8\pi j}$$

where g_1 and g_2 are the functions discussed in Appendix A

$$g_{\frac{1}{2}} = \frac{\exp\left(jk\left[A^2 \mp 2AB \cos(\phi + \tau z) + B^2 + (z-d)^2\right]^{1/2}\right)}{\left[A^2 \mp 2AB \cos(\phi + \tau z) + B^2 + (z-d)^2\right]^{1/2}}$$

where

$$A = r \sin \theta$$

$$B = b$$

$$d = r \cos \theta$$

Using Equation (A-5) and the shifting theorem for Fourier transforms we obtain

$$\tilde{F}^*(\beta)=\frac{-1}{16\pi}\sum_{n\ \text{even}}\begin{Bmatrix} J_n(b[k^2-(\beta-(n-1)\tau)^2]^{1/2})\ H_n^{(1)}(r\sin\theta[k^2-(\beta-(n-1)\tau)^2]^{1/2}) \\ \cdot e^{j(\beta-(n-1)\tau)\ r\cos\theta}e^{jn\phi} \\ -J_n(b[k^2-(\beta-(n+1)\tau)^2]^{1/2})\ H_n^{1}(r\sin\theta[k^2-(\beta-(n+1)\tau)^2]^{1/2}) \\ e^{j(\beta-(n+1)\tau)\ r\cos\theta}e^{jn\phi} \end{Bmatrix} \quad (13)$$

In this way, using Parseval's theorem, the first equation in (3) becomes

$$A_x(r)=\frac{+\cos\psi}{8}\sum_{n\ \text{even}}^{\infty}\int_{-\infty}\tilde{I}(\beta)\,d\beta\begin{Bmatrix} J_n(b[k^2-(\beta-(n-1)\tau)^2]^{1/2})H_n^{(1)}(r\sin\theta[k^2-(\beta-(n-1)\tau)^2]^{1/2}) \\ \cdot e^{j(\beta-(n-1)\tau)\ r\cos\theta}e^{jn\phi} \\ -J_n(b[k^2-(\beta-(n+1)\tau)^2]^{1/2}H_n^{(1)}(r\sin\theta[k^2-(\beta-(n+1)\tau)^2]^{1/2}) \\ e^{j(\beta-(n+1)\tau)\ r\cos\theta}e^{jn\phi} \end{Bmatrix}$$

2.3 The Far-Field Radiation Pattern

The asymptotic estimation of this integral follows that given in Appendix B. In this case the change of variables (Equation B-4) is

$$\beta-(n-1)\tau = k\cos\alpha$$

or

$$\beta-(n+1)\tau = k\cos\alpha$$

Thus we have

$$A_x(r)\sim+j\pi\cos\psi\sum_{n\ \text{even}}G_oJ_n(kb\sin\theta)[\tilde{I}(k\cos\theta_+(n+1)\tau)-\tilde{I}(k\cos\theta_+)(n+1)\tau)]e^{jn\phi}$$

where

$$G_o=\frac{e^{-jkr_o}}{4\pi r_o}$$

In this way Equation (3) becomes

$$\vec{A_x}(\vec{r})\sim+j\pi\cos\psi\sum_{n\ \text{even}}G_oJ_n(\rho)[\tilde{I}(k\cos\theta_+(n-1)\tau)-\tilde{I}(k\cos\theta_+(n+1)\tau)]e^{jn\phi} \quad (4)$$

$$\vec{A_y}(\vec{r})\sim\pi\cos\psi\sum_{n\ \text{even}}G_oJ_n(\rho)[\tilde{I}(k\cos\theta_+(n-1)\tau)+\tilde{I}(k\cos\theta_+(n+1)\tau)]e^{jn\phi}$$

$$\vec{A_z}(\vec{r})\sim 2\pi\sin\psi\sum_{n\ \text{odd}}G_oJ_n(\rho)\tilde{I}(k\cos\theta_+n\tau)e^{jn\phi}$$

where

$$\rho = kb \sin\theta$$

These series are rapidly convergent if $\tilde{I}(k\cos\theta+n\tau)$ is bounded on n because of the properties of $J_n(\rho)$. The ratio of the first two of these to $J_o(\rho)$ is shown in Figure 2. In addition, it will be shown later that for the backfire bifilar helix $|\tilde{I}_n(k\cos\theta+n\tau)|$ also decreases rapidly with n. Thus the radiation field of the backfire bifilar helix may be represented by the first terms of Equation (4) with little error giving

$$\begin{aligned} A_x(\vec{r}) &\sim J\pi\cos\Psi\, G_o\, J_o(\rho)[\tilde{I}(k\cos\theta-\tau)-\tilde{I}(k\cos\theta+\tau)] \\ A_y(\vec{r}) &\sim \pi\cos\Psi\, G_o\, J_o(\rho)[\tilde{I}(k\cos\theta+\tau)+\tilde{I}(k\cos\theta-\tau)] \\ A_z(\vec{r}) &\sim 2\pi\sin\Psi\, G_o\, J_1(\rho)[\tilde{I}(k\cos\theta+\tau)e^{j\phi}+\tilde{I}(k\cos\theta-\tau)e^{-j\phi}] \end{aligned} \qquad (5)$$

From Equation (5) it is obvious that the backfire bifilar helix radiation pattern is the sum of right-handed and left-handed circularly-polarized components. The ratio of these components on the axis of the antenna is given by

$$r = \frac{\tilde{I}(1-k)}{\tilde{I}(\pm 1-k)}$$

The axial ratio of the polarization ellipse is deduced from this by the equation

$$AR = \frac{1+r}{1-r} \qquad (6)$$

Computed values of the axial ratio are described in Chapter 6 of this report.

The relation between the radiation pattern of the backfire bifilar helix and the Fourier spectrum of its current distribution is established. The spectrum of the current distribution on the semi-infinite helix will be deduced from the determinantal equation for the infinite helix. The determinantal equation for the infinite bifilar helix is derived in the next chapter.

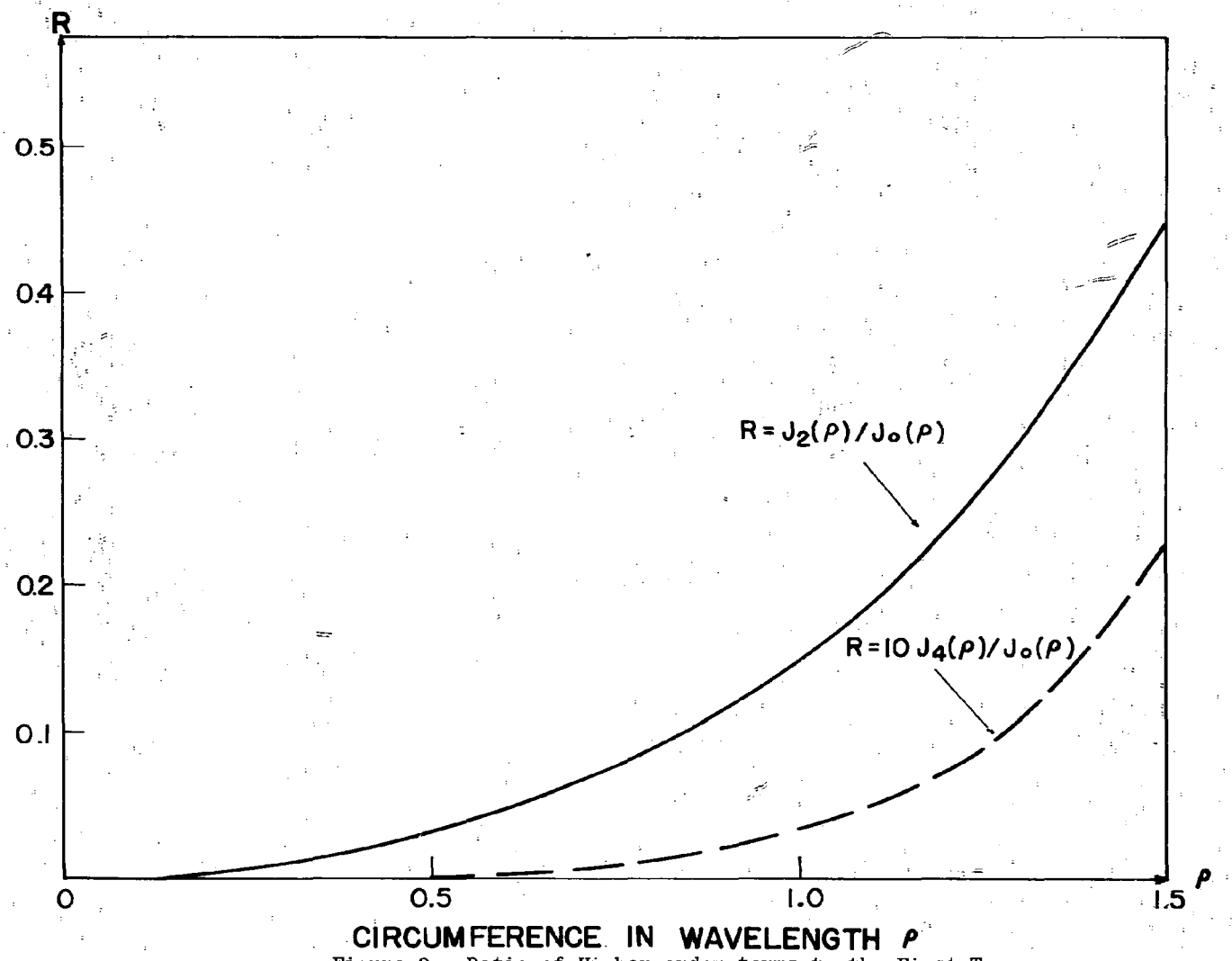

Figure 2. Ratio of Higher order terms to the First Term in the Series Expansion for the Pattern of the Bifilar Helix

3. THE BIFILAR HELIX DETERMINANTAL EQUATION

3.1 The Complete Circuit Equation

The electromagnetic field in an infinite homogeneous isotropic medium can be obtained from the magnetic vector potential $\vec{A}$ and the scalar potential V using the relations

$$\vec{H} = \nabla \times \vec{A}$$
$$\vec{E} = -jk\zeta \vec{A} - \nabla V \tag{7}$$

If the divergence of $\vec{A}$ is chosen to be

$$\nabla \cdot \vec{A} = -jk/\zeta \; V$$

these potentials satisfy the scalar and vector wave equations,

$$(\nabla^2 + k^2)V = -\frac{\rho}{\epsilon}$$

$$(\nabla^2 + k^2)\vec{A} = -\vec{I}$$

The solution of these equaltions can be written in terms of the Green's function of the medium

$$G(\vec{r}, \vec{r}') = \frac{\exp[-jk|\vec{r}-\vec{r}'|]}{4\pi |\vec{r}-\vec{r}'|}$$

as

$$V(\vec{r}) = \frac{1}{\epsilon}\iiint G(\vec{r}, \vec{r}')\rho(\vec{r}') \, dv$$
$$A(r) = \iiint G(\vec{r}, \vec{r}') \, I(\vec{r}') \, dv \tag{8}$$

Using the equation of continuity

$$\nabla \cdot \vec{I} = -jw\rho$$

in Equation (8) with Equation (7), there results

$$V = j\zeta/k \iiint G(\vec{r}, \vec{r}') \, \nabla \cdot I \, (\vec{r}') \, dv \tag{9}$$
$$\nabla V = -E - jk\zeta \iiint G(\vec{r}, \vec{r}') \, I(\vec{r}') \, dv$$

which forms the basis of the complete circuit equation.

The circuit equation for the bifilar helix is obtained by replacing the conducting boundaries of thehelical wires by the current distribution on the surface required to produce zero tangential electric intensity there. The equation is simplified by linearizing the boundary condition. This is based on two thin wire approximations; first, it is assumed that the current distribution on the surface of the wires can be replaced with a line current distribution at the center of the wire, and, second, it is assumed that, if the electric field is zero along only one line of the surface, the resulting solution will be a reasonable approximation to the exact solution. These assumptions are good if the wires are sufficiently thin.

In this analysis the current will be assumed to exist on the line defined in cartesian coordinates by

$$p_1 = (b \cos \tau z' [\ b \sin \tau z',\ z')$$

$$p_2 = (-b \cos \tau z',\ -b \sin \tau z',\ z')$$

and the null line will be taken as defined by

$$q_1 = (b' \cos \tau z\ ,\ b' \sin \tau z,\ z)$$

$$q_2 = (-b' \cos \tau z,\ -b' \sin \tau z,\ z)$$

where

$$b' = b-a$$

b = distance from helix axis to wire centerline

a = wire radius

Thus, the currents and potentials can be considered a function of the z coordinate alone. Because of the constant pitch angle of the helix,

$$\psi = \cot^{-1} (2\pi b/p)$$

an elementary displacement along the axis is related to one along the wire by

$$dz = \sin \psi\ dp$$

Thus on wire one

$$\nabla\cdot\vec{I}(\vec{r}') = \sin\psi \frac{dI(z')}{dz}$$

$$\nabla V(r') = \sin\psi\, \hat{u}_1(z) \frac{dV(z)}{dz}$$

$$\vec{I}(\vec{r}') = u_1(z')\, I_1(z')$$

where $\hat{u}_1 = -\hat{x}\cos\psi \sin\tau z + \hat{y}\cos\psi\cos\tau z + \hat{z}\sin\psi$

In these equations it is assumed that the pitch angle of the null line ψ' is equal to the pitch angle ψ of the centerline of the wire. The correct result is

$$\cot\psi' = \frac{b'}{b}\cot\psi = (1-\delta)\cot\psi$$

where

$$\delta = a/b$$

The approximation ($\psi' = \psi$) is consistent with the thin-wire assumption used throughout this study.

3.2 The Determinantal Equation for the Monofilar Helix

Equation (9) will be applied first to a single wire helix so that the modification of the determinantal required for the balanced bifilar helix will be made evident. The current is confined to the line p_1, and the potential is evaluated on the line q_1. Since the electric field strength is assumed zero along this line, Equation (9) becomes

$$V(z) = j\frac{\zeta}{k}\int_{-\infty}^{\infty} G_{11}(z, z')\sin\psi \frac{dI_1(z')}{dz}\, dz'$$

$$\sin\psi \frac{dV_z}{d} = -jk\zeta\int_{-\infty}^{\infty} G_{11}(z, z')\, \hat{u}_1(z)\cdot\hat{u}_1(z')\, I_1(z')\, dz' \qquad (10)$$

If the first equation is differentiated with respect to z, multiplied by $\sin\psi$, and equated to the second equation; the result is

$$\int_{-\infty}^{\infty} [\sin^2\psi \frac{dG_{11}(z, z')}{dz}\frac{dI(z')}{dz} + k^2(\hat{u}_1(z)\cdot\hat{u}_1(z')\, G_{11}(z, z')\, I(z')]\, dz' = 0 \qquad (11)$$

where

$$G_{11}(z, z') = \frac{\exp[-jk[b^2+b'^2-2bb'\cos\tau(z-z') + (z-z')^2]^{1/2}]}{4\pi[b^2+b'^2-2bb'\cos\tau(z-z') + (z-z')^2]^{1/2}}$$

and

$$\hat{u}_1(z) \cdot \hat{u}_1(z') = C_{11}(z-z') = \cos^2\psi \cos\tau(z-z') + \sin^2\psi$$

are even functions of the difference in z coordinates at the source and observation points.

Because G and C are functions of the difference in the z coordinate, Equation (11) is a convolution integral

$$\int_{-\infty}^{\infty} Z_{11}(z-z')\, I_1(z')\, dz' = 0 \qquad (12)$$

where Z_{11} is the operator

$$Z_{11}(z-z') = \frac{-dG_{11}(z-z')}{dz} \frac{d}{dz'} -k^2 G_{11}(z-z') -k^2 \cot^2\psi \cos\tau(z-z')\, G_{11}(z-z')$$

The Fourier transform of $G_{11}(z-z')$ is deduced from the result of Appendix A by

$$G_{11}(z) = \frac{g_1^*(z)}{4\pi}$$

where

$$g_1(z) = \frac{\exp(jk[A^2-2AB\cos(\phi+\tau z)+B^2+(z-d)^2]^{1/2})}{[A^2-2AB\cos(\phi+\tau z)+B^2+(z-d)^2]^{1/2}}$$

and where

$$A = b$$

$$B = b'$$

$$\phi = 0$$

$$d = 0$$

is

$$\tilde{G}_{11}(\beta) = \frac{j}{8\pi} \sum_{n=-\infty}^{\infty} J_n(b[k^2-(\beta-n\tau)^2]^{1/2})\, H_n^{(2)}(b[k^2-(\beta-n\tau)^2]^{1/2})$$

or

$$\tilde{G}_{11}(\beta) = \frac{1}{4\pi^2} \sum_{n=-\infty}^{\infty} I_n(b[(\beta-n\tau)^2-k^2]^{1/2})\, K_n(b[(\beta-n\tau)^2-k^2]^{1/2})$$

For convenience we will define a new function

$$B_n(\beta) = I_n(b'[(\beta-n\tau)^2-k^2]^{1/2})\, K_n(b[(\beta-n\tau)^2-k^2]^{1/2})$$

The function, $\tilde{G}_{11}(\beta)$ now has the simpler representation

$$\tilde{G}_{11}(\beta) = \frac{1}{4\pi^2} \sum_{n=-\infty}^{\infty} B_n(\beta)$$

The Fourier transform of $Z(z)$ is given by

$$\tilde{Z}_{11}(\beta) = (\beta^2-k^2)\, \tilde{G}_{11}(\beta) - \frac{k^2\cot^2\psi}{2} [\tilde{G}_{11}(\beta+\tau)+\tilde{G}_{11}(\beta-\tau)]$$

This function has infinitely many branch points located at

$$\beta = n\tau \pm k \qquad\qquad n = 0, \pm 1, \pm 2, \cdots$$

The Fourier transform of Equation (12) is

$$\tilde{Z}_{11}(\beta)\, \tilde{I}_1(\beta) = 0 \tag{13}$$

The spectrum of the current on the infinite monofilar helical waveguide given by Equation (13) must be a distribution of point support at the roots of $\tilde{Z}(\beta)$ and, therefore, is a polynomial of delta distributions there. However, by analytic continuation of the distribution [7] into the complex β-plane, it can be shown that the order of the distribution must be one less than the order of the root. Since the roots of $\tilde{Z}(\beta)$ are of first order, no derivatives of the delta appear. The current distribution, therefore, is a sum of traveling waves with propagation constants given by the roots of $\tilde{Z}(\beta)$.

In investigating the roots of $\tilde{Z}(\beta)$, Kogan[2] rearranges terms in the form

$$\frac{\sum_{n=-\infty}^{\infty} [B_n(\beta+\tau) + B_n(\beta-\tau)]}{2 \sum_{n=-\infty}^{\infty} B_n(\beta)} = \text{Tan}^2 \psi \left(\frac{\beta^2}{k^2} - 1\right)$$

The function on the left can be called $F_2(\beta)$ and, following Kogan[2], is sketched in Figures 3 and 4. It can be seen that $F_2(\beta)$ is approximately equal to one in the range

$$\frac{k}{\tau} < \left| \frac{\beta}{\tau} - n \right| < 1 - \frac{k}{\tau} \qquad n = 0, \pm 1, \pm 2, \ldots$$

except near $\beta = \tau \pm k$ where the terms $B_o(\beta-\tau)$ in the numerator have a logarithmic singularity contributed by the modified Hankel function of zero order or near $\beta = k$ where $B_o(\beta)$ in the denominator is logarithmically singular. In this range the root of $\tilde{Z}(\beta)$ is given approximately by

$$\frac{\beta^2}{k^2} = 1 + \cot^2 \psi$$

or

$$\beta = k/\sin \psi$$

The roots of $\tilde{Z}(\beta)$ are at the intersection of $F_2(\beta)$ and the parabola

$$F_1(\beta) = \text{Tan}^2 \psi \left[\frac{\beta^2}{k^2} - 1\right]$$

For k small it can be seen that there are three roots: one near $\beta = k/\sin \psi$, one near $\beta = 1-k$, and one near $\beta = 1+k$. Since $\tilde{Z}(\beta)$ is an even function of β, there are also three corresponding roots on the negative β-axis.

The functional dependence of the roots of $\tilde{Z}(\beta)$ on the frequency, k, is conveniently displayed on the Brillouin diagram, also called the β-k diagram, shown in Figure 5. In this figure, due to Sensiper[1], the variables are normalized with respect to τ ($\tau = 2\pi/p$). The deviation of the curve from the

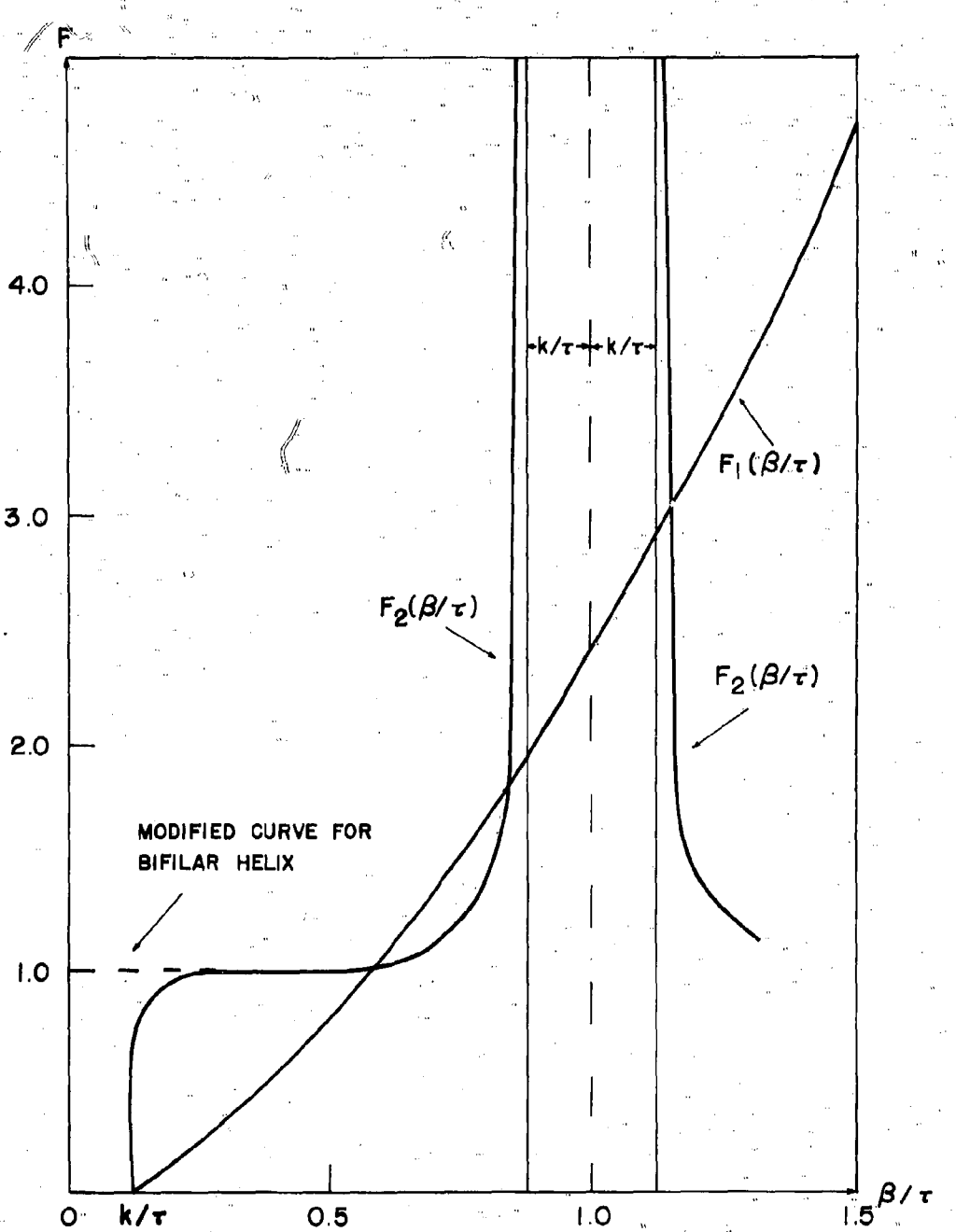

Figure 3. Graphical Solution for the Roots of the Helix Determinantal Equation when $k < k_c$

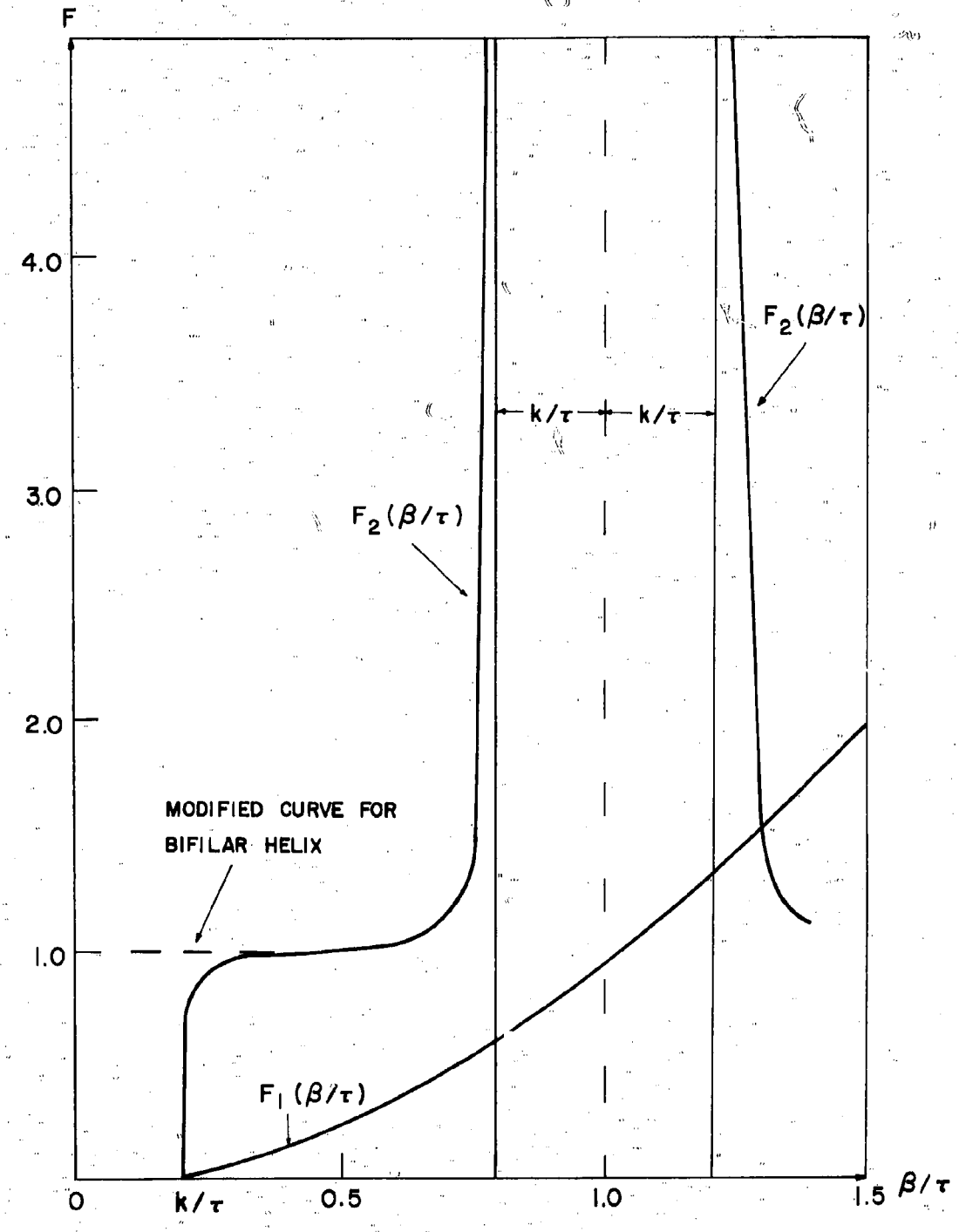

Figure 4. Graphical Solution for the Roots of the Helix Determinantal Equation when $k > k_c$

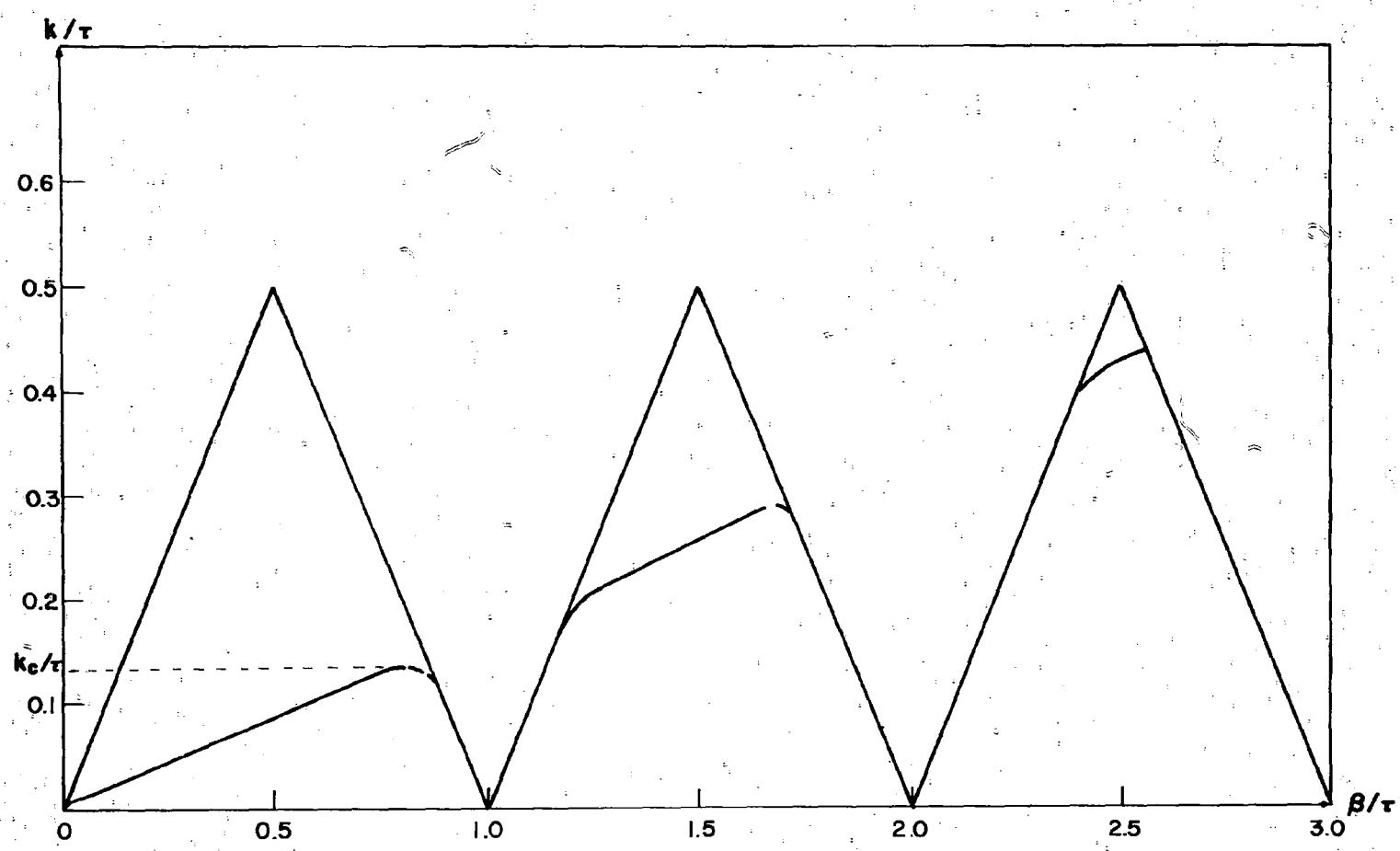

Figure 5. Brillouin Diagram for a Monofilar Helical Waveguide

asymptote,

$$\beta = k/\sin\psi$$

near $\beta = 0$ can be interpreted as coupling between the current wave and a linearly polarized plane wave, and the deviation near $\beta = \tau \pm k$ can be interpreted as coupling with circularly polarized plane waves. This coupling is indicated by the logarithmic singularities and depends upon the wire thickness $\delta(\delta=a/b)$ of $F_2(\beta)$ shown in Figure 3.

3.3 The Determinantal Equation for the Bifilar Helix

When the second conductor is added to the problem, Equation (12) becomes

$$\int_{-\infty}^{\infty} [Z_{11}(z-z')\, I_1(z') + Z_{12}(z-z')\, I_2(z')]\, dz' \qquad (14)$$

where

$$Z_{12}(z-z') = \frac{d}{dz} G_{12}(z-z') \frac{d}{dz} - k^2 C_{12}(z-z')\, G_{12}(z-z')$$

In this equation

$$G_{12}(z-z') = \frac{\exp(-jk[b^2+b'^2+2bb'\cos\tau(z-z')+(z-z')^2]^{1/2})}{4\pi[b^2+b'^2+2bb'\cos\tau(z-z')+(z-z')^2]^{1/2}}$$

relates the potential at wire one to the current on wire two, and

$$C_{12}(z-z') = \hat{u}_1(z) \cdot \hat{u}_2(z') = -\cos^2\psi \cos\tau(z-z') + \sin^2\psi$$

is the cosine of the angle between the line element at the source point and the line element at the observation point.

The fourier transform of $G_{12}(z)$ is

$$\tilde{G}_{12}(\beta) = \frac{1}{4\pi^2} \sum_{n=-\infty}^{\infty} (-1)^n B_n(\beta)$$

and that of $Z_{12}(z)$ is

$$\tilde{Z}_{11}(\beta) = (\beta^2 - k^2)\, \tilde{G}_{12}(\beta) + \frac{k^2\cot^2\psi}{2} [\tilde{G}_{12}(\beta+\tau) + \tilde{G}_{12}(\beta-\tau)]$$

It follows then that the Fourier transform of Equation (14) is

$$\tilde{Z}_{11}(\beta)\,\tilde{I}_1(\beta) + \tilde{Z}_{12}(\beta)\,\tilde{I}_\beta(\beta) = 0 \tag{15}$$

If the excitation of the bifilar helix is balanced ($I = I_1 = -I_2$) Equation (15) becomes

$$\tilde{Z}(\beta)\,\tilde{I}(\beta) = 0 \tag{16}$$

where

$$\tilde{Z}(\beta) = \tilde{Z}_{11}(\beta) - \tilde{Z}_{12}(\beta)$$

or

$$\tilde{Z}(\beta) = (\beta^2-k^2)[\tilde{G}_{11}(\beta)-\tilde{G}_{12}(\beta)] - \frac{k^2\cot^2\psi}{2}\left[\begin{matrix}\tilde{G}_{11}(\beta-\tau)+\tilde{G}_{11}(\beta-\tau)\\ +\tilde{G}_{12}(\beta+\tau)+\tilde{G}_{12}(\beta-\tau)\end{matrix}\right]$$

When this is written in terms of the functions $B_n(\beta)$, it becomes

$$4\pi^2\tilde{Z}_{(\beta)} = (\beta^2-k^2)\sum_{n\ \text{odd}} B_n(\beta) - \frac{k^2\cot^2\psi}{2}\sum_{n\ \text{even}}[B_n(\beta+\tau)+B_n(\beta-\tau)] \tag{17}$$

All branch points ($\beta = n\tau \pm k$) for n even have been removed. If the equation for the roots of Equation (17) is cast in Kogan's form, we obtain

$$F_2(\beta) = \frac{\sum_{n\ \text{even}}[B_n(\beta+\tau)+B_n(\beta-\tau)]}{2\sum_{n\ \text{odd}} B_n(\beta)}$$

This function is similar to that of the monofilar helix except that the logarithmic singularity at $\beta = k$ has been removed. The resulting modification to the monofilar helix is shown in Figures 3 and 4. The Brillouin diagram, shown in Figure 6, no longer shows the dispersive character of the monofilar helix in the neighborhood of $\beta = 0$.

3.4 Convergence and Asymptotic Representation of the Determinantal Equation

To establish the convergence of the series representation of $\tilde{Z}(\beta)$ and its asymptotic representation, it is sufficient to study the function

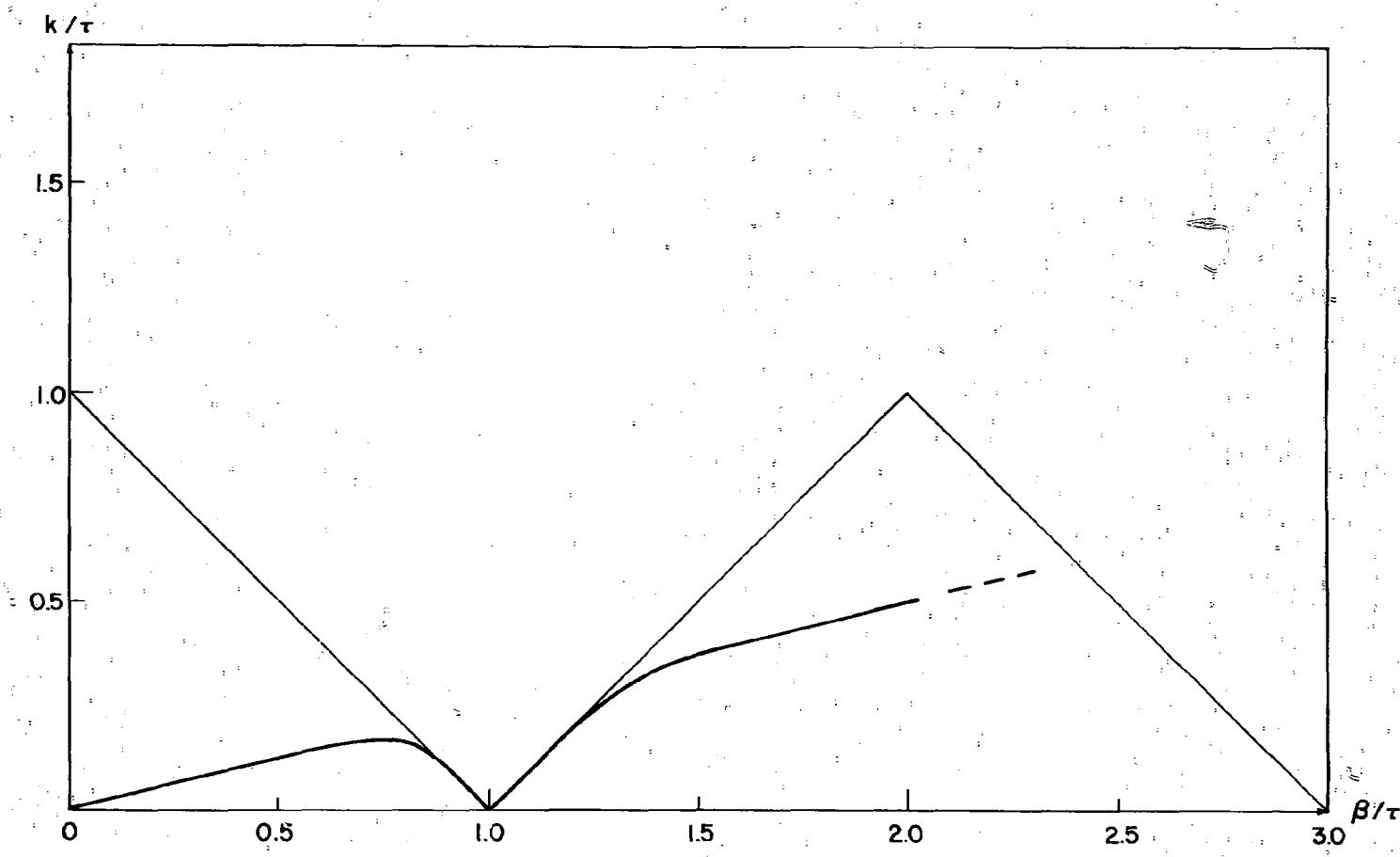

Figure 6. Brillouin Diagram for a Bifilar Helical Waveguide

$$\tilde{G}_{11}(\beta) = \frac{1}{2\pi} \int_{-\infty}^{\infty} \frac{e^{-jk[b^2+b'^2-2bb'\cos \tau z+z^2]^{1/2}}}{4\pi[b^2+b'^2-2bb'\cos \tau z+z^2]^{1/2}} e^{j\beta z} dz$$

$$= \frac{1}{4\pi^2} B_o(\beta) + \frac{1}{4\pi^2} \sum_{n=1}^{\infty} (B_n(\beta)+B_n(-\beta)) \qquad (18)$$

where

$$B_n(\beta) = I_n(b'\gamma n)\ Kn\ (b\ \gamma n)$$

$$\gamma_n^2 = (\beta-n\tau)^2 - k^2$$

When $k<\tau$ all the terms in the series Equation (18) are positive except at most one term. It follows that, if the series representation of $\tilde{G}_{11}(\beta)$ converges, then $\tilde{G}_{12}(\beta)$ converges absolutely.

A result of Watson[8]

$$I_n(x)\ K_n(x) = \int_0^{\infty} \frac{z}{z^2+x^2} J_n^2(z)\ dz$$

shows that $I_n(x)\ K_n(x)$ is positive monotone decreasing. Since

$$\lim_{x\to o} I_n(x)\ K_n(x) = \frac{1}{2n}$$

it follows that

$$I_n(x)\ K_n(x) \leq \frac{1}{2n}$$

for all real x. The recurrence formula for the modified Hankel function

$$\frac{dx^n K_n(x)}{dx} = -x^n\ K_{n-1}(x)$$

tells us that $x^n K_n(x)$ is also positive decreasing for positive x and, if $x_1 > x_2$, it follows that

$$x_1 K_n(x_1) < x_2 K_n(x_2)$$

Thus

$$I_n(x_2)\ K_n(x_1) < \left(\frac{x_2}{x_1}\right)^n I_n(x_2)\ K_n(x_2) \leq \frac{1}{2n} \left(\frac{x_2}{x_1}\right)^n$$

But, in Equation (18),

$$\frac{x_2}{x_1} = \frac{b'}{b} = \frac{b-a}{b} = 1-\delta$$

so that,

$$B_n(\beta) < \frac{(1-\delta)^n}{2n}$$

Therefore

$$4\pi^2 \tilde{G}_{11}(\beta) < B_o(\beta) + \sum_{n=1}^{\infty} \frac{(1-\delta)^n}{n}$$

or

$$\tilde{G}_{11}(\beta) < \frac{1}{4\pi^2} (B_o(\beta) - \ln \delta)$$

where

$$\delta = \frac{a}{b}$$

is the ratio of the wire radius to the mean radius of the helix. This inequality is valid where no $\gamma_n(\beta)$ is imaginary. If one is imaginary, that term may be excluded from the series without affecting its convergence. Thus the series representation of $\tilde{G}_{11}$ is convergent everywhere.

When $\tilde{Z}(\beta)$ is evaluated for β small, the usual small argument approximation for the large order terms of the series does not apply because the argument of the Bessel functions,

$$b[(\beta - n\tau)^2 + k^2]^{1/2}$$

increases with the order of the function. In this case, Debye approximations are more appropriate. These are[9]

$$I_n(b'\gamma_n) \approx \frac{\exp([n^2+(b\gamma_n)^2]^{1/2} - n \sinh^{-1} \frac{n}{b\gamma_n})}{\sqrt{2\pi}\ [n^2+(b'\gamma_n)^2]^{1/4}}$$

$$K_n(b\gamma_n) \simeq \sqrt{\frac{\pi}{2}} \frac{\exp\left([n^2+(b\gamma_n)^2]^{1/2} - n \sinh^{-1}\frac{n}{b\gamma_n}\right)}{[n^2+(b\gamma_n)^2]^{1/4}}$$

The term

$$[n^2+(b\gamma_n)^2]^{1/2} = [\, n^2+n^2(b\tau)^2-2n\,\frac{\beta}{\tau}\,(b\tau)^2+\,[(\frac{\beta}{\tau})^2-(\frac{k}{\tau})^2](b\tau)^2\,]^{1/2}$$

can be approximated for large n by

$$[n^2+(b\gamma_n)^2]^{1/2} \simeq n\sqrt{1+\cot^2\psi} - \frac{\beta}{\tau}\frac{\cot^2\psi}{\sqrt{1+\cot^2\psi}}$$

$$\simeq \frac{n}{\sin\psi} - \frac{\beta}{\tau}\frac{\cos^2\psi}{\sin\psi}$$

where the relation

$$b\tau = \cot\psi$$

has been used. The term

$$n \sinh^{-1}\frac{n}{b\gamma_n} = n \ln\left(\frac{n}{b\gamma_n} + [1+(\frac{n}{b\gamma_n})^2]^{1/2}\right)$$

can be written

$$n \sinh^{-1}\frac{n}{b\gamma_n} = n \ln\left(\frac{n+[n^2\cot^2\psi-2\,\frac{\beta}{\tau}\,n\cot^2\psi - (\frac{k}{\tau})^2\cot^2\psi+n^2]^{1/2}}{\cot\psi\,[(\frac{\beta}{\tau}-n)^2-(\frac{k}{\tau})^2]^{1/2}}\right)$$

and approximated

$$n \sinh^{-1}\frac{n}{b\gamma_n} \simeq n \ln\left(\frac{n+\frac{n}{\sin\psi} - \frac{\beta}{\tau}\,\frac{\cos^2\psi}{\sin\psi}}{n\cot\psi\,(1-\frac{\beta}{n\tau})}\right)$$

$$n \sinh^{-1}\frac{n}{b\gamma_n} \simeq n \ln\left(\frac{1+\sin\psi}{\cos\psi}\,[\,1-\frac{\beta}{n\tau}\,\frac{\cos^2\psi}{1+\sin\psi}\,]\,[1+\frac{\beta}{n\tau}]\right)$$

$$\simeq n \ln\left(\frac{1+\sin\psi}{\cos\psi}\,[1-\frac{\beta\sin\psi}{n\tau}]\right)$$

Thus the modified Handel function can be approximated by

$$K_n(b\gamma_n) \simeq \sqrt{\frac{\pi}{z}} \frac{\exp\left[-\frac{n}{\sin\psi} + \frac{\beta}{\tau}\frac{\cos^2\psi}{\sin\psi}\right]}{\sqrt{n/\sin\psi}} \left(\frac{1+\sin\psi}{\cos\psi}\right)^n \left(1+\frac{\beta}{n\tau}\sin\psi\right)^n$$

but since,

$$\lim_{n\to\infty}\left(1+\frac{\beta\sin\psi}{n\tau}\right) = \exp\frac{\beta\sin\psi}{\tau}$$

we have

$$K_n(b\gamma_n) \sim \sqrt{\frac{\pi\sin\psi}{2n}}\left(\frac{1+\sin\psi}{\cos\psi}\right)^2 \exp\left[-\frac{n-\frac{\beta}{\tau}}{\sin\psi}\right]$$

Similarly, using

$$b'\tau = \cot\psi' = (1-\delta)\cot\psi$$

we have

$$I_n(b'\gamma_n) \sim \sqrt{\frac{\sin\psi}{2\pi n}}\left(\frac{\cos\psi}{1+\sin\psi}\right)\exp\left[\frac{n-\beta/\tau}{\sin\psi'}\right]$$

Thus the Bessel function product in Equation (18) can be approximated for n large by

$$B_n(\beta) \sim B'_n(\beta) = \frac{\sqrt{\sin\psi\sin\psi'}}{2n}\left[\frac{\cos\psi'(1+\sin\psi)}{\cos\psi(1+\sin\psi')}\right]^n \exp -(n-\frac{\beta}{\tau})\left(\frac{1}{\sin\psi}-\frac{1}{\sin\psi'}\right)$$

The rate of convergence of the series representation of $\tilde{g}_{11}(\beta)$ can be increased by using Kummer's transformation[10]. Since the terms $B'_n(\beta)$ can be summed, the result is

$$\tilde{G}_{11}(\beta) = \frac{1}{4\pi^2}\left\{-\sqrt{\sin\psi\sin\psi'}\cosh\frac{\beta}{\tau}\left(\frac{1}{\sin\psi}-\frac{1}{\sin\psi'}\right)\right]$$
$$\ln\left[1-\frac{\cos\psi(1+\sin\psi)}{\cos\psi(1+\sin\psi)}\exp\left(\frac{1}{\sin\psi}-\frac{-1}{\sin\psi'}\right)\right] \qquad (19)$$
$$+B_o(\beta)+\sum_{n=1}^{\infty}\left[B_n(\beta)-B_n(\beta)+B_n(-\beta)-B_n(-\beta)\right]\Bigg\}$$

Equation (19) is in the form used in the numerical calculations of this study. The expressions in the first term are somewhat complicated, and it

is interesting to apply further approximations based on the assumption of small relative wire size δ. The algebra involved is straightforward but tedious. The result for the first term is

$$-\sin\Psi \ln\frac{\delta}{\sin\Psi} \tag{20}$$

This term controls the "sharpness" of the corners of the Brillouin diagram. It determines, in effect, the degree of coupling between the current wave on the helical wire and the axial plane waves of linear and circular polarization. As this term becomes larger, the corners become sharper. When it is small, the corners will be well rounded, and the coupling can be considered large. The magnitude of this factor is controlled by the relative wire size, δ, and the sine of the pitch angle. As the wire size increases and also as the pitch angle decreases, coupling is increased, and the Brillouin diagram will depart considerably from the asymptote

$$\beta = k/\sin\Psi$$

On the other hand, when the wire is thin and the pitch angle is large, coupling is small and the asymptotic form of the Brillouin diagram well approximates the current distribution.

It proves to be quite difficult to obtain an asymptotic estimation of $\tilde{G}_{11}(\beta)$ for large β from the series representation. It can, however, be obtained rather easily from the integral representation in Equation (18). The integrand has branch points at the roots of the denominator

$$b^2+b'^2-2bb'\cos\tau z+z^2 = 0$$

This equation has no real roots. If $z = x+jy$, the real and imaginary parts of this equation become

$$b^2+b'^2-2bb' \cosh \tau y \cos \tau x+x^2-y^2 = 0$$
$$bb' \sinh \tau y \sin \tau x = -xy \qquad (21)$$

The first of these equations is satisfied when

$$f(x, y) = g(x, y)$$

where

$$f(x, y) = 2bb' \cosh \tau y \cos x+y^2$$
$$g(x, y) = b^2+b'^2+ x^2$$

The functions f(o, y) and g(o, y) are shown in Figure 7 where $\eta = \tau y$. Since

$$f(x, y) \leq f(o, y)$$
$$g(x, y) \geq g(o, y)$$

it is obvious that the imaginary parts of the roots at

$$f(o, y) = g(o, y)$$

have the smallest magnitude, since the second equation in (21) is satisfied for all y when x = 0. This root then is the solution of the transcendental equation

$$b^2+b'^2-2bb' \cosh \tau y-y^2 = 0$$

If this equation is multiplied by τ^2 and the substitutions

$$b' = (1-\delta)b$$
$$\eta = \tau y$$
$$\cot \psi = \tau b$$

are used, the result is

$$1+(1-\delta)^2-2(1-\delta) \cosh \eta = (\eta \operatorname{Tan} \psi)^2$$

Where δ is small η is given approximately by

$$\eta \simeq \delta \cos \psi$$

The integral in Equation (18) is evaluated by deforming the contour upward and along branch cuts extending from the branch points parallel to

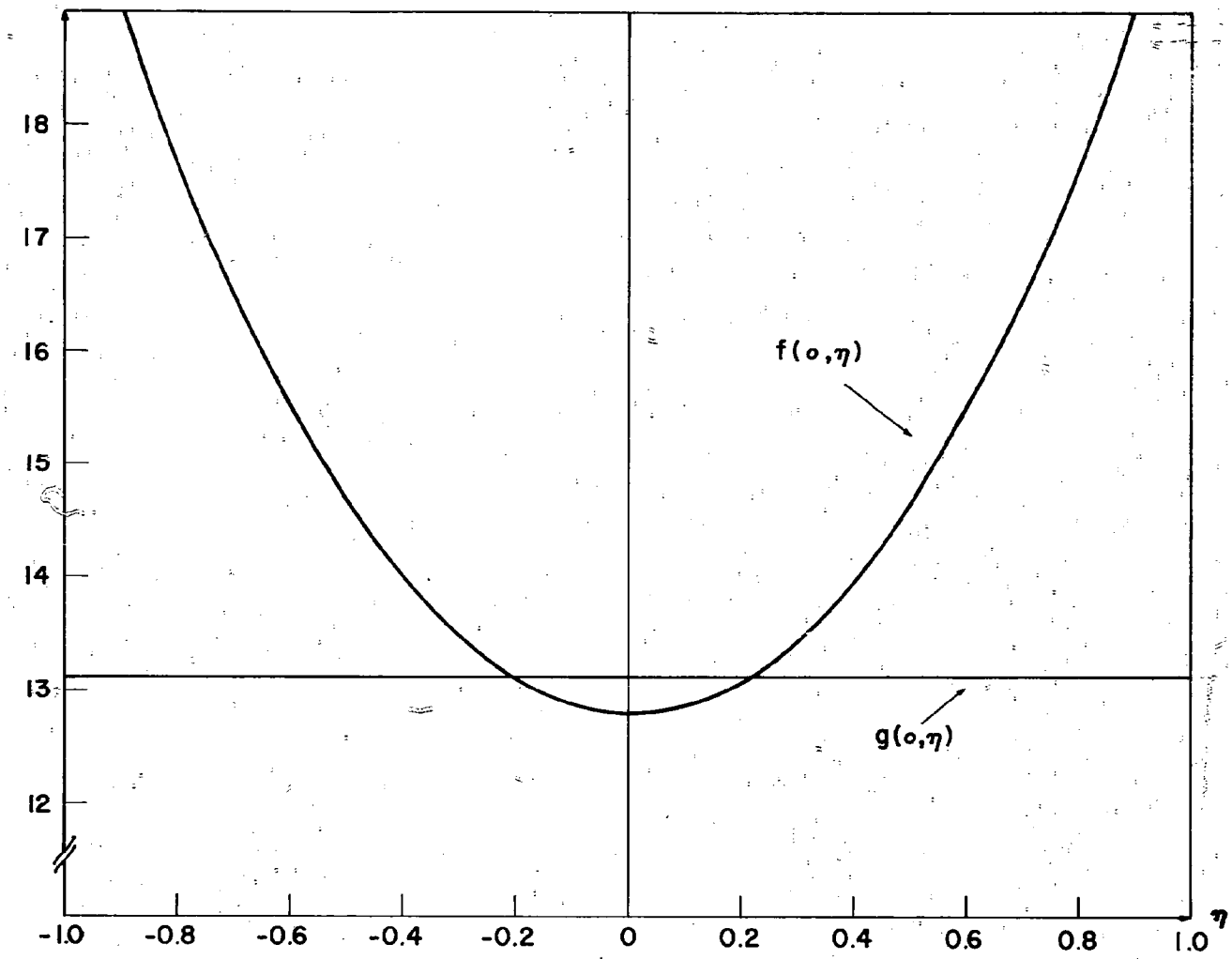

Figure 7. Graphical Solution for the Exponent in the Asymptotic Form of $\tilde{Z}$ (β)

the y axis. The contribution of the branch point at $z = j\,\eta/\tau$ is evaluated by the method of van der Waerden[11]. According to this method

$$S = j(jz+n/\tau)^{1/2}$$

is chosen as a local uniformizer and a Laurent expansion of the integrand about $S = 0$ is obtained.

$$\frac{\exp(-jk[b^2+b'^2-2bb' \cos \tau z+z^2]^{1/2})}{[b^2+b^2-2bb' \cos \tau z+z^2]^{1/2}} = \frac{a_{-1}}{S} + a_o + a_1 S + \ldots$$

where

$$a_{-1} = \frac{1}{\sqrt{-2(\tau bb' \sin \eta+\frac{\eta}{\tau})}} = \frac{-j}{\sqrt{2/\tau[(1-\delta) \cot^2\psi \sin \eta+\eta]}}$$

The integral of the first term is

$$2j\, a_{-1}\, e^{-\beta \frac{\eta}{\tau}} \int_{-\infty}^{\infty} e^{-\beta S^2} ds$$

or

$$2j\, a_{-1}\, e^{\frac{-\beta\eta}{\tau}} \sqrt{\frac{\pi}{\beta}}$$

van der Waerden[11] shows that the remainder of the integral at this branch point is of order

$$R = O(e^{-\frac{\beta\eta}{\tau}} \beta^{-3/2})$$

The exponent at the remaining branch points are larger than η/τ, and the contribution of these terms may be neglected for β large. Thus, we have the result

$$\tilde{g}_{11}(\beta) \sim \frac{\sqrt{2\pi}\; e^{\frac{-\beta\eta}{\tau}}}{\sqrt{\frac{\beta}{\tau}[(1-\delta) \cot^2\psi \sinh \eta+\eta]}} \qquad (22)$$

and

$$\tau^2 \tilde{Z}(\beta) = \frac{(\frac{\beta}{\tau})^{3/2} \; e^{-\frac{\beta\eta}{\tau}}}{\sqrt{8\pi[(1-\delta)\cot^2\psi \sinh \eta+\eta]}} \qquad (23)$$

and the exponent is approximately

$$\frac{\eta}{\tau} \simeq a \sin \psi$$

The factor $A(\delta)$,

$$A(\delta) = \frac{1}{\sqrt{8\pi[(1-\delta)\cot^2\psi \sinh \eta+\eta]}} \qquad (24)$$

is given approximately by

$$A(\delta) = \frac{1}{4\pi}\sqrt{\frac{p \sin \psi}{a}}$$

4. THE SOLUTION OF THE SEMI-INFINITE BIFILAR HELIX

4.1 The Modified Circuit Equation for the Semi-infinite Helix

The semi-infinite bifilar helix will be taken as two helical conducting wires originating in the $z = 0$ plane of a cartesian coordinate system and extending in the positive z direction. There will be no conducting structure for negative values of the z coordinate, and the structure will be considered to be coincident with that described in the preceeding section for positive values of the z coordinate. The lack of conducting structure in the negative half-space forces the current distribution, $I_+(z)$, to be identically zero there. Since there is no conducting boundary in the negative half-space, the electric field strength tangent to the null line in this space, $E_-(z)$, need no longer be zero. However, $E_-(z)$ must be identically zero for positive z.

The positive subscript is used to indicate a function of z, identically zero for all negative z. The negative subscript denotes a function which vanishes for positive z.

Equation (10), in this case, becomes

$$V(z) = j\,\zeta/k \int_{-\infty}^{\infty} G_{11}(z,\, z')\, \sin\psi\, \frac{d}{dz}\, I_{1_+}(z')\, dz'$$

$$\sin\psi\, \frac{dV(z)}{dz} = -E_-(z) - jk\zeta \int_{-\infty}^{\infty} G_{11}(z,\, z')\, \hat{u}_1(z) \cdot \hat{u}_1(z')\, I_{1_+}(z')\, dz'$$

where only one wire is considered. The potential V(z) is eliminated by multiplying the derivative of the first equation by $\sin\psi$ and equating to the second equation. The result, after a simple algebraic manipulation is

$$-j\, k/\zeta\, E_-(z) = \int_{-\infty}^{\infty} Z_{11}(z-z')\, I_{1_+}(z')\, dz'$$

This is the modified circuit equation for the semi-infinite helix. The circuit equation for the semi-infinite bifilar helix is obtained from this by including the contribution of the second wire as was done in Chapter 3. Replacing the expression on the left with $V_-(z)$ gives the result

$$V_-(z) = \int_{-\infty}^{\infty} Z(z-z')\ I_+(z')\ dz' \tag{25}$$

for the circuit equation of the semi-infinite bifilar helix.

4.2 The Source Problem

The Fourier transform of the convolution integral Equation (25) is

$$\tilde{V}_1(\beta) = \tilde{Z}(\beta)\ \tilde{I}_+(\beta) \tag{26}$$

This equation contains two unknown functions of β. Since the support of $V_-(z)$ is the negative z axis, its transform

$$\tilde{V}_-(\beta) = \frac{1}{2\pi} \int_{-\infty}^{\infty} V_-(z)\ e^{j\beta z} dz$$

is regular in the lower half of the complex β-plane; and since the support of $I_+(z)$ is the positive axis, its transform

$$\tilde{I}_+(\beta) = \frac{1}{2\pi} \int_{-\infty}^{\infty} I_+(z)\ e^{j\beta z} dz$$

is regular in the upper half of the complex β-plane. It will be assumed that $V_-(z)$ and $I_+(z)$ are of decaying exponential order at infinity so that their regions of regularity include the real β-axis. The procedure for solving Equation (26) used in this study depends upon factorizing $\tilde{Z}(\beta)$ in the form

$$\tilde{Z}(\beta) = \frac{Z_+(\beta)}{Z_-(\beta)} \tag{27}$$

where $Z_+(\beta)$ is regular in the upper half-plane and $Z_-(\beta)$ is regular in the lower half-plane. By the Wiener-Hopf technique[12], Equation (26) can be

written

$$\tilde{V}_-(\beta)\, Z_-(\beta) = \tilde{I}_+(\beta)\, Z_+(\beta) = J(\beta) \qquad (28)$$

If the factors of $\tilde{Z}(\beta)$ have a common strip of regularity including the real β-axis, then each side of Equation (28) must be the analytic continuation of the other in its region of regularity, and it follows that each side is an entire function, $J(\beta)$. If this function has polynomial growth at infinity, it is a polynomial, say $P_n(\beta)$, by Liouville's theorem. The factorization of $\tilde{Z}(\beta)$ is not unique because, $Z_+(\beta)$ and $Z_-(\beta)$ may be multiplied by the same polynomial, $Q_n(\beta)$, without changing Equation (27).

To obtain a unique solution of Equation (28) it is necessary to determine the asymptotic behavior of the factors at large values of β. This is equivalent to determining the behavior of $I_+(z)$ near the origin. In this problem, this determines the source conditions on the current distribution.

The backfire bifilar helical antenna will be fed at $z = 0$ from a balanced transmission line on its axis. In the mathematical model considered here, the transmission line and the wires connecting it to the helix will be neglected, and the current distribution $I_+(z)$ will start from some finite value at the origin. This discontinuity in the current at the origin implies an oscillating point charge distribution at the end of the wire. An infinitely long thin straight wire driven by an oscillating point charge at its end has been discussed by Schelkunoff[13]. The point charges can be considered as the source of the currents flowing in the helical wires. They will be replaced in the physical antenna by the transmission line and the connecting wires.

The discontinuity in the current distribution at the origin implies that the transform $\tilde{I}_+(\beta)$ behaves as $1/\beta$ at infinity. The current distribution

$I_+(z)$ can be represented as the sum of a decaying exponential on the positive z-axis starting from $I_+(0)$ and a function which vanishes with some power of z for z small and vanishes exponentially for z large

$$I_+(z) = I_+(0)\, e^{-\alpha z} + f(z)$$

The Fourier transform of the first term is $(\beta+j\alpha)^{-1}$ and, hence, decays as $1/\beta$. Since $f(z)$ is of order z^n with n positive for small z, its transform must decay as $B^{-(1+n)}$ for β large and may be neglected for large β when compared with the transform of the first term. Now, since

$$\tilde{I}_+(\beta) \sim B/\beta$$

and

$$Z(\beta) \sim A\, e^{-\frac{\beta\eta}{\tau}} \left(\frac{\beta}{\tau}\right)^{3/2}$$

from Equation (23), it follows that

$$\tilde{V}_-(\beta) = \tilde{I}_+(\beta)\, \tilde{Z}(\beta) \sim AB\, e^{-\frac{\beta\eta}{\tau}} \left(\frac{\beta}{\tau}\right)^{1/2}$$

Thus if $\tilde{Z}(\beta)$ is factorized so that

$$Z_+(\beta) \sim \beta$$

$$Z_-(\beta) \sim \frac{e^{+\beta\eta/\tau}}{A\sqrt{\beta/\tau}}$$

Equation (28) becomes

$$\tilde{V}_-(\beta)\, Z_-(\beta) = \tilde{I}_+(\beta)\, Z_+(\beta) = B \tag{29}$$

and the solution for $\tilde{I}_+(\beta)$ is given by

$$\tilde{I}_+(\beta) = \frac{B}{Z_+(\beta)} \tag{30}$$

As mentioned before, the factorization of $\tilde{Z}(\beta)$ is not unique, and the factors obtained here could be multiplied by a polynomial $Q_n(\beta)$. This would multiply each expression in Equation (29) by the same polynomial. The result then would be

$$\tilde{I}_+(\beta) = \frac{BQ_n(\beta)}{Z_+(\beta)\, Q_n(\beta)} = \frac{B}{Z_+(\beta)}$$

Thus, although the factorization of $\tilde{Z}(\beta)$ is not unique, the solution for $\tilde{I}_+(\beta)$, based upon the source condition

$$I_+(z) \longrightarrow I_+(0)$$

$$z \longrightarrow 0$$

is unique.

4.3 The Wiener-Hopf Factorization

A function $K(\beta)$ can be factorized by theorem C of Noble[12] in the form

$$K(\beta) = K_+(\beta)\, K_-(\beta)$$

provided that $K(\beta)$ is regular and non-zero in a strip containing the real β-axis and further that $K(\beta)$ tends to +1 as the magnitude of β becomes large on the axis. The required factors then are given by Cauchy's integral formula as

$$K_+(\beta) = \exp\left[\frac{1}{2\pi j}\int_{-\infty}^{\infty} \frac{\ln K(x)}{x-\beta}\, dx\right], \quad \Im m(\beta) > 0$$

$$K_-(\beta) = \exp\left[\frac{-1}{2\pi j}\int_{-\infty}^{\infty} \frac{\ln K(x)}{x-\beta}\, dx\right], \quad \Im m(\beta) < 0 \qquad (31)$$

These functions are bounded and non-zero in their regions of regularity, and they tend asymptotically to +1 along the real axis. This theorem will be used to factorize $\tilde{Z}(\beta)$ after it has been properly conditioned.

Some typical graphs of the function

$$\frac{4\pi^2}{\tau^2}\tilde{Z}(\beta) = \left[\left(\frac{\beta}{\tau}\right)^2 - \left(\frac{k}{\tau}\right)^2\right] \sum_{n \text{ odd}} B_n(\beta) - \frac{(k/\tau \cot \psi)^2}{2} \sum_{n \text{ even}} \left[B_n(\beta+\tau)+B_n(\beta-\tau)\right] \qquad (32)$$

for real values of β are plotted in Figures 8 and 9. In Figure 8 the frequency is below the critical frequency ($k<k_c$), and in Figure 9 the frequency is above the critical frequency ($k>k_c$). In the first instance there are three roots of $\tilde{Z}(\beta)$ on the positive β-axis, and, of course, three corresponding roots on the negative β-axis since $\tilde{Z}(\beta)$ is an even function of β. The analysis given here will be restricted to the second case, where the frequency is above the critical value k_c, and where there is only one real root, β_o on the positive β-axis.

The reason for this restriction is the experimentally observed fact that below the critical frequency a current traveling wave corresponding to the smallest root of $\tilde{Z}(\beta)$ dominates the current distribution. This result is shown in Figure 11 of Chapter 6. The dominance of the contribution of this root is explained by considering the residue of the inverse of $\tilde{Z}(\beta)$ at these roots. The residues are inversely proportional to the derivatives of $\tilde{Z}(\beta)$ at its roots. The derivative at the smallest root is always smaller since the function is logarithmic in the vicinity of the two larger roots, and therefore, its residue is the largest. Above the critical frequency this root has vanished and only the relatively weak root at β_o remains.

The branch points of $\tilde{Z}(\beta)$ at

$$\beta = n_T \pm k \qquad (n = \pm 1, \pm 3, \ldots)$$

all lie on the real axis. This makes it impossible to factorize the function $\tilde{Z}(\beta)$ into factors with a common strip of regularity including the real axis. This difficulty can be surmounted by assuming that the medium is slightly dissipative

$$k = k_o - j\alpha \simeq \omega\sqrt{\mu\epsilon} - j\frac{\sigma}{2}\sqrt{\frac{\mu}{\epsilon}}$$

The location in the complex β-plane of the branch points and zeros of $\tilde{Z}(\beta)$ for a dissipative medium is shown in Figure 10. The branch cuts

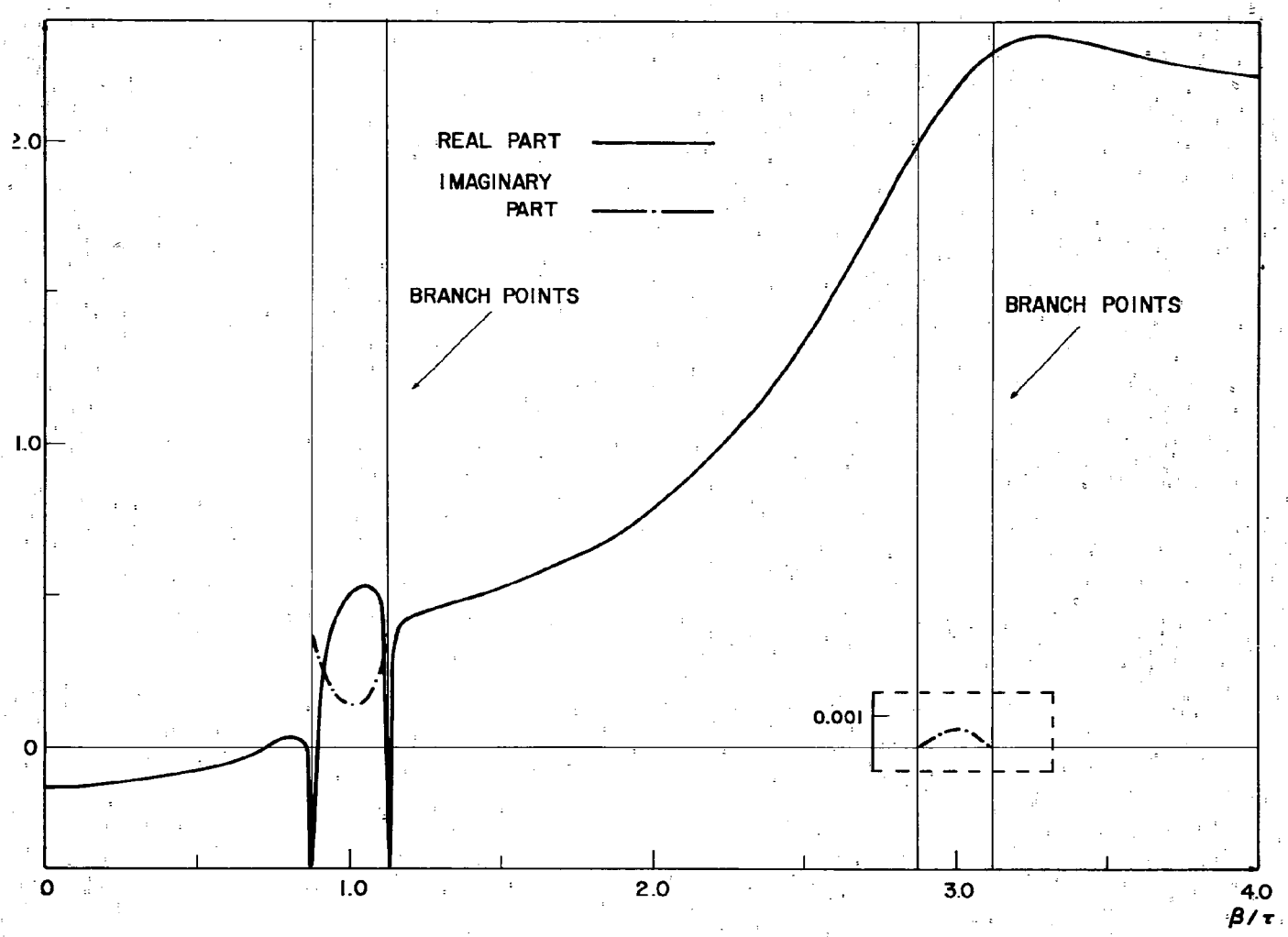

Figure 8. The Bifilar Helix Determinantal Function $k < k_c$

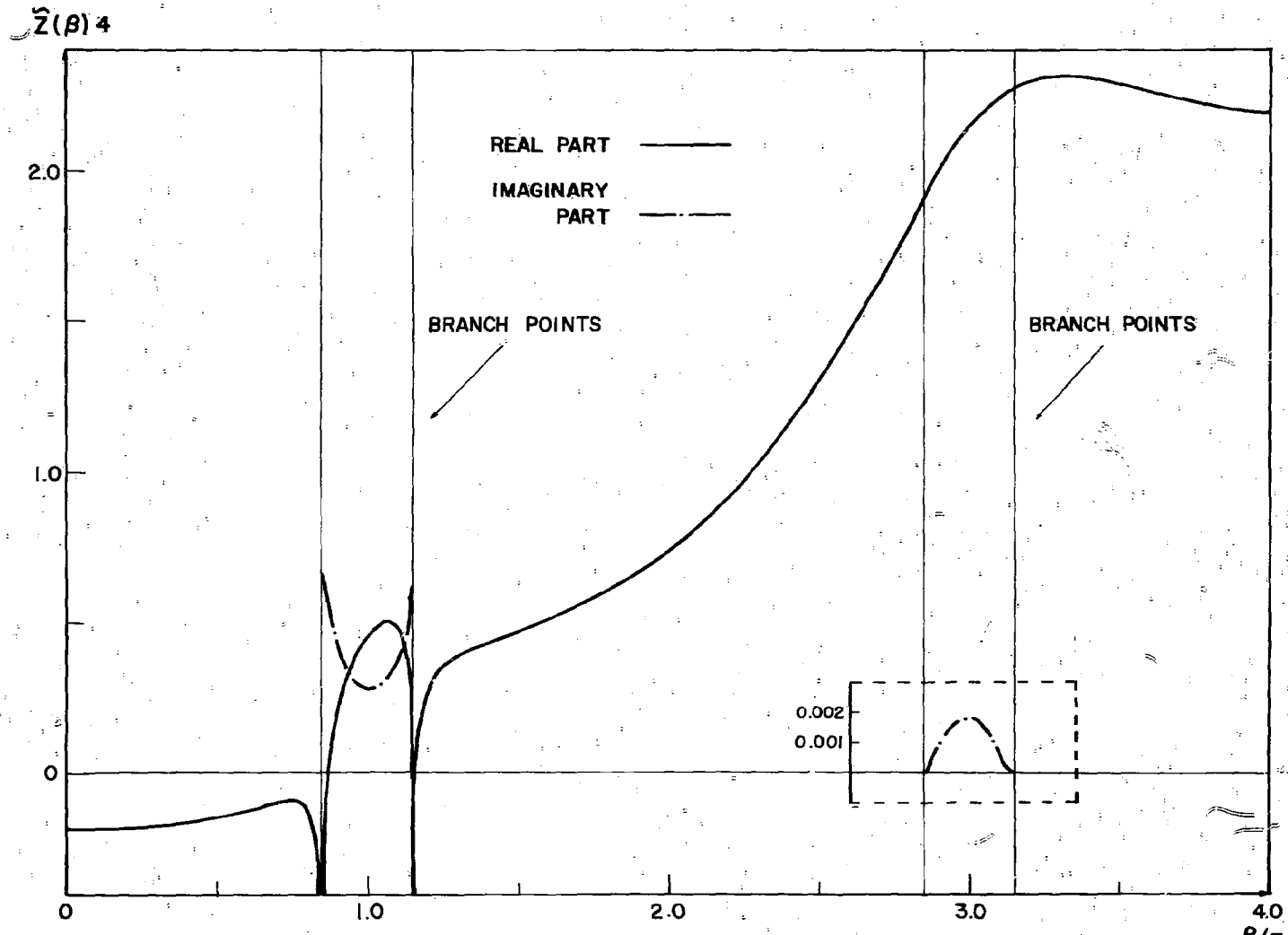

Figure 9. The Bifilar Helix Determinantal Function $k > k_c$

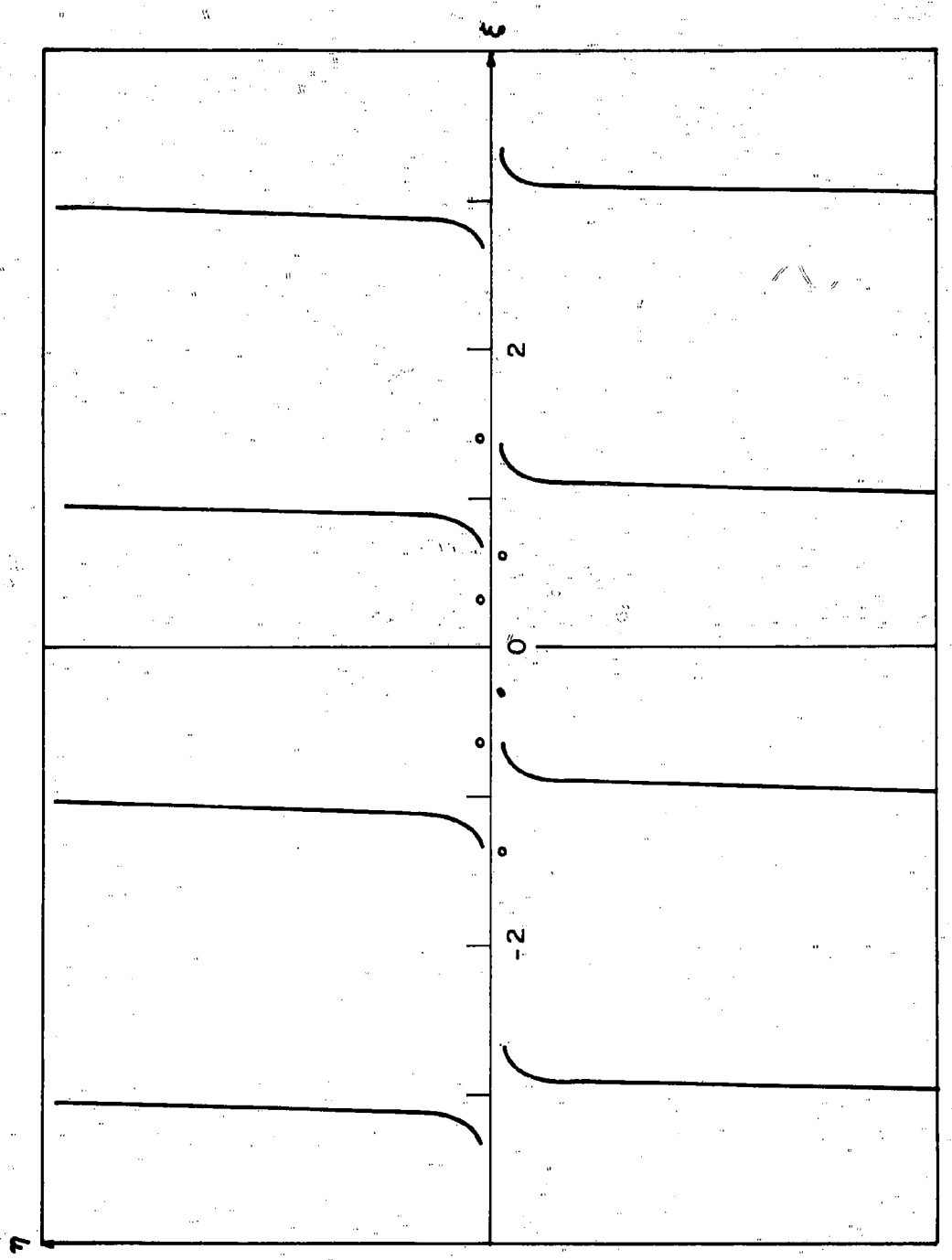

Figure 10. The Zeros and Branch Points of $\tilde{Z}(\beta)$ in the Complex β-plane

shown are chosen to satisfy the condition

$$\varphi_e([(\beta-n\tau)^2-k^2]^{1/2}) = 0$$

If $\beta = \xi + j\eta$ the equation of the branch line is

$$(\xi-n\tau)\eta = -k\alpha$$

This provides a strip of regularity of $\tilde{Z}(\beta)$ of width 2α including the real axis.

The function $\tilde{Z}(\beta)$ can be written as the product of two factors

$$\tilde{Z}(\beta) = R(\beta)\ K(\beta) \tag{33}$$

such that $K(\beta)$ is non-zero in the strip and tends to +1 as β becomes large.

The factor $K(\beta)$ is chosen so that it can be factored by Equation (31). It is particularly chosen so that its function values are real over as much of the real β-axis as possible. This allows a relatively simple estimate for the magnitude of $K_+(\beta)$ to be obtained as shown in Equation (41). The factor $R(\beta)$ remaining will be factored by a variety of devices. These factors are

$$R(\beta) = A\frac{\beta^2-\beta_o^2}{(\beta^2-\beta_o^2)^{1/4}}\ e^{-\frac{\eta}{\tau}\sqrt{\beta^2-k^2}} \tag{34}$$

and

$$K(\beta) = \frac{\tilde{Z}(\beta)\ e^{n/\tau\sqrt{\beta^2-k^2}}}{(\beta^2-\beta_o^2)\ A}\ (\beta^2+k^2)^{1/4} \tag{35}$$

β_o is the root of $\tilde{Z}(\beta)$ and the factor $(\beta^2-\beta_o^2)$ removes the zeros from $K(\beta)$ satisfying one of the requirements of Theorem C. The exponential factor is chosen to give the correct asymptotic form and to be easily factorizable[12]. The factor $(\beta^2+k^2)^{1/4}$ is chosen to give asymptotic behavior like $|\beta^{1/2}|$. This factor is chosen because it is real on the real β-axis. The term k in the factor is arbitrary as any other constant larger than α would make this factor regular inside the strip of width 2α. With this choice of factors $K(\beta)$ is real for real k everywhere on the real axis except in the segments $|\beta-n\tau| < k$.

These segments will be called the "visible regions" of the real β-axis since only this part of the Fourier spectrum contributes to the radiation pattern as is shown in Equation (4).

The function K(β) is well behaved except a logarithmic singularity at

$$|\beta| = \pm 1 \pm k$$

This singularity is integrable in Equation (21), and K(β) can be factorized by Noble's Theorem C.

4.4 Factorization of the Log-integrable Function

If K(β) is represented in polar form

$$K(\beta) = M(\beta) \exp [j\phi(\beta)]$$

we may write

$$K_+(\beta) = \exp \left[\frac{1}{2\pi j} \int_{-\infty}^{\infty} \frac{\ln M(x) + j\phi(x)}{x-\beta} \, dx \right] \tag{36}$$

The integral may be separated into its real and imaginary parts;

$$\int_{-\infty}^{\infty} \frac{\ln K(x)}{x-\beta} \, dx = -\pi\phi(\beta) + \int_{-\infty}^{\infty} \frac{\ln \frac{M(x)}{M(\beta)}}{x-\beta} \, dx + j\left(\pi \ln M(\beta) + \int_{-\infty}^{\infty} \frac{\phi(x) - \phi(\beta)}{x-\beta} \, dx\right) \tag{37}$$

The imaginary part of this integral gives the magnitude of $K_+(\beta)$,

$$|K_+(\beta)| = \sqrt{M(\beta)} \exp \left[\frac{1}{2\pi} \int_{-\infty}^{\infty} \frac{\phi(x) - \phi(\beta)}{x-\beta} \, dx \right] \tag{38}$$

and the real part gives the phase. The computation of phase involves the evaluation of an infinite integral while the magnitude is given by a sum of integrals over the visible range only

$$\int_{-\infty}^{\infty} \frac{\phi(x)}{x-\beta}\,dx = \sum_{n=-\infty}^{\infty} \int_{n\tau-k}^{n\tau+k} \frac{\phi(x)}{x-\beta}\,dx$$

where the integral over the range containing β is understood in the sense of the cauchy principal value.

To show that the contribution to the phase integral of all terms except for $n = \pm 1$, the following estimate of the phase is obtained. The relative size of the phase values for n=1 and n=2 can be obtained from Figures 8 and 9. The function $Z(\beta)$ may be written

$$4\pi^2 \tilde{Z}(\beta) = \sum_{n \text{ odd}} \mathcal{Z}_n(\beta)$$

where

$$\mathcal{Z}_n(\beta) = \begin{cases} (\beta^2-k^2) I_n(b'\gamma_n) K_n(b\gamma_n) \\ -\frac{k^2 \cot^2\psi}{2} \left[I_{n-1}(b'\gamma_n) K_{n-1}(b\gamma_n) + I_{n+1}(b'\gamma_n) K_{n+1}(b\gamma_n) \right] \end{cases} \tag{39}$$

If β is in the n-th visible range the n-th term of this series will be complex

$$\mathcal{Z}_n(\beta) = -\frac{\pi}{2}(\beta^2-k^2) J_n(b'\gamma_n) \left[N_n(b\gamma_n) + jJ_n(b\gamma_n) \right]$$

$$+\frac{\pi k^2 \cot^2\psi}{4} \begin{cases} J_{n-1}(b'\gamma_n) \left[N_{n-1}(b\gamma_n) + jJ_{n-1}(b\gamma_n) \right] \\ J_{n+1}(b'\gamma_n) \left[N_{n+1}(b\gamma_n) + jJ_{n+1}(b\gamma_n) \right] \end{cases} \tag{40}$$

where

$$\gamma_n = \left[k^2 - (\beta - n\tau)^2 \right]^{1/2}$$

For large values of n the first term dominates, and the phase of $\mathcal{Z}_n$ is given by

$$\phi_n(\beta) \simeq \tan^{-1} \left[-\frac{J_n(b\gamma_n)}{N_n(b\gamma_n)} \right] \qquad (|\beta - n\tau| < k)$$

which is well approximated with the small argument form of the Bessel functions

when

$$k \cot \psi << n\tau$$

The result is

$$\phi_n(\beta) \sim \frac{\pi}{n!\,(n-1)!} \left[\frac{\left[\left(\frac{\beta}{\tau} - n\right)^2 - \left(\frac{k}{\tau}\right)^2\right] \cot^2 \psi}{4} \right]^n$$

which tends toward zero very rapidly when n increases. The remaining terms of the series, being positive real, increase the real part of the function in the visible range, thus making the phase of the function even smaller than the phase of the complex term.

The phase of $K(\beta)$ is the same as that of $\tilde{Z}(\beta)$ except for $|\beta| < \beta_o$. Here division by $\beta^2-\beta_o^2$ makes $K(\beta)$ positive where $\tilde{Z}(\beta)$ is negative. Only in the range $(\beta) < k$ is there a non-zero phase contributed to $K(\beta)$ by the exponential factor. Therefore, the phase integral will be approximated by

$$\int_{-\infty}^{\infty} \frac{\phi(x)}{x-\beta}\,dx \approx \Sigma \int_{n_\tau-k}^{n_\tau+k} \frac{\phi(x)}{x-\beta}\,dx \qquad n = -1,\ 0,\ 1$$

If β is in the range $(\tau-k,\ \tau+k)$ the integral in that range is written

$$\int_{\tau-k}^{\tau+k} \frac{\phi(x) - \phi(\beta)}{x-\beta}\,dx + \phi(\beta) \int_{\tau-k}^{\tau+k} \frac{1}{x-\beta}\,dx$$

or

$$\int_{\tau-k}^{\tau+k} \frac{\phi(x) - \phi(\beta)}{x-\beta}\,dx + \phi(\beta) \ln\left(\frac{\tau+k-\beta}{\beta-\tau+k}\right) + j\pi\phi(\beta)$$

Thus the magnitude of $K_+(\beta)$ is given approximately by

$$|K_+(\beta)| \approx \sqrt{M(\beta)}\left(\frac{k+\tau-\beta}{k-\tau+\beta}\right) \frac{\phi(\beta)}{2\pi} \exp \frac{1}{2\pi} \left[\int_{\tau-k}^{\tau+k} \frac{\phi(x)-\phi(\beta)}{x-\beta}\,dx + \int_{k}^{+k} \frac{\phi(x)}{x-\beta}\,dx + \int_{-\tau+k}^{-\tau+k} \frac{\phi(x)}{x-\beta}\,dx \right] \tag{41}$$

The magnitude of $K_+(\beta)$ is given by two integrals over a finite range while the computation of phase involves the evaluation of an infinite integral. The integrals of these functions are not known in closed form, and they must be evaluated by numerical tenchiques. It was decided to evaluate only the magnitude of $Z_+(\beta)$ for this reason, and also because this is sufficient to determine the magnitude of the radiation pattern.

4.5 Factorization of the Remainder Function

Since $K_+(\beta)$ tends toward +1 for large β, the remainder function

$$R(\beta) = A \frac{\beta^2-\beta^2}{[\beta^2+k^2]^{1/4}} \exp\left(-\frac{n}{\tau}\sqrt{\beta^2-k^2}\right)$$

must be factorized to give the desired asymptotic behavior

$$R_+(\beta) \sim A\beta$$

In addition, R_+, R_- and their inverses must be regular in the indicated half planes.

The zeros $(\pm\beta_o)$ of R can be assigned to the appropriate half plane by considering the medium to be slightly dissipative

$$k = k_o - j\alpha$$

The root β_o is a function of k and can be expanded in a Taylor series about k_o. The change in β_o due to the assumption of a small loss, correct to the first order in α, is given by

$$\beta_o + j\eta = \beta_o - j\alpha \frac{\partial \beta_o}{\partial k}$$

Since β_o increases with k, as seen in Figure 6, the root at $+\beta_o$ is shifted to the lower half plane by a small loss, and thus, belongs to R_+. Similarly, the root at $-\beta_o$ is a root of R_-.

The exponential factor of R may be factorized by a method due to

W S Ament given in Noble[12].

By this method, the radical in the experiment is written in the form

$$-\sqrt{\beta^2-k^2} = (k^2-\beta^2)(\beta^2-k^2)^{-1/2}$$

where the first factor is entire, the transformation $\beta = k \cos\theta$ is used to remove the branch points of the second factor

$$g = (\beta^2-k^2)^{1/2} = \frac{1}{jk \sin\theta}$$

As shown in Figure 10, the branch point at $\beta=k$ is in the lower half plane and, therefore, must be assigned to g_+. This branch point corresponds to the pole at $\theta = 0$ in the θ plane. Therefore,

$$g = g_+ + g_- = \frac{\pi-\theta}{j\pi \sin\theta} + \frac{\theta}{j\pi \sin\theta}$$

is the required separation of g. When these functions are transformed back to the β-plane,

$$g_-(\beta) = \frac{\pi + j \ln \frac{\beta+\sqrt{\beta^2-k^2}}{k}}{\pi\sqrt{\beta^2-k^2}}$$

has a branch point only at $\beta=k$ and

$$g_-(\beta) = \frac{-j \ln \frac{\beta+\sqrt{\beta^2-k^2}}{k}}{\pi\sqrt{\beta^2-k^2}}$$

has a branch point in the finite β-plane only at $\beta=-k$. The factor of the exponential function, that is regular in the upper half plane, then is

$$\exp\left[\frac{-\eta\sqrt{\beta^2-k^2}}{\tau\pi}\ \pi + j \ln \frac{\beta+\sqrt{\beta^2-k^2}}{k}\right] \qquad (42)$$

This function has unit magnitude for all negative β less than $-k$.

The remaining factor of R, can be written $\beta-jk$

$$\frac{1}{(\beta^2+k^2)^{1/4}} = \frac{1}{(\beta-jk)^{1/2}}\left(\frac{\beta-jk}{\beta+jk}\right)^{1/4}$$

The pole in the first factor is in the upper half plane, so this factor is part of R_-. The contribution of the second factor to R_+ can be obtained by Noble's theorem C as in Section 4.4. If this factor is called G, G_+ is given by

$$G_+(\beta) = \exp\left(\frac{-1}{4\pi}\int_{-\infty}^{\infty}\frac{\cot^{-1}\frac{x}{k}}{x-\beta}\,dx\right) \tag{43}$$

and its magnitude is given by the principal value of this integral.

The magnitude of the remainder function then is the product of Equation (42) and Equation (43) with the zero at β. This may be written explicitly as

$$|R_+(\beta)| = |\beta-\beta_o|\left|\exp\left[-\eta\frac{\sqrt{\beta^2-k^2}}{\pi}\left(\pi+j\ln\frac{\beta+\sqrt{\beta^2-k^2}}{k}\right)\right]\exp\left[-\frac{1}{4\pi}\,P\int_{-\infty}^{\infty}\frac{\cot^{-1}\frac{x}{k}}{x-\beta}\,dx\right]\right| \tag{44}$$

The method used for the numerical evaluation of Equations (41) and (44) is discussed in the next chapter.

5. EVALUATION OF THE SOLUTION BY NUMERICAL ANALYSIS

5.1 The Quadrature Formula

A Gaussian quadrature formula[14] is used in this study to evaluate the integrals in Equations (41) and (44). It is used because it offers a potential accuracy comparable to other available quadrature formulas while using only half as many ordinates. This is an important consideration here because of the complexity of the integrand. In selecting a particular Gaussian quadrature formula for an integral of the form

$$I = \int_a^b w(x)\ f(x)\ dx$$

attention must be given to the weighting function $\beta(x)$.

For the weighting function $w(x) = 1$ and the interval $(-1, 1)$, the Legendre-Gauss quadrature is used. This quadrature formula has been well tabulated[15] and can be easily instrumented. The error function for this quadrature formula is

$$E = \frac{2^{2m+1}(m!)^4}{(2m+1)[(2m)!]^3}\ f^{(2m)}(g)$$

where ζ is in $(-1, 1)$. The integrand in Equation (41) behaves as

$$\phi_{(x)} \approx \frac{1}{\ln(1-x)}$$

as x approaches -1. The first derivative of this function and all higher derivatives are unbounded near the end points of the interval. Since ζ can be any point in the interval, no bound on the error of the quadrature formula can be obtained. This situation could be corrected by using the weighting function

$$w_{(x)} = \frac{1}{\ln x}$$

in a small region near the endpoints of the interval (1-k, 1+k).

The use of a logarithmic weighting function near the end points of the interval would require the construction of a new set of orthogonal polynomials on the interval of integration. This involves the moments of the weighting function which must be evaluated in terms of the exponential-integral functions. Since this difficulty is caused by the behavior of the integrand near the endpoints of integration, and since the contribution of the end regions to the integral is obviously small, it was decided to use a sixteen point Legendre-Gauss quadrature. Although no bound can be set for the error of this quadrature formula it is reasonable to expect that the error will be small.

5.2 The Statement of the Problem in the Form Used by the Automatic Digital Computer

In preparing a problem for Automatic digital computation, greatest attention must be given to the most frequent computations in the program. The Legendre-Gauss quadrature of the integral in Equation (41) can be considered as controlling the program from the point of view of running time. This is caused by the comparatively long time required to calculate the eighteen Bessel function values required for each ordinate point. Since the quadrature points do not depend on the particular values of β for which the integral is evaluated, it was decided to compute the ordinate values in a separate program called the "table generator". This program computes the function in Equation (17) subject to the approximation in Equation (19) at each of the sixteen quadrature points and at the thirty-six observation points given by

$$\beta = \tau + k \cos \theta$$

where θ takes on increments of 5° from 5° to 180°. If $F(\frac{\beta}{\tau}) = \frac{4\pi^2}{\tau^2} Z(\beta)$ is used to represent the approximate form of the bifilar helix determinantal equation, then

$$F\left(\frac{\beta}{\tau}\right) = 2 \sum_i \left[\left(\frac{\beta^2}{\tau^2} - \frac{k^2}{\tau^2}\right) \beta_2(\beta) - \frac{\frac{k^2}{\tau^2}\cot^2\psi}{2} \left(\beta_{i-1}(\beta)+\beta_{i+1}(\beta)\right)\right] \qquad (45)$$

$$-e^{-x}\frac{\beta}{\tau}\left[\left(\frac{\beta^2}{\tau^2} - \frac{k^2}{\tau^2}\right)\left[\ln\left(\frac{1-ye^{-x}}{1+ye^{-x}}\right) + 2\left(\frac{y^3e^{-3x}}{3} + ye^{-x}\right)\right] - \frac{k^2}{\tau^2}\cot^2\psi \cosh x \left[\ln(1-y^2e^{-2x}) + \frac{y^4e^{-4x}}{4} + y^2e^{-2x}\right]\right]\sqrt{\sin\psi \sin\psi'}$$

with $i = \pm 1, \pm 3$

is the expression used in the machine computations, where

$$x = \frac{1}{\sin\psi} - \frac{1}{\sin\psi'}$$

$$y = \frac{\cos\psi' (1+\sin\psi)}{\cos\psi (1+\sin\psi')}$$

The input data for the table generator is the normalized frequency ($\frac{k}{\tau} = \frac{P}{\lambda}$), the cotangent of the pitch angel ψ and the relative wire size δ. The constants x and y in Equation (45) are then computed as are those functions of these constants not depending on β. These are stored for use in the later calculations. The eight roots of the sixteenth Legendre polynomial in (0,1) are then used to compute the values of $F(\beta/\tau)$ in the range $(0, 1-k/\tau)$. The results of this calculation together with the sixteen quadrature points and thirty-six observation points in the range $(1-k/\tau, 1+k/\tau)$ are emitted on punch cards for use by the subsequent integrating program. This program also finds the zero, $\frac{\beta_o}{\tau}$, of $F(\beta/\tau)$ that must be used in the subsequent calculation.

The zero seeking routine used in this program starts with an initial value of the argument increment size, and direction of search. The increment size is doubled at each step until the function values change sign. When this occurs a second approximation to the root is obtained. The value of the function at this approximate root is calculated, and if it is larger than 10^{-6}, the search is again

initiated toward the true root location with an increment one tenth as large as the last increment used. This process continues until either the function value at the approximate root is sufficiently small (less than 10^{-6}), or until the increment becomes too small to modify the argument of the function (less than one in the eighth significant figure).

The second and final program in the set computes $I_+(\tau+k\cos\theta)$ and $I_+(-\tau+k\cos\theta)$ using the tabulated data provided by the table generator. For each value of θ in 5^o increments, it computes the following factors.

$$P_o(\theta) = \frac{\beta}{\tau} - \frac{\beta_o}{\tau}$$

$$P_o(\theta) = \begin{cases} 1 & \beta < k \\ e^{\frac{-\eta\sqrt{\beta^2-k}}{\tau}} & \beta > k \end{cases}$$

$$P_2(\theta) = e^{-\frac{1}{4\pi}\int_{-\infty}^{\infty} \frac{\cot^{-1}(\frac{x}{k})}{x-\beta}\,dx}$$

$$P_3(\theta) = \left(\left| \frac{F(\beta/\tau)}{(\beta/\tau)^2-(\frac{\beta_o}{\tau})^2} \left[(\beta/\tau)^2+(k/\tau)^2\right]^{1/4} e^{\eta\sqrt{(\frac{\beta}{\tau})^2-(\frac{k}{\tau})^2}} \right| \right)^{1/2}$$

$$P_4(\theta) = e^{\frac{\beta/\tau}{\pi}\int_{1-\frac{k}{\tau}}^{1+\frac{k}{\tau}} \frac{\phi(x)-\phi(\frac{\beta}{\tau})}{x^2-(\beta/\tau)^2}\,dx}$$

where $$\frac{\beta}{\tau} = 1+\frac{k}{\tau}\cos\theta$$

The constant β_o in the first factor is the one positive real root of $Z_+(\beta)$, and is supplied by the table generator. The variable β is generated in the integrating program at 5^o increments in the polar angle θ corresponding to direction of observation of the antenna. The first factor can be interpreted as the contribution of the higher waveguide mode, whose propagation constant is β_o, to the radiation pattern. The next two factors, $P_1(\theta)$ and $P_2(\theta)$, are

included to insure the proper asymptotic behavior of $Z_+(\beta)$ and consequently of $\tilde{I}_+(\beta)$. The values are generated in the integrating program independently of the function values of $F(\frac{\beta}{\tau})$ supplied by the table generator. These factors have relatively little effect on the value of $\tilde{I}_+(\beta)$ in the visible range.

The last two factors, $P_3(\theta)$ and $P_4(\theta)$, exercise primary control over the shape of the radiation pattern. The factor $P_3(\theta)$ depends primarily upon the magnitude of $F(\frac{\beta}{\tau})$ at the observation points. $P_4(\theta)$ depends upon the phase at the observation points as well as the phase at the quadrature points. The integrating routine obtains the real and imaginary parts of $F(\frac{\beta}{\tau})$ from the table supplied by the table generator and converts them to polar form. The magnitude is then used to compute P_3 while the phase is integrated to obtain the value of P_4.

The product of these factors is taken for the magnitude of $Z_+(\beta)$. The inverse of the product is then interpreted as the magnitude of the Fourier spectrum of the current distribution The vector potential for the backfire bifilar helix results when the current spectrum is multiplied by the function

$$J_o(\frac{k}{\tau} \cot \psi \sin \theta)$$

as indicated in Equation (5). The radiation pattern can be deduced from this as indicated in Chapter 2. Radiation patterns were computed for a range of pitch angles, relative frequency k/τ, and relative wire sizes δ. The results of these computations are discussed in the next section where they are compared with experimental results.

6. EXPERIMENTAL AND THEORETICAL RESULTS

6.1 The Experimental Study

The study of the bifilar backfire helical antenna was started as part of a larger investigation of the properties of periodic radiating structures. This investigation in turn was started in an effort to learn more about the behavior of log-periodic antennas[16-18]. In this connection it is suggested[19] that the properties of a log-periodic structure, as a function of distance from the apex, are related to those of a periodic structure whose period is given by the local period of the log-periodic structure. In this sense the bifilar helix is an analog of the two arm equiangular spiral antenna[18].

The portion of a log-periodic antenna, nearest the feed point at or near the apex of the structure, acts as a transmission line carrying the energy to the larger portion. The energy is carried to the so-called "active region" of the structure whose position and size varies linearly with frequency. This region is thought to be primarily responsible for the radiation from the antenna. Beyond this region, the current decays rapidly. These characteristics of the log-periodic antenna are observed for the bifilar helix when the variation of distance from the apex is replaced with a variation of frequency.

The operation of the helix as a waveguide is discussed in Chapter 3. There it is seen that the propagation constant is given approximately by

$$\beta = k/\sin \psi$$

until the edge of the visible range is approached. That is until

$$\frac{k}{\sin \psi} = \tau k$$

This equation defines the cutoff frequency or critical frequency of the principal waveguide mode of an infinitely thin helical conductor. This critical

frequency, normalized with respect to τ, is called χ to avoid confusion with the critical frequency for a finite size helical conductor. It is given explicitly by

$$\chi = \frac{\sin \psi}{1+\sin \psi} \tag{46}$$

The critical frequency marks the boundary between the frequencies for which the helical structure is primarily a waveguide and the frequencies for which it is a useful antenna.

Several models of the bifilar helical antenna were constructed for a range of χ between 0.05 and 0.4. The physical dimensions of these models are given in Table I. These are based upon a frequency of 1.5 Gc. The pitch of the helix is determined from the wavelength at the base frequency by

$$p = \chi \lambda \tag{47}$$

The pitch angle is given by

$$\psi = \sin^{-1}\left(\frac{\chi}{1-\chi}\right) \tag{48}$$

and the mean radius of the helix is given by

$$b = \frac{\lambda}{2\pi} \sqrt{1-2\chi} \tag{49}$$

The waveguide operation of these models was studied by sampling the fields near the antenna with a current loop moving parallel with the axis of the helix. A typical amplitude response of this loop as a function of distance from the feed point is shown in Figure 11. The antenna was fed by a balanced two wire line. Below the critical frequency, the propagation constant of the waveguide mode can be easily determined by the standing wave on the structure. The propagation constants measured in this way are shown in Figure 12. It is noted that the cutoff frequency for each of these models is somewhat below χ due to the finite wire thickness. The cutoff frequency for the models tested in this investi-

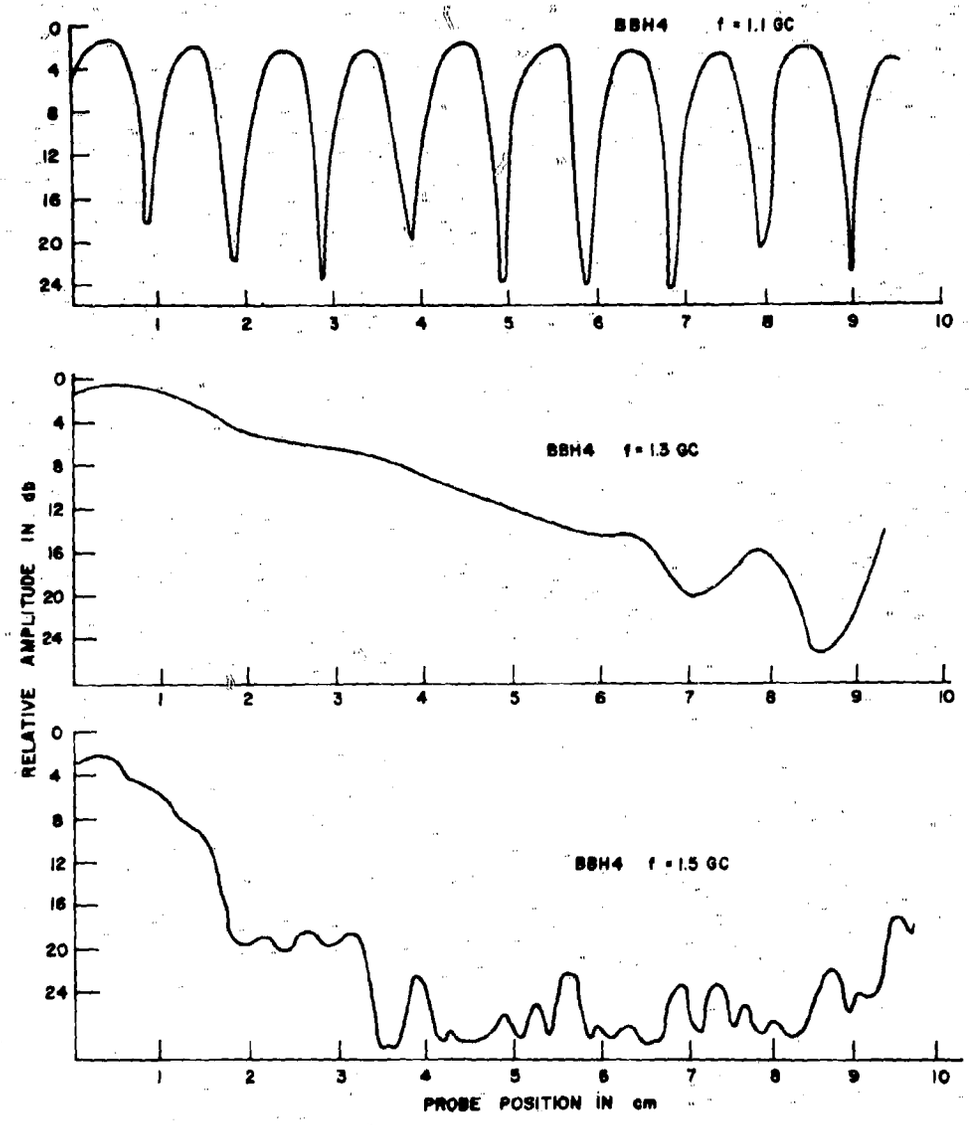

Figure 11. Current Amplitude Distribution on a Bifilar Helix

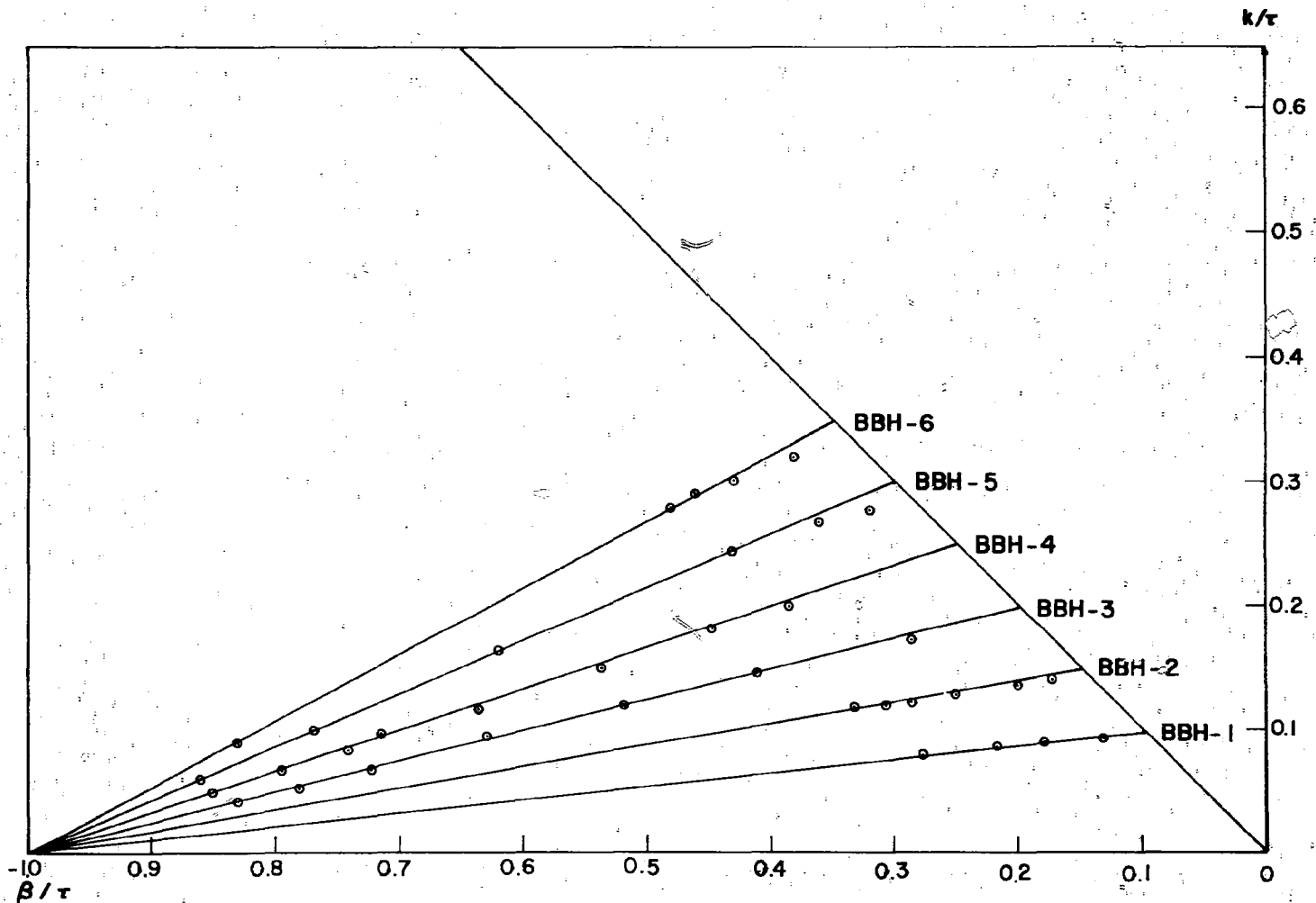

Figure 12. Measured Propagation Constants of the Principal Waveguide Mode on the Bifilar Helix

Table I

The Physical Parameters of the Experimental Models of the Bifilar Helical Antenna

Code Name	χ	Pitch p(cm)	Radius b(cm)	Relative* Wire Size δ	Pitch Angle ψ (degrees)
BBH-1	0.1	2	2.663	.0227	6.38
BBH-2	0.15	3	2.847	.0242	10.18
BBH-3	0.2	4	2.465	.0262	14.49
BBH-4	0.25	5	2.251	.0287	19.47
BBH-5	0.30	6	2.013	.0323	25.37
BBH-6	0.35	7	1.743	.0371	32.60
BBH-7+	0.40	16	2.85	.0226	41.82

*No. 16 AWG Tinned copperwire was used in the construction of the models.

+The base frequency for this model was changed from 1.5 Gc to .75 Gc for mechanical reasons.

gation is plotted as a function of the pitch angle ψ in Figure 13, where it is compared with χ, the normalized cutoff frequency for an infinitely thin wire model.

An unusual feature of the standing wave pattern of the waveguide mode on the bifilar helix was noted during the course of the measurements. The apparent guide wavelength increases with frequency from a minimum at zero frequency equal to the pitch of the helix to a maximum at the cutoff frequency, the maximum being somewhat less than the free space wave length. This indicates that the principal waveguide mode on the bifilar helix is a backward wave. The phase constant decreases with increasing frequency, and therefore, the phase velocity and the group velocity must have opposite signs. The group velocity must be directed away from the feed point (i.e. in the positive direction), therefore the phase velocity is in the negative direction as indicated in Figure 12.

The measured results in Figure 12 do not seem to agree with the calculated results shown in Figure 6. However, Figure 6 gives the phase progression of the current along the helical conductor, while Figure 12 gives the phase progression of the near fields of the bifilar helix. The results of Figure 6 agree with the results of Marsh[5] for phase measurements along the wire. When measurements along the helix parallel to the axis are made, an additional phase shift of 2π radians per turn is observed. This is the expected result since the test probe is now moving from one conductor to the other as it travels along the helix. At zero frequency therefore, the phase changes by π radians as each conductor is crossed. From another point of view, the additional 2π radians of phase shift results from the rotation of a tangent to the helical conductor as it moves along a turn of the helix.

It is seen in Figure 11, that above the cutoff frequency, the standing wave

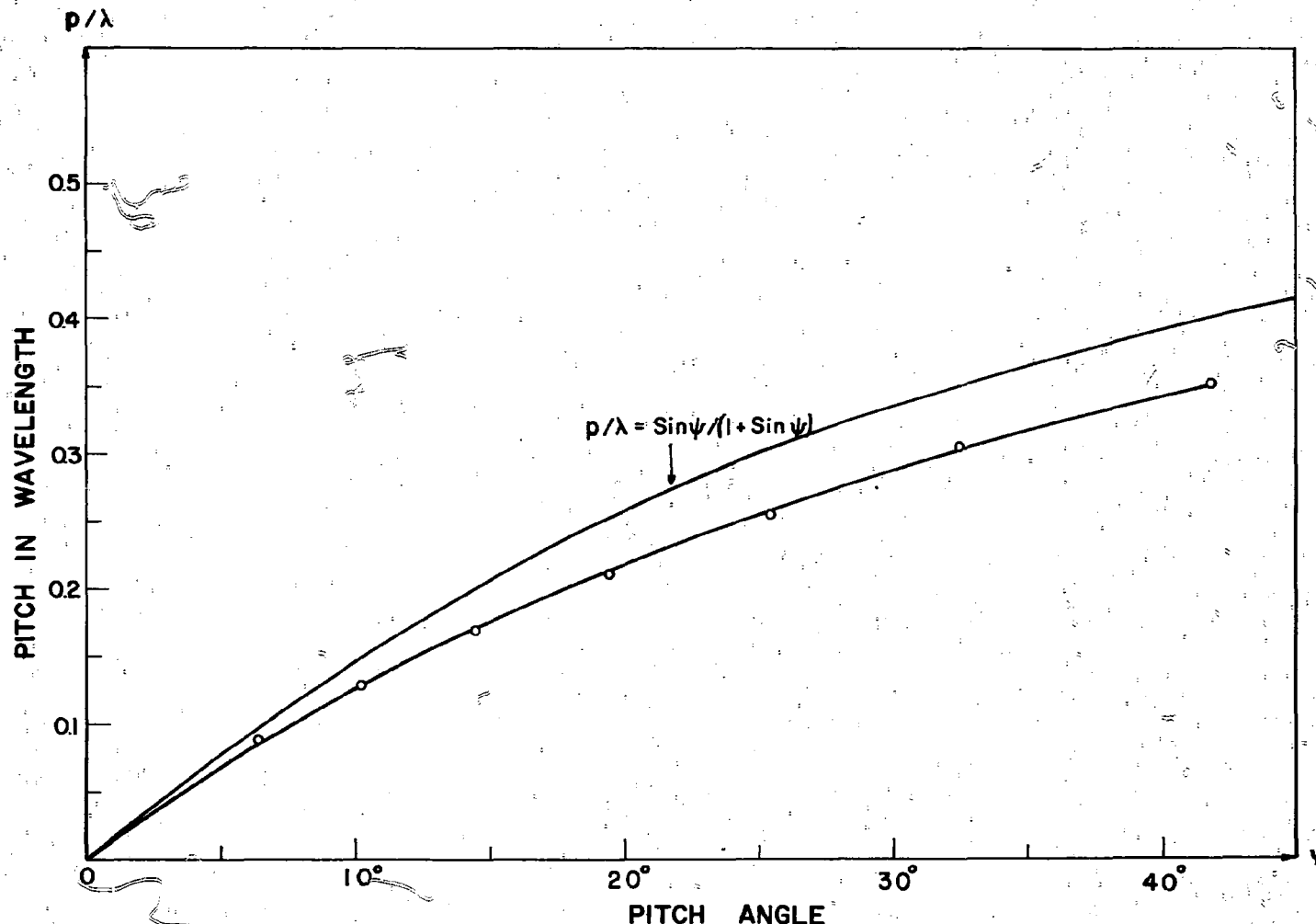

Figure 13. Measured Values of the Principal-Mode Cut-off Frequency for the Bifilar Helix

has vanished and is replaced by a decaying amplitude distribution. As frequency is increased further the rate of decay increases. This is shown in greater detail in Figure 14. At these higher frequencies, a standing wave distribution again appears with a maximum amplitude about twenty decibels below the input level. This is the higher order helical waveguide mode. The excitation of this mode increases with frequency from a negligible level near the cutoff frequency of the principal mode. The development of this mode places an upper limit on the frequencies for which the bifilar helix behaves as a backfire antenna.

Phase measurements made in the near field above the cutoff frequency are shown in Figure 15. In this figure the phase is normalized to the free space propagation constant and is plotted in centimeters. The first curve shows that the phase is leading as the probe moves away from the feedpoint. The first curve, slightly above the cutoff frequency, k_c, shows leading phase over most of the length of the structure. As frequency is increased, the direction of phase progression near the end of the structure changes and is away from the feedpoint. The point at which the phase progression changes from leading to lagging moves near to the feed point as frequency is increased. This corresponds to the point at which the feed region currents have decayed to the level of the higher order helical waveguide mode.

The near field phase measurements indicate that, although they do not correspond to a proper mode, the feed region currents have a backward wave character above the critical frequency, k_c. This leading phase characteristic persists as long as the feed region currents are dominant on the structure. On the remainder of the structure the higher order waveguide mode, with its lagging phase or forward wave characteristic, dominates the current distribution. The fact that in the feed region the direction of phase progression

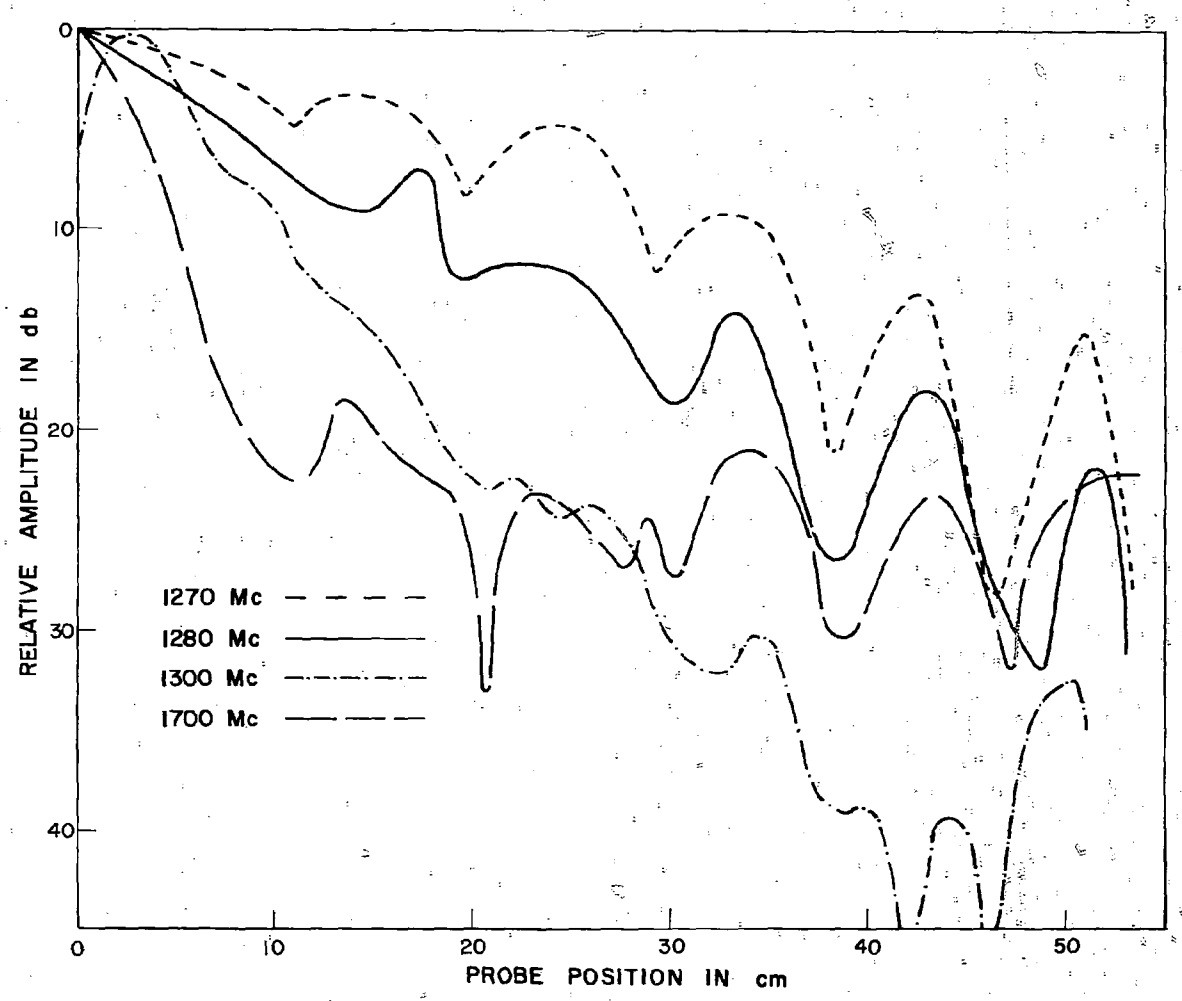

Figure 14. Current Amplitude Distribution above the Critical Frequency

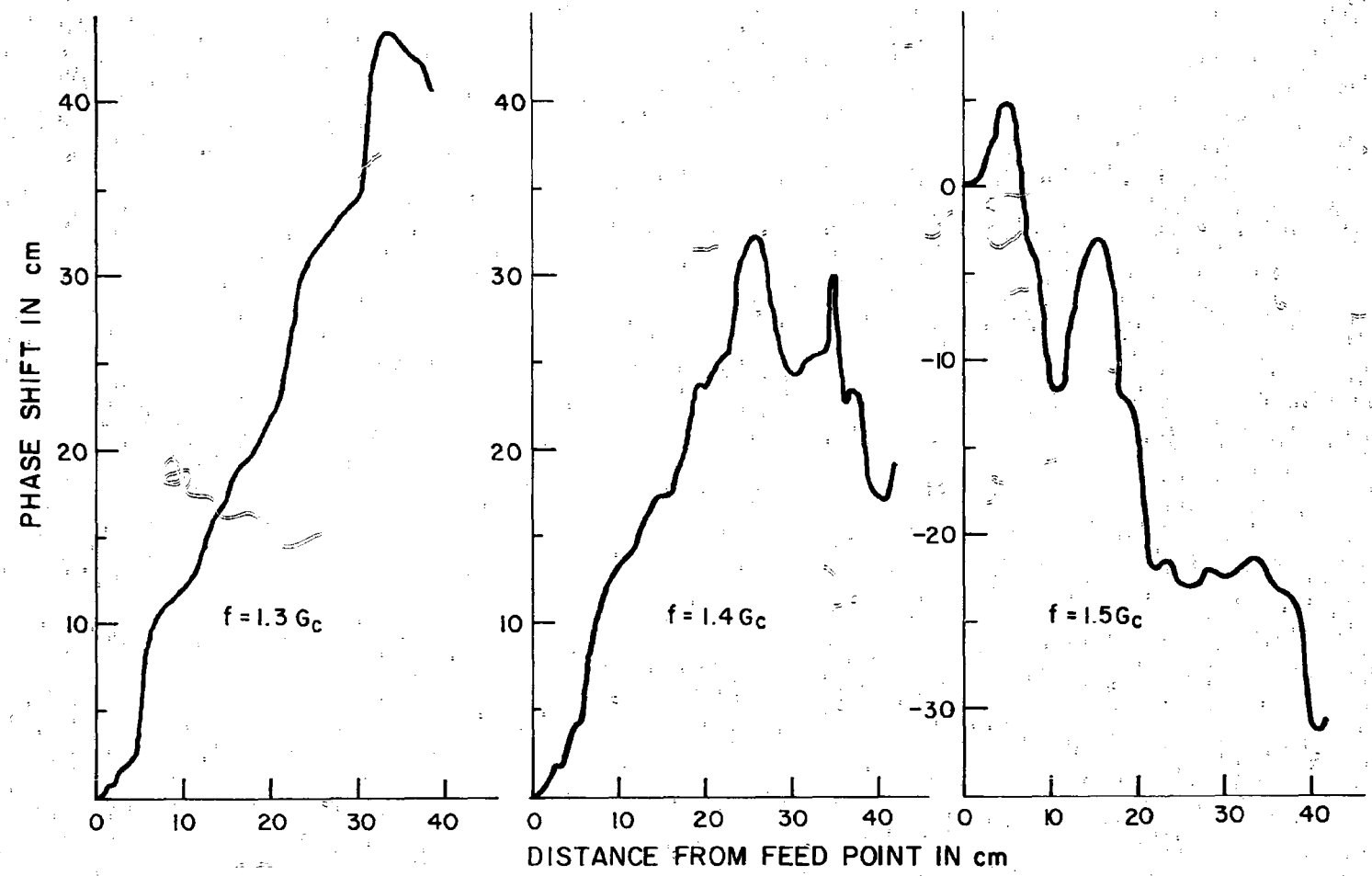

Figure 15. Near-Field Phase Measurements for the Bifilar Helix BBH-4

is toward the feedpoint, is consistent with the "backfire" radiation of the bifilar helical antenna, since an antenna tends to radiate in the direction of the phase progression of current.

The measured radiation patterns for the backfire bifilar helical antenna are presented in Figure 16. The patterns are plotted so that their centers give the helix radius and pitch in wavelengths at the frequency for which the pattern was measured. Two curves are also provided for reference to the Brillouin diagram for the bifilar helix. The curve

$$b/\lambda = \frac{\sqrt{1-2\ p/\lambda}}{2\pi}$$

gives the frequency at which the propagation constant asymptote

$$\beta = k/\sin\psi$$

intersects the edge of the visible range given by

$$\beta = \tau - k$$

This corresponds to the cutoff frequency of the principal mode on a helical waveguide with infinitely thin conductors. The curve

$$\frac{b}{\lambda} = \frac{\sqrt{1+2\ p/\lambda}}{2\pi}$$

gives the frequency at which the propagation constant asymptote intersects the edge of the visible range given by

$$\beta = \tau + k$$

This curve is given by Kraus[20] as the upper frequency limit for beam mode operation of the helical antenna. The range of parameters for this antenna given by Kraus is indicated by the broken line

The critical frequency can be determined by studying the radiation patterns shown in Figure 16. As the critical frequency is approached from above, the patterns show increasing directivity characterized, in general, by

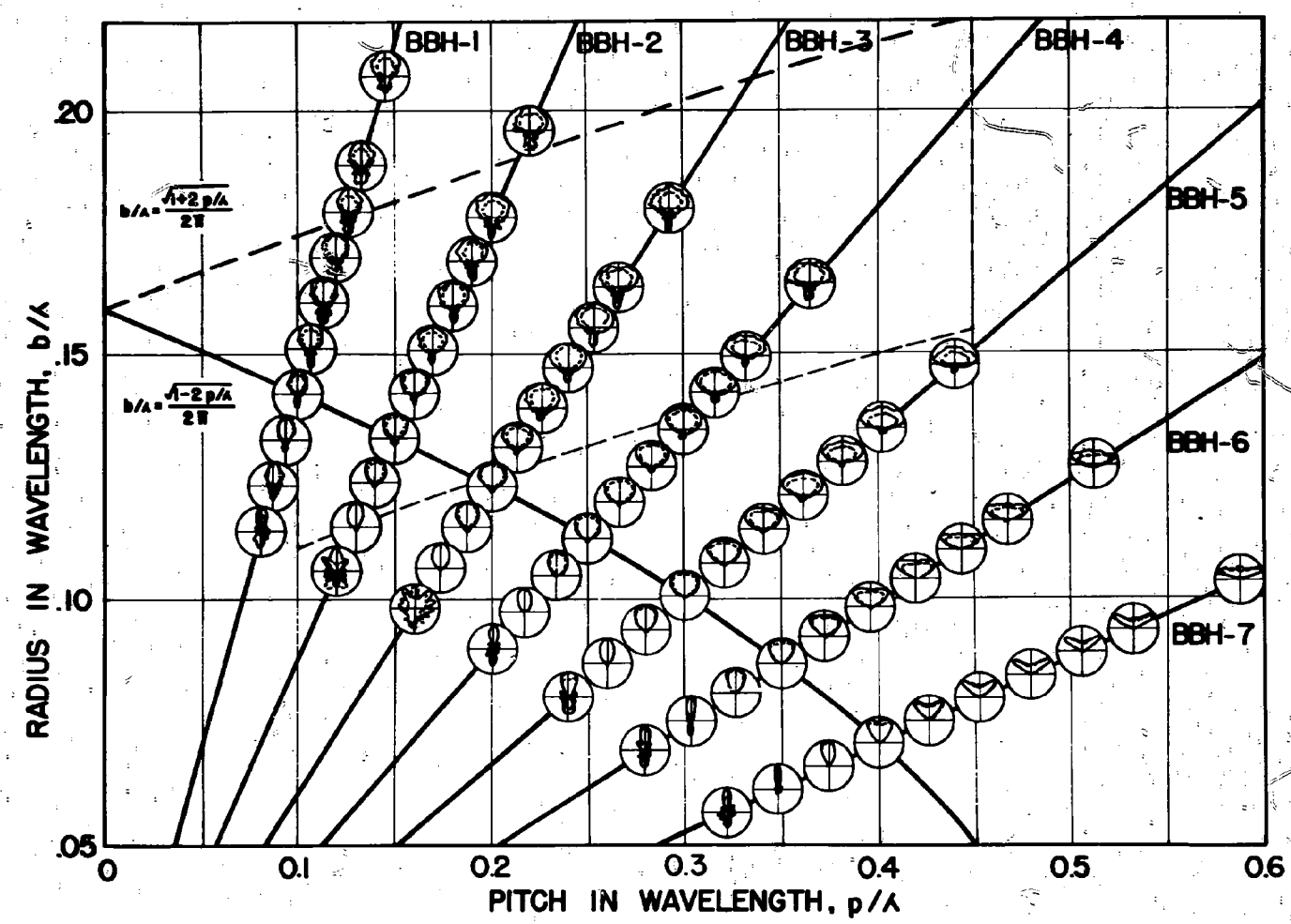

Figure 16. Measured Radiation Patterns of the Backfire Bifilar Helical Antenna

a single lobe with little or no "endfire" radiation or back lobe. Below the critical frequency, the patterns have many lobes and the pattern shape changes rapidly with frequency. This indicates the standing wave current distribution on the antenna. As the frequency is increased the patterns tend to broaden and, for larger pitch angles, tend to form a split beam. This is due to two effects: first, the phase progression in the feed region tends to become faster than light, and second, the rate of current decay in the feed region increases, decreasing the effective aperture. The splitting of the main beam is not observed for smaller pitch angles because the effective aperture is too small to form distinct beams. For the larger pitch angles, the rate of current decay is smaller, and the larger effective aperture can produce a well-defined beam. This result is consistent with Equation (20) where it was shown that the coupling of the antenna current to the radiated field is controlled by $\delta/\sin\psi$. Since the relative wire size δ does not change appreciably over the range of models tested, the decreasing pitch angle serves to increase the coupling and hence the rate of current decay.

6.2 Comparison of Computed Patterns with Measured Patterns

The effect of wire size is not shown in the experimental results of this study, but it is illustrated in the computed patterns shown in Figures 17-23. The patterns for the largest wire size ($\delta = 0.2$) show the least variation with frequency. The patterns for the smallest wire size ($\delta = 0.002$) have the greatest directivity near the critical frequency, but tend to broaden faster with frequency. It can also be seen from the computed results that a change in wire size is more effective in changing the shape of the radiation pattern for larger pitch angles. This again indicates the dependence of the performance of the backfire bifilar helical antenna on $\delta/\sin\psi$.

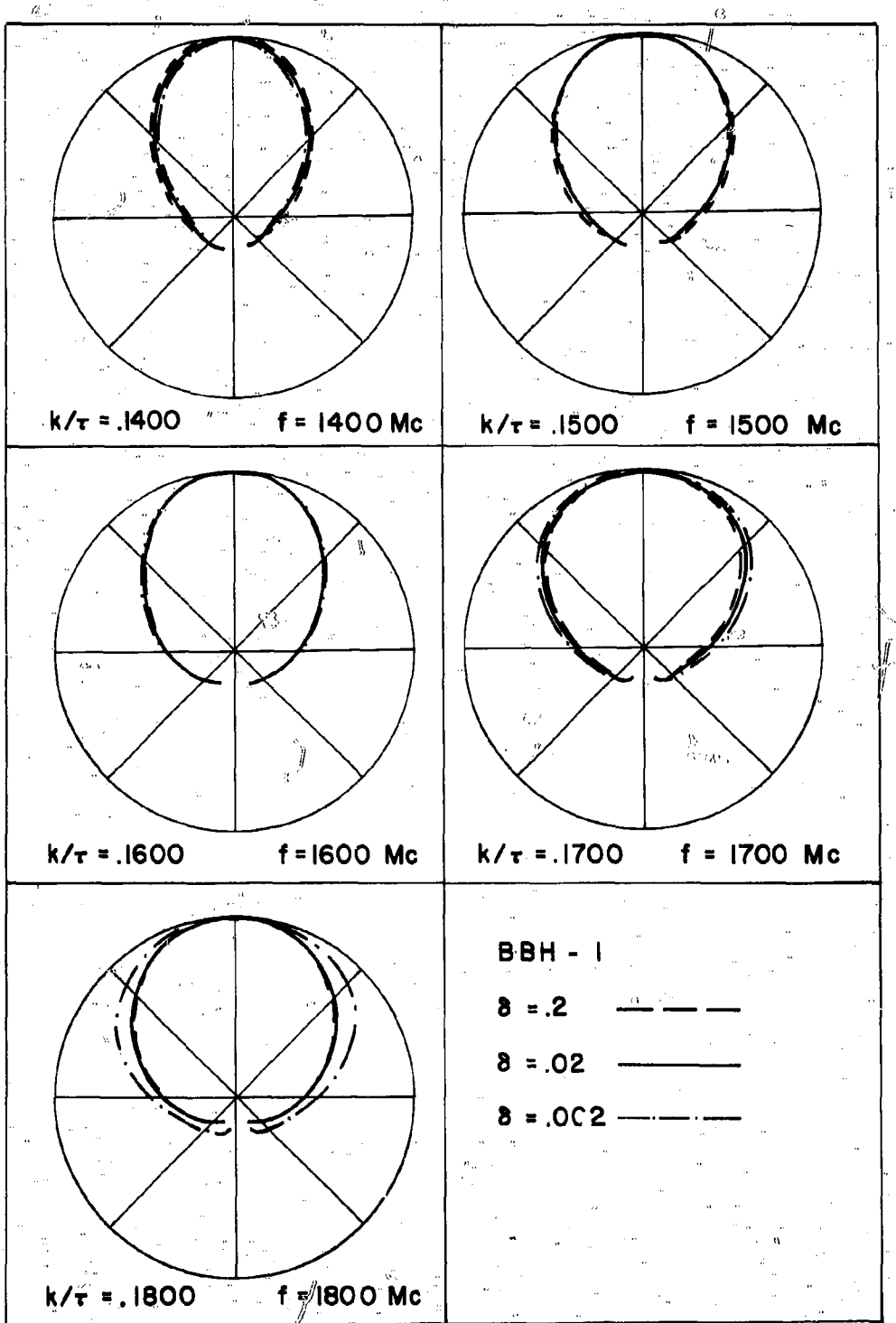

Figure 17. Computed Radiation Patterns for BBH-1

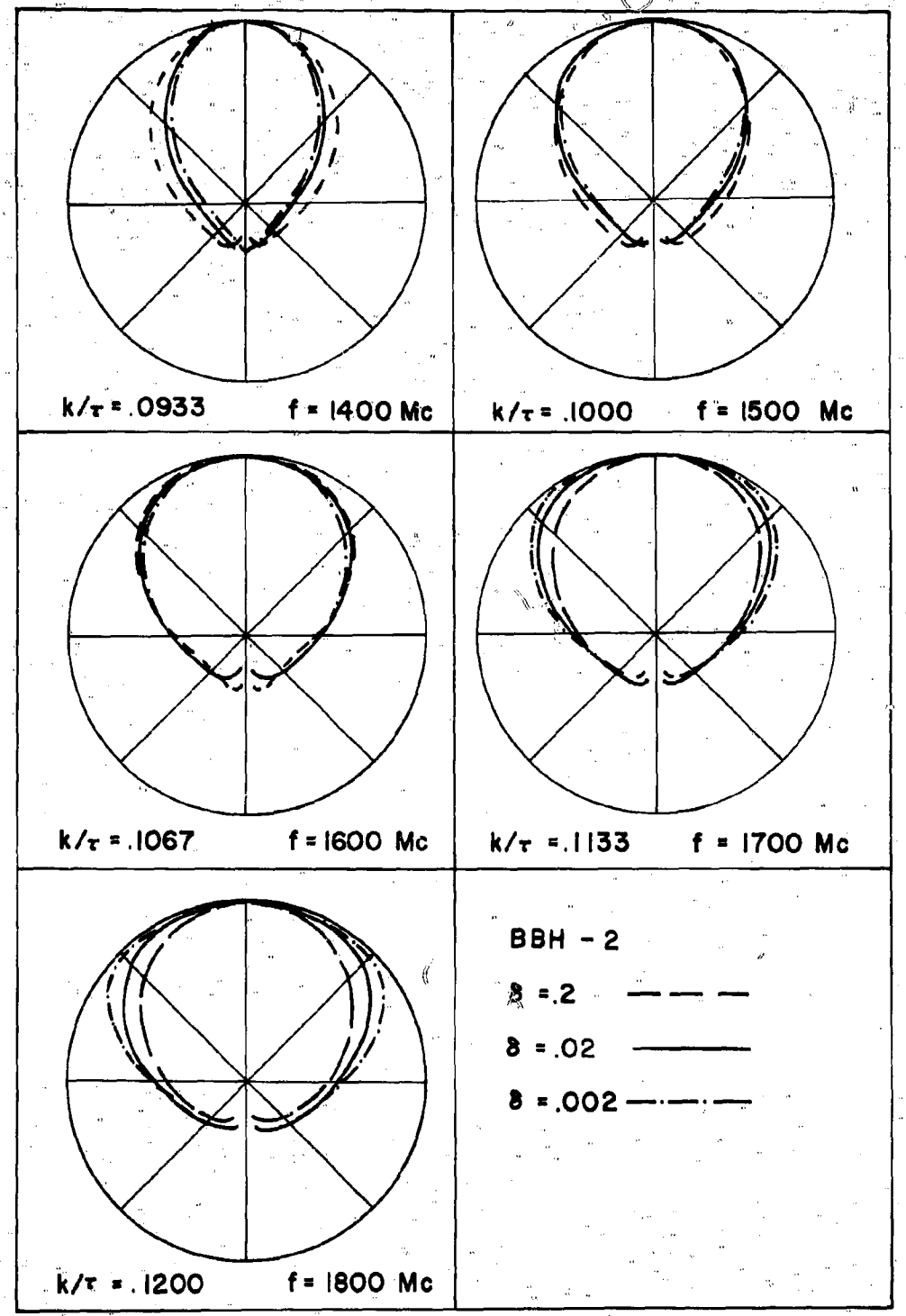

Figure 18. Computed Radiation Patterns for BBH-2

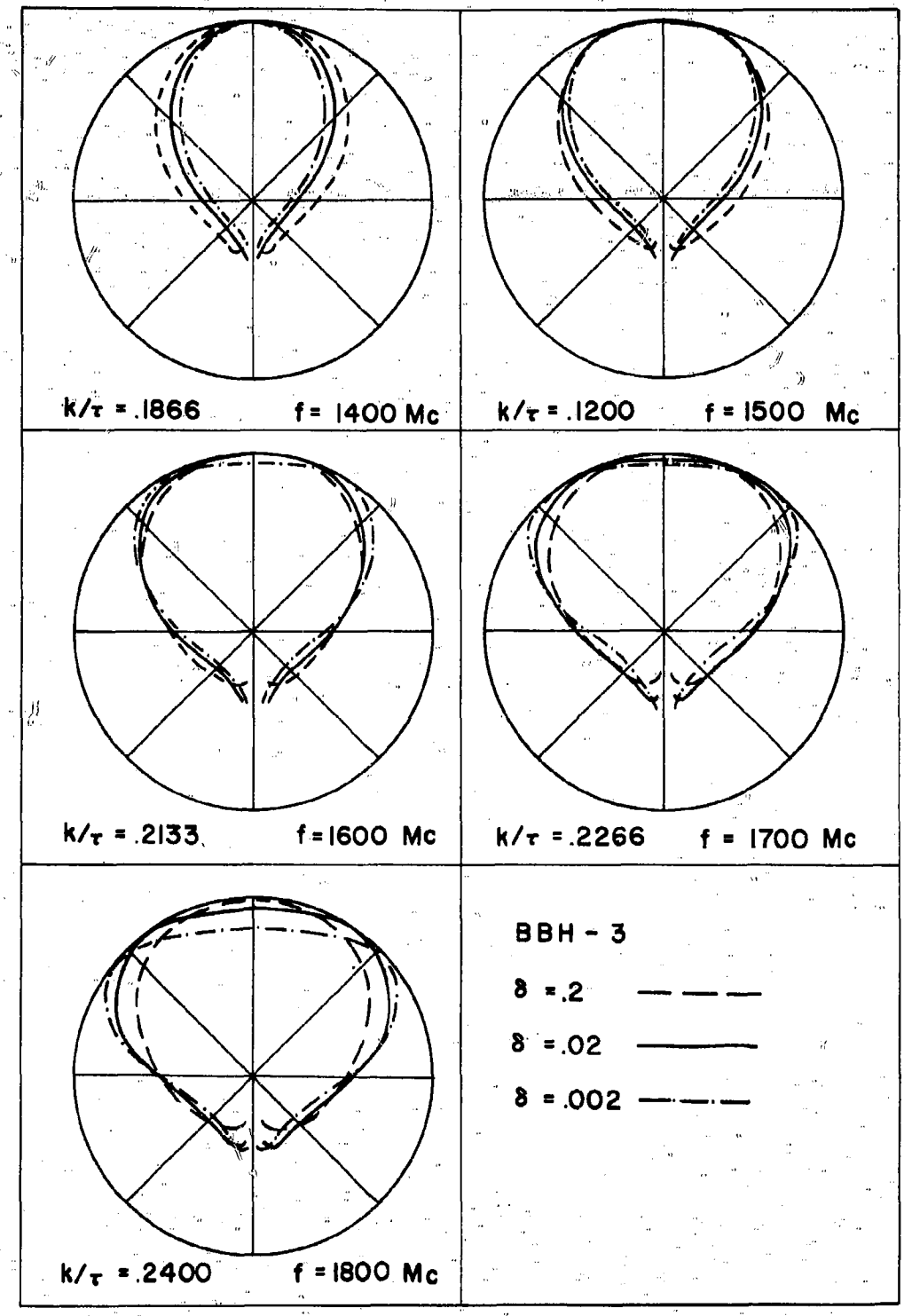

Figure 19. Computed Radiation Patterns for BBH-3

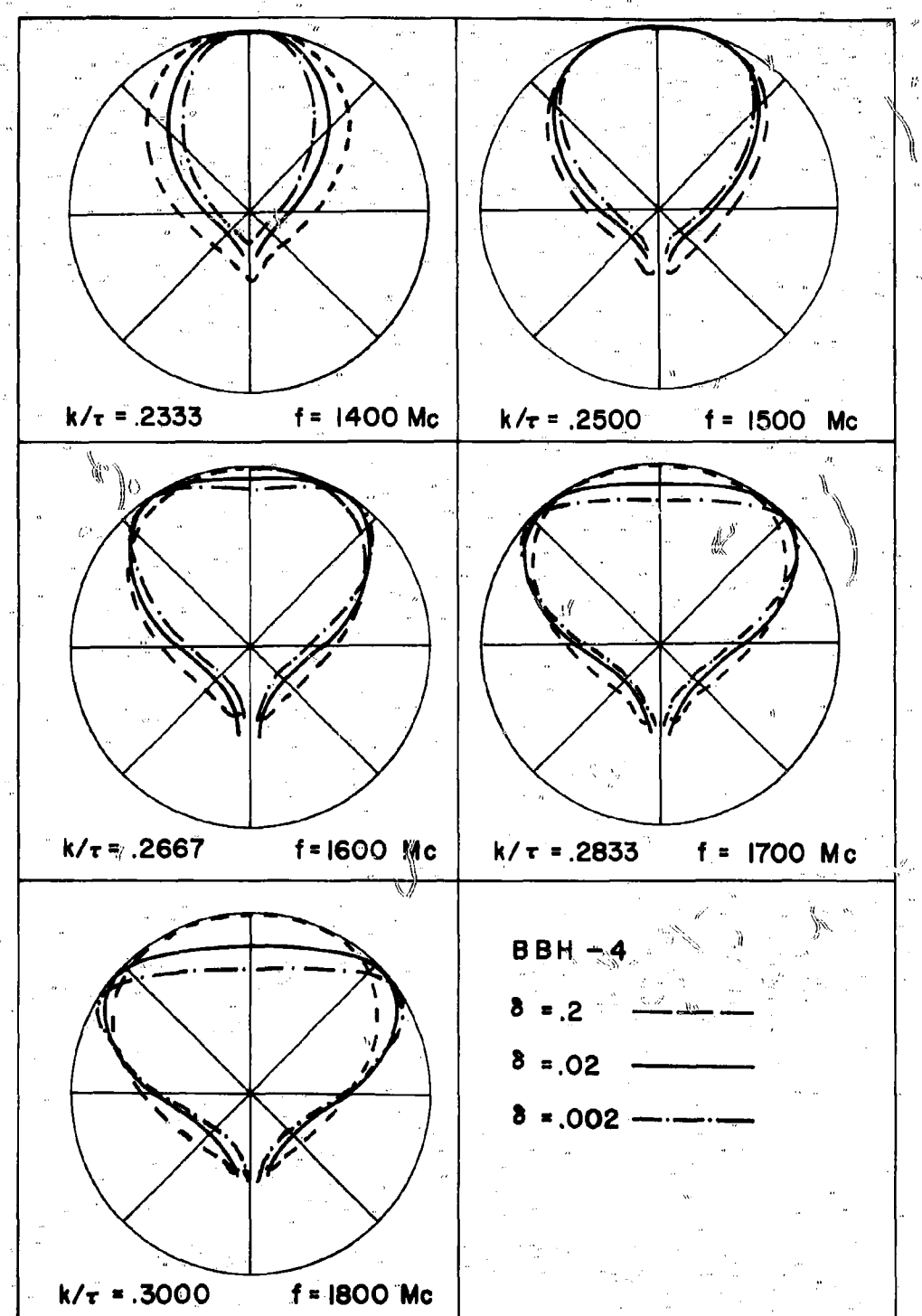

Figure 20. Computed Radiation Patterns for BBH-4

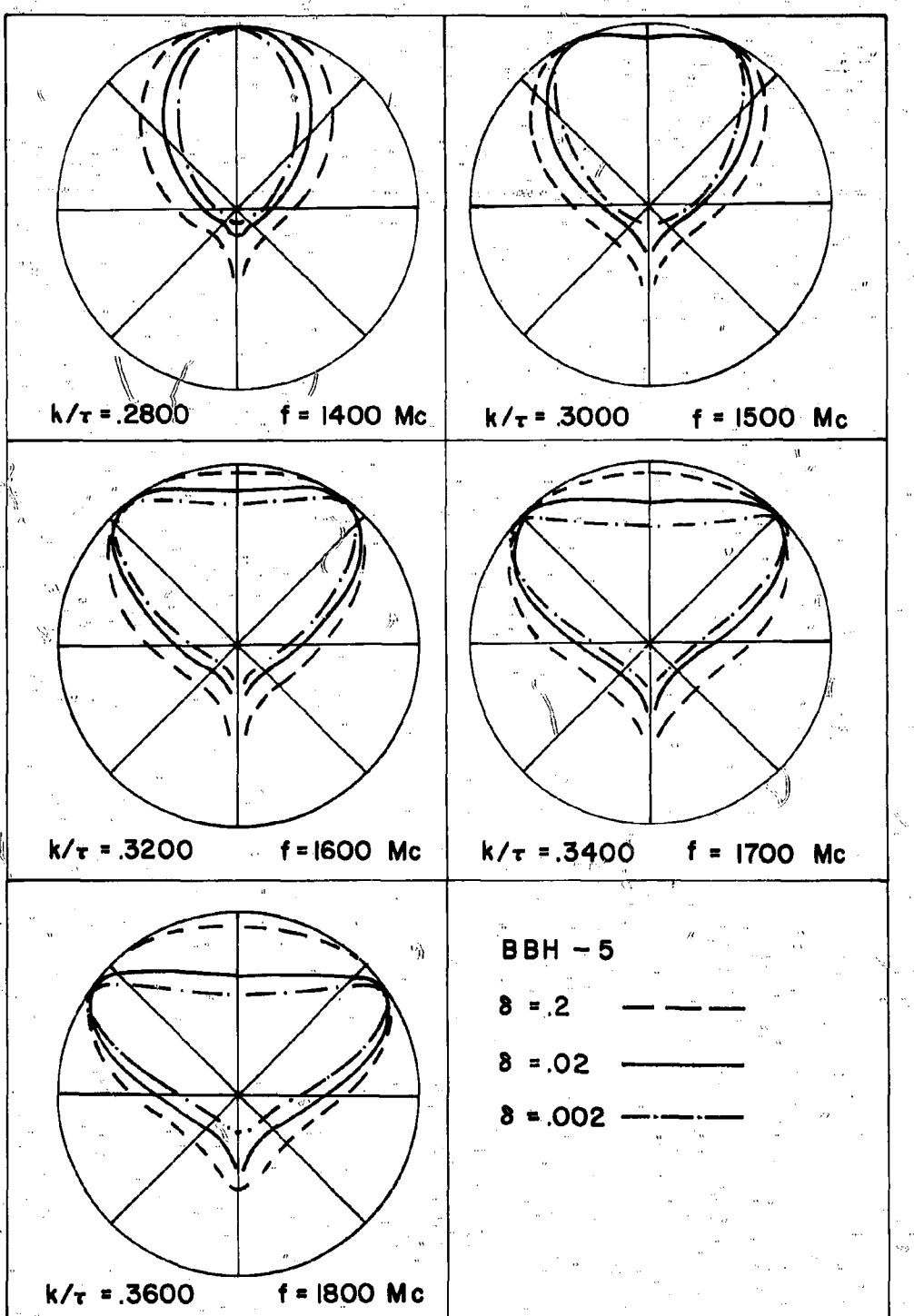

Figure 21. Computed Radiation Patterns for BBH-5

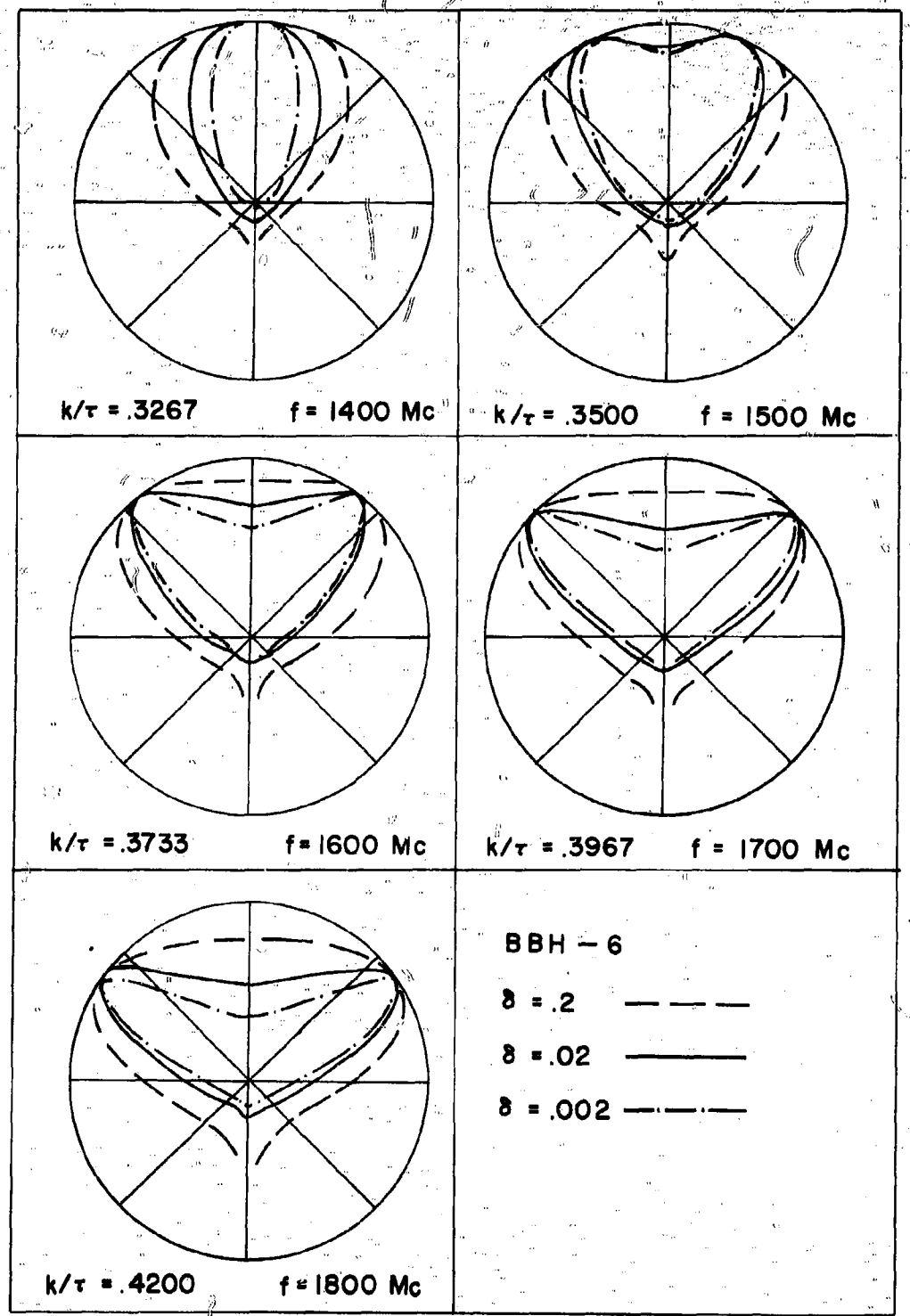

Figure 22. Computed Radiation Patterns for BBH-6

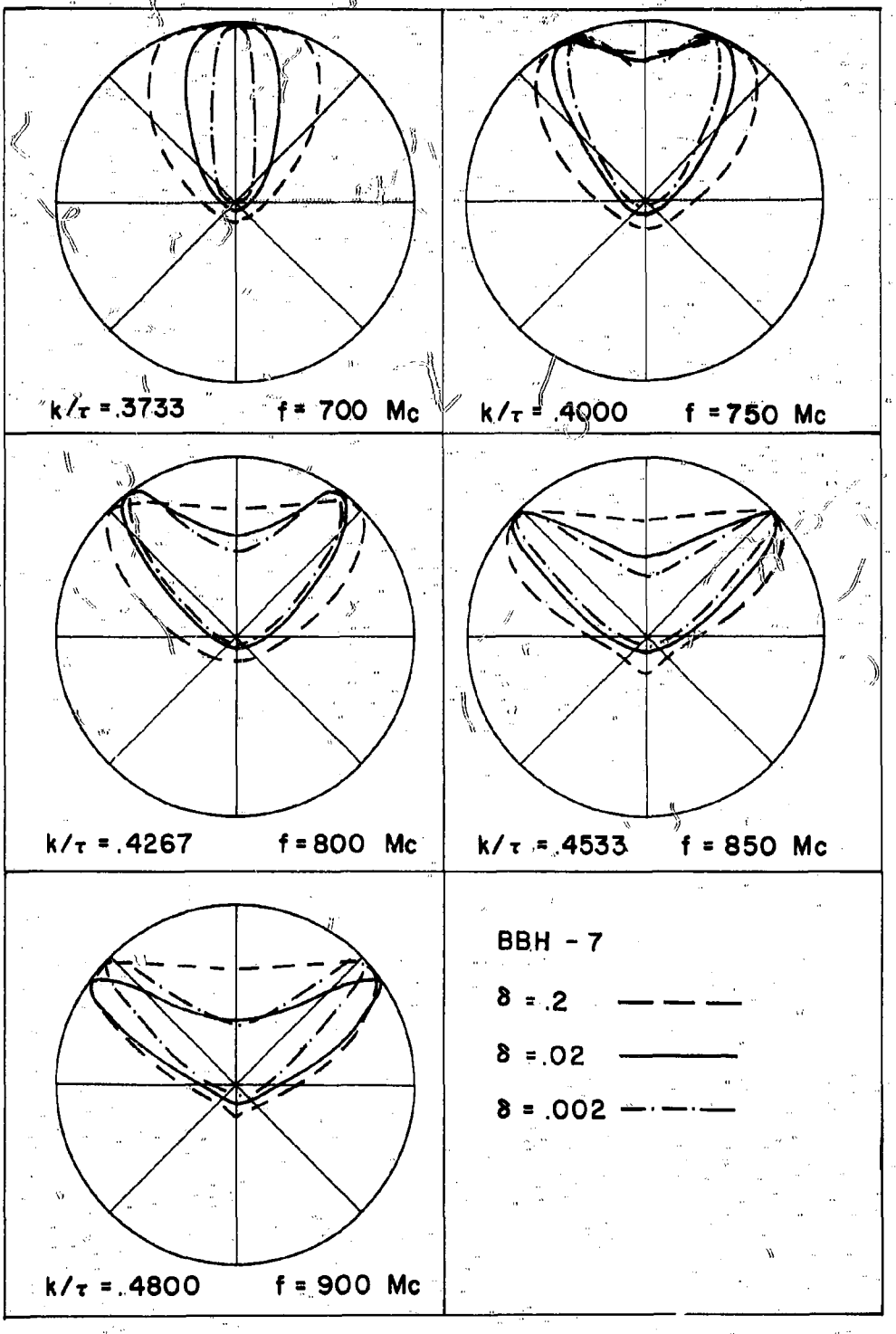

Figure 23. Computed Radiation Patterns for BBH-7

One pattern was computed for each of the antenna models for the normalized frequency

$$\frac{k}{\tau} = \chi$$

This corresponds to the model frequency of 1.5 Gc. One pattern was computed for a frequency one hundred megacycles below this frequency, and three were computed in increments of one hundred megacycles above this frequency. It was considered desirable for uniformity to use the same wire sizes for the entire range of antenna parameters. The value ($\delta = 0.02$) was chosen as a convenient number near the values obtained for the experimental models. Wire sizes of one tenth and ten times this value were used to show the effect of wire size on the performance of the antenna.

The computed patterns for the wire size $\delta = (0.02)$ are compared with measured patterns in Figures 24-30. The agreement between the measured pattern and the computed patterns is good in the main beam. There is a considerable difference in the shapes of the computed and measured patterns in the direction of the structure (back lobe). The radiation in this direction is controlled by the length of the helical antenna in the manner described in the next chapter. In this chapter we will limit our discussion to a comparison between the main beams of the computed and measured patterns.

In the patterns for BBH-1, Figure 24, the agreement between the computed and measured patterns is quite good. The relative wire size of the experimental model $\delta = 0.0227$. This does not differ much from the value ($\delta = 0.02$) used in the computation. In addition it can be seen in Figure 18 that the shape of the radiation is little dependent on the relative wire size. For BBH-2 through BBH-6 the relative wire size increses, and the agreement between the measured pattern and the patterns computed for $\delta = 0.02$ becomes poorer. The agreement is

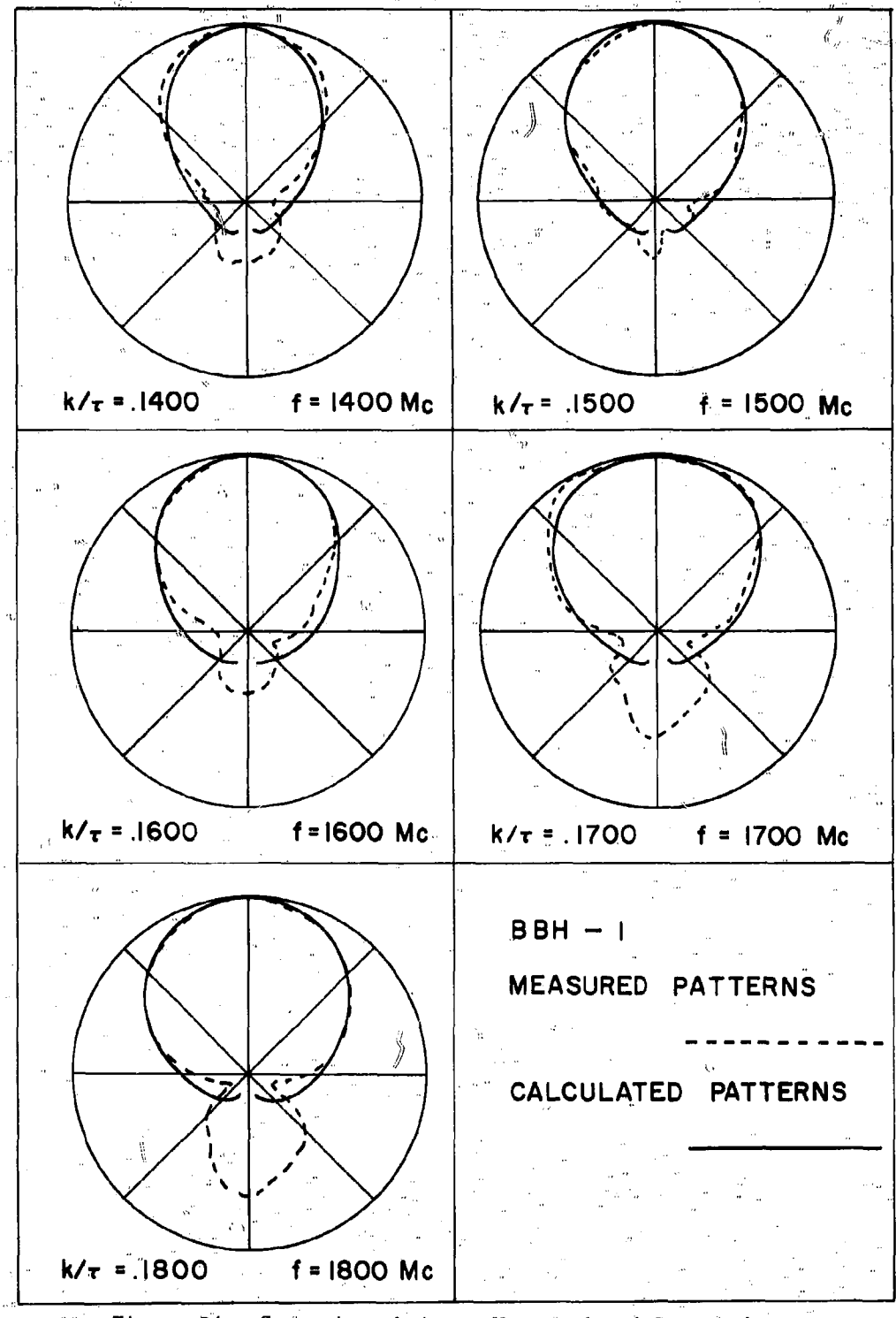

Figure 24. Comparison between Measured and Computed Patterns for BBH-1

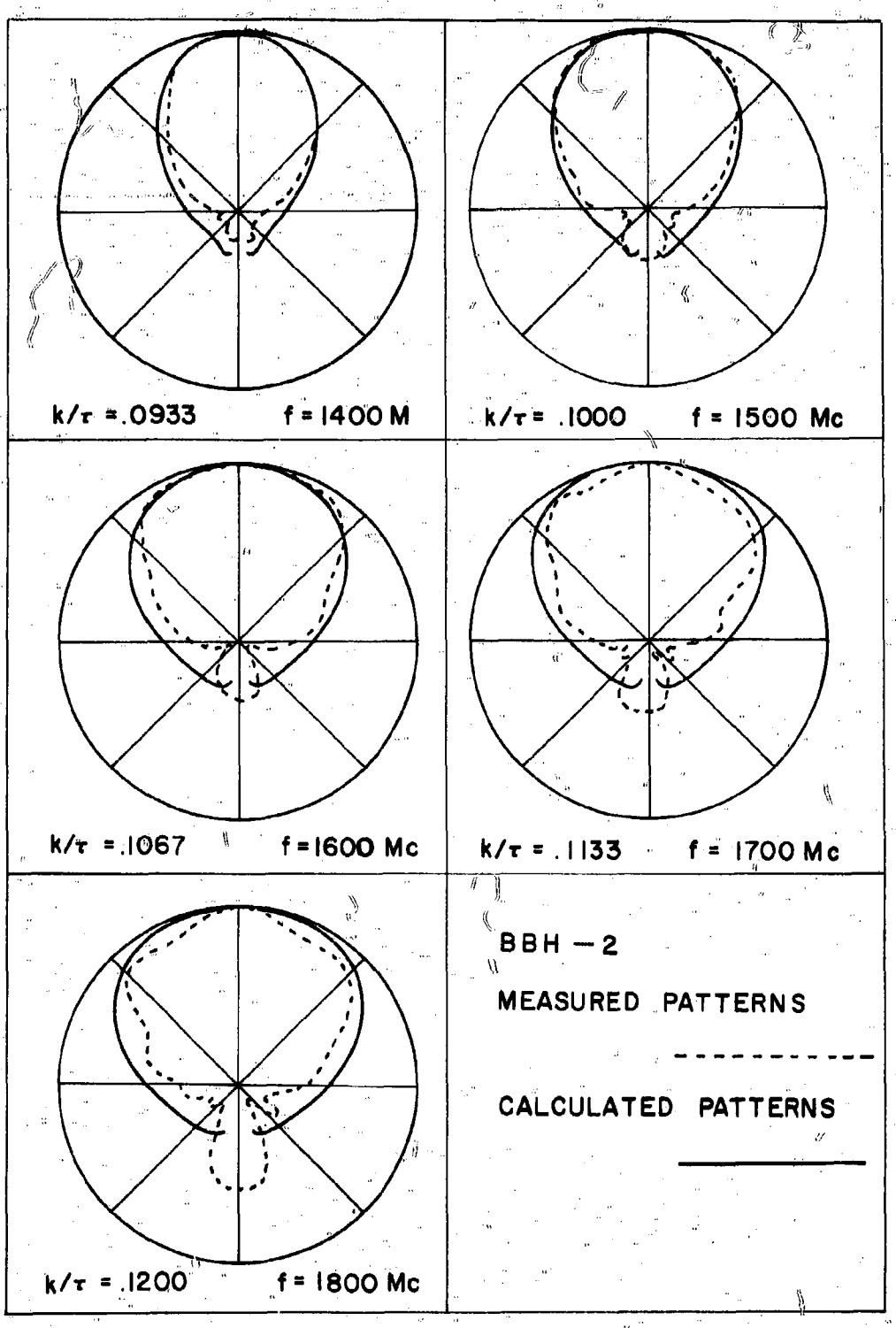

Figure 25. Comparison between Measured and Computed Patterns for BBH-2

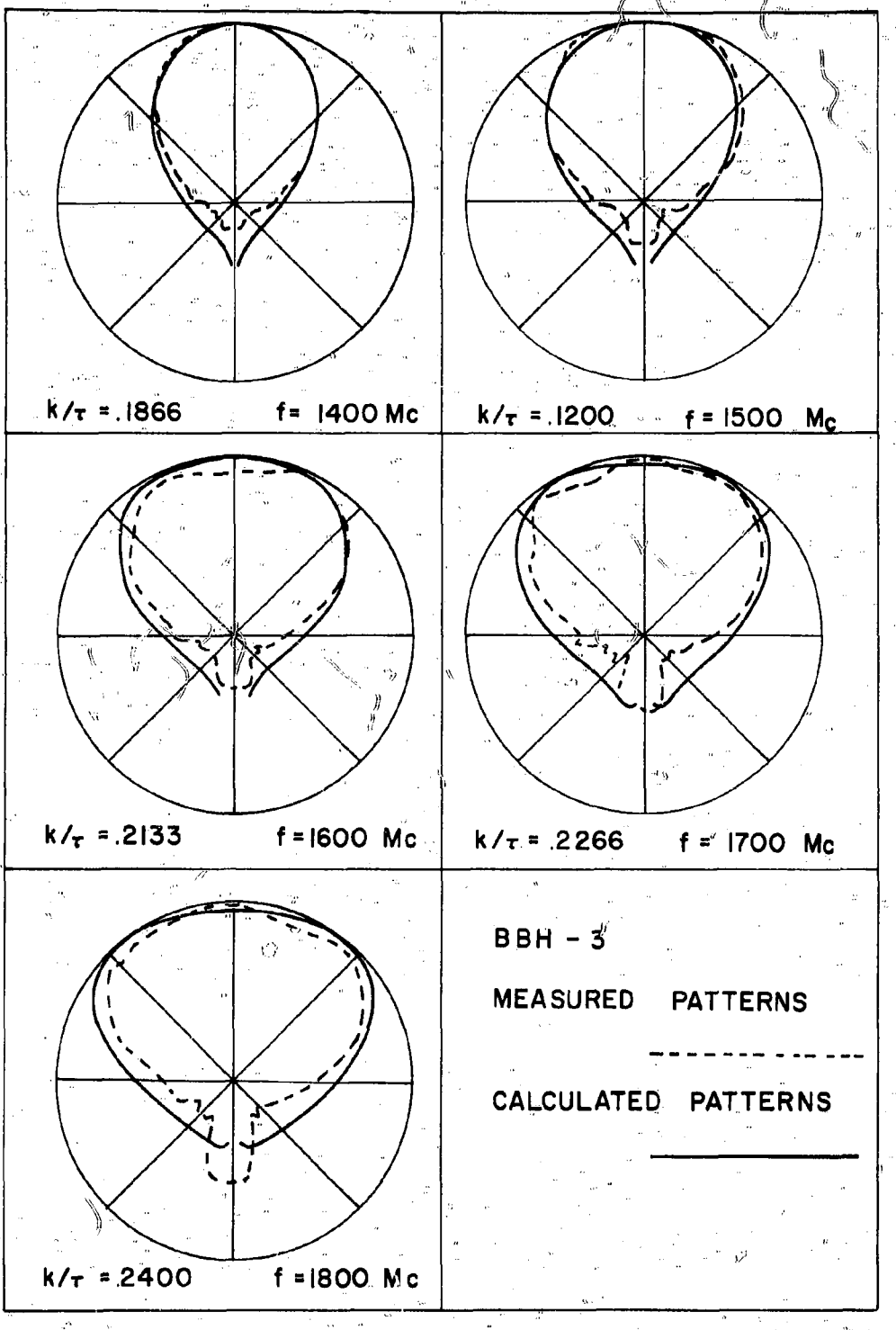

Figure 26. Comparison between Measured and Computed Patterns for BBH-3

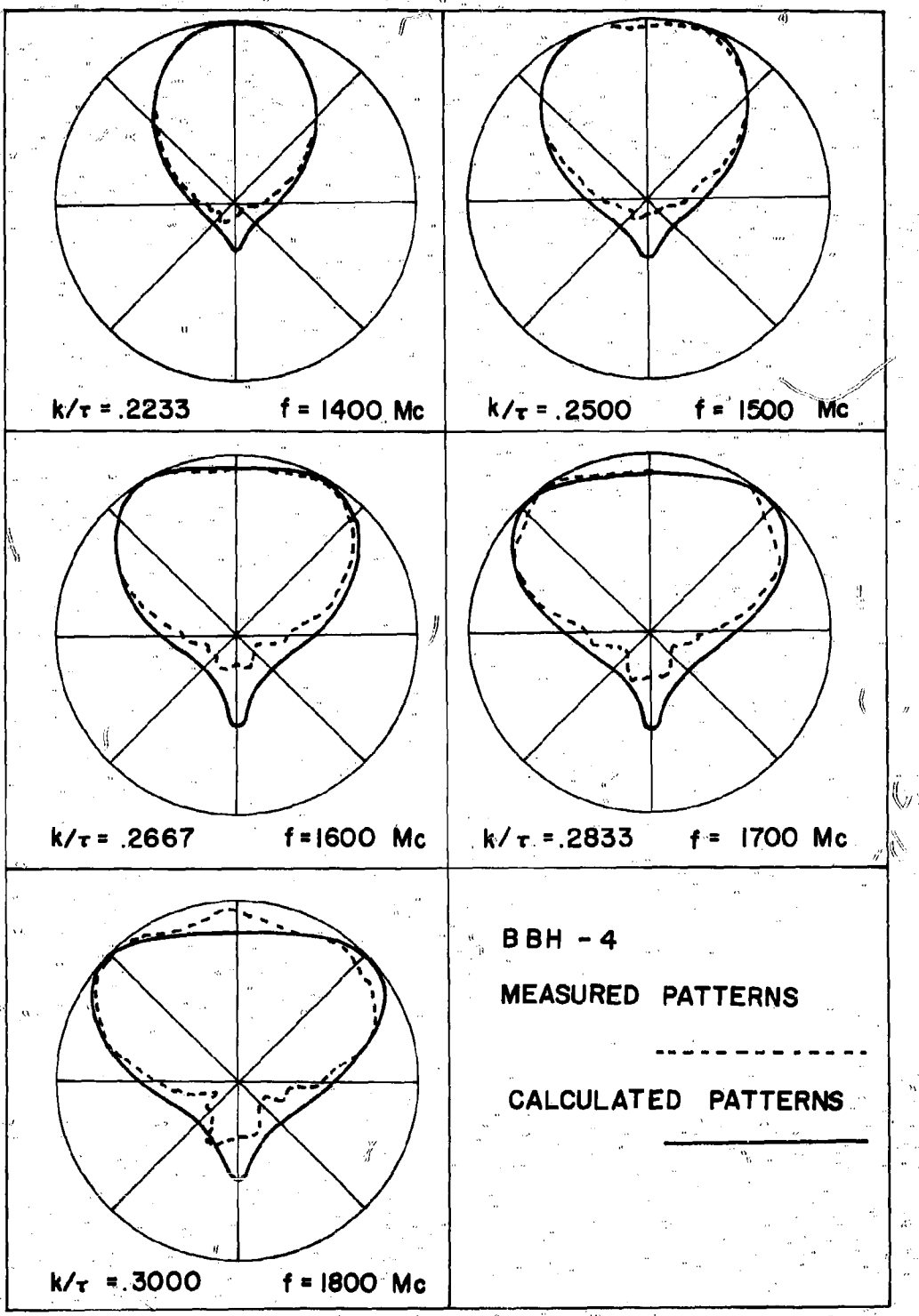

Figure 27. Comparison between Measured and Computed Patterns for BBH-4

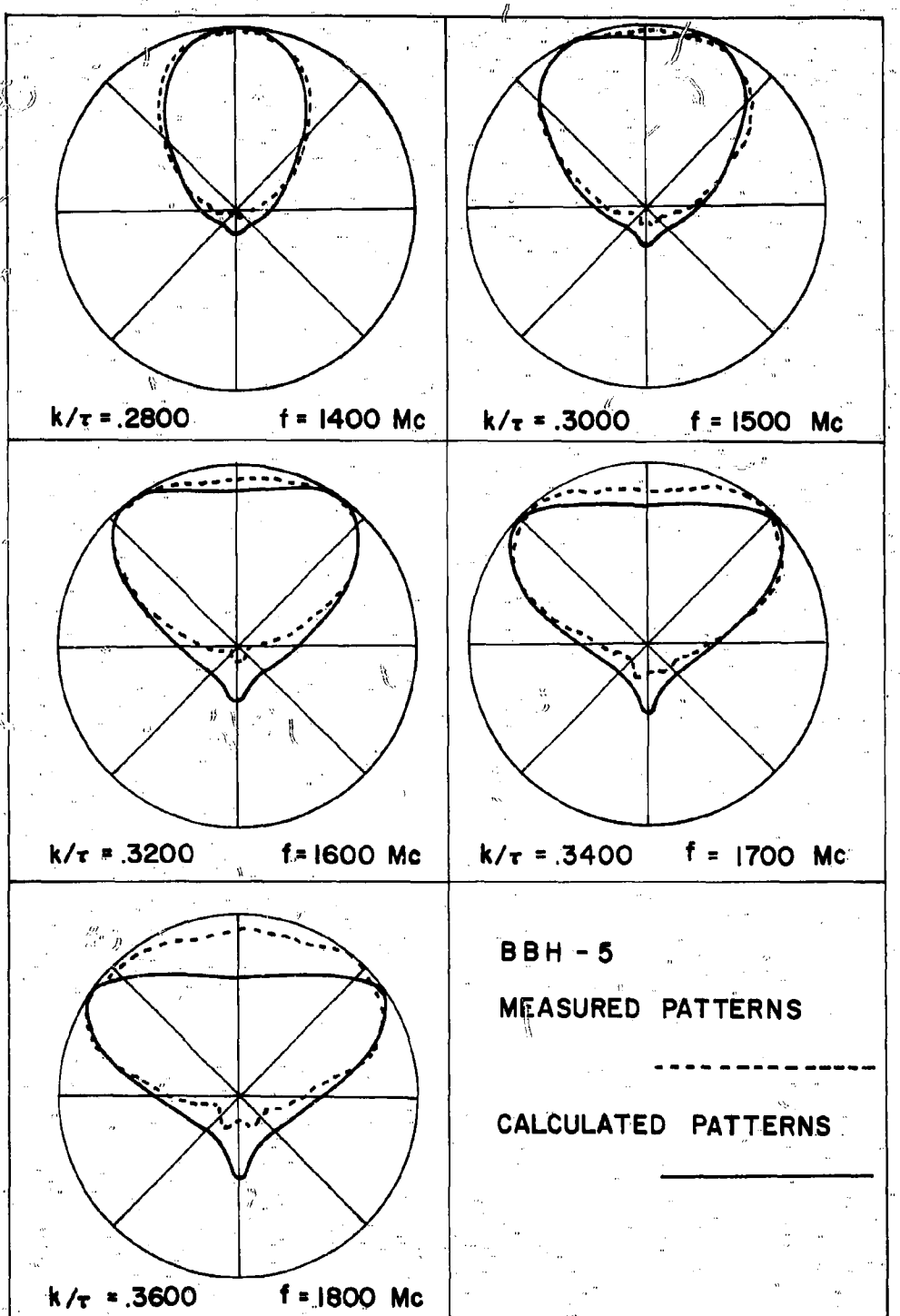

Figure 28. Comparison between Measured and Computed Patterns for BBH-5

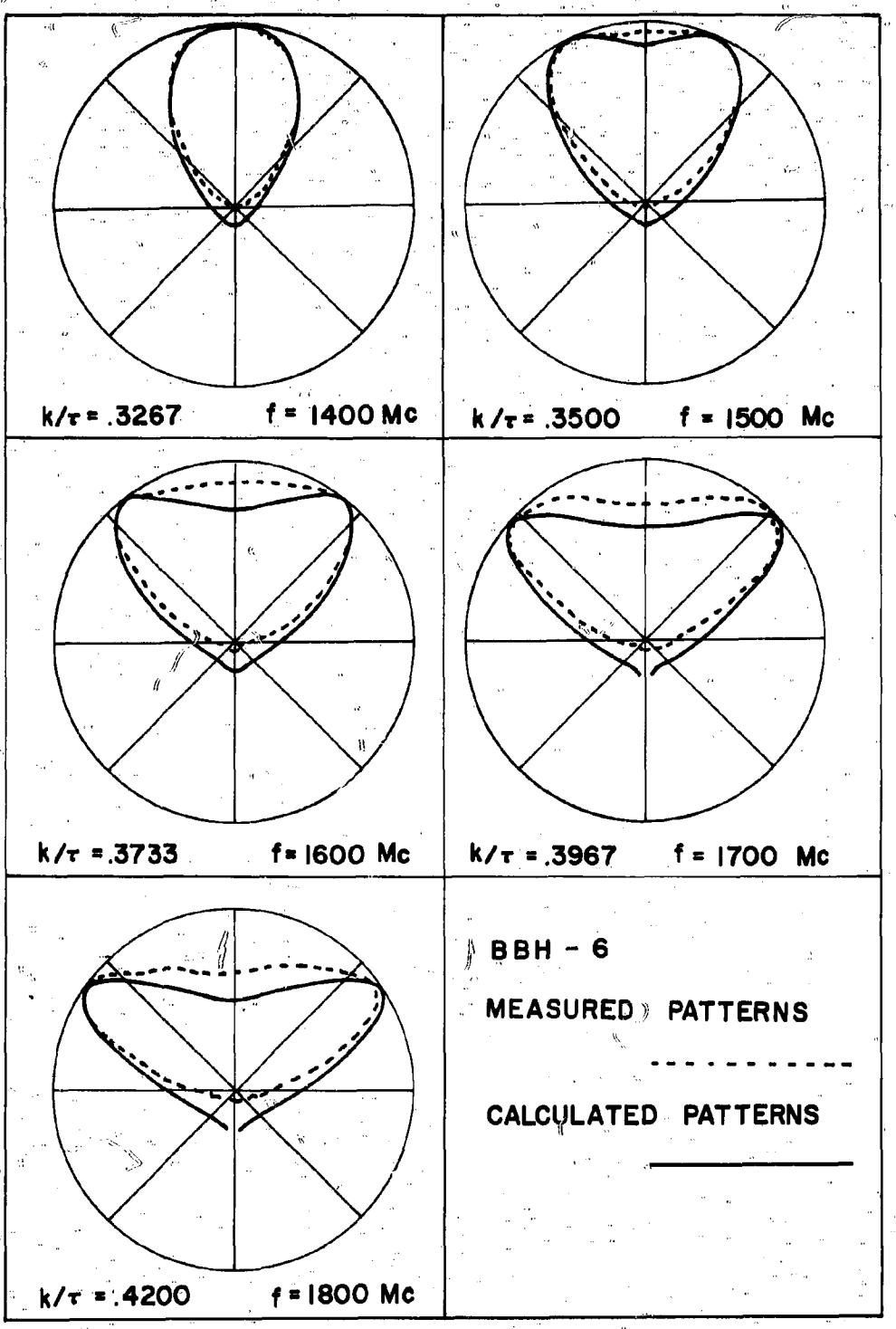

Figure 29. Comparison between Measured and Computed Patterns for BBH-6

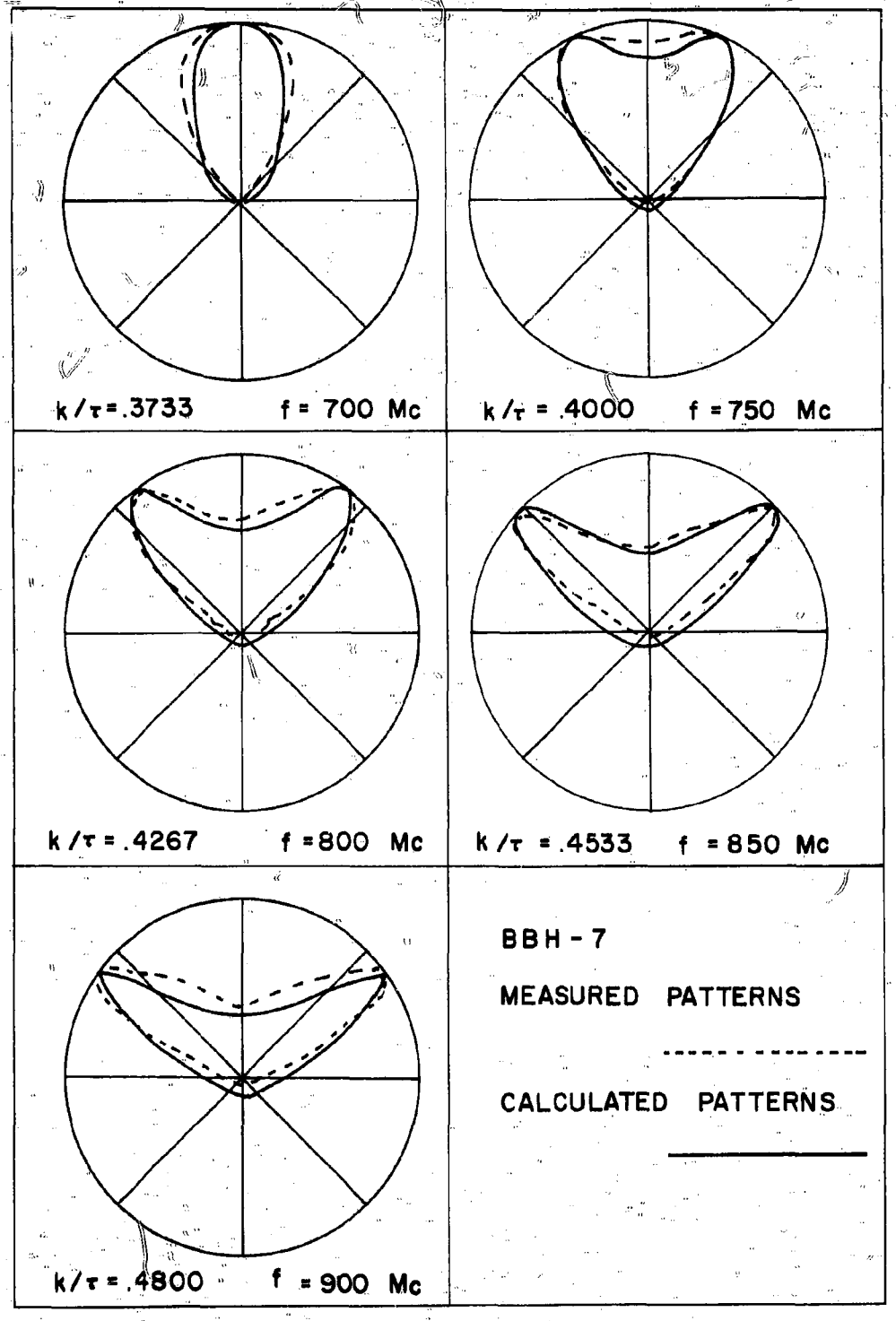

Figure 30. Comparison between Measured and Computed Patterns for BBH-7

best for the lower frequencies where the relative wire size has less control over the pattern shape. The measured and computed patterns show the greatest difference for BBH-6 where the relative wire size ($\delta = 0.037$) has its largest value. When BBH-7 was constructed it was found that the polystyrene foam core used to support the helical wires had insufficient strength when sized for the design frequency of 1.5 Gc. The design frequency was changed to 0.75 Gc. This doubled the radius of the helix and halved the relative wire size to $\delta = 0.0226$. This is evident in Figure 30 from the improved agreement between the measured and computed patterns.

Computed values of the axial ratio on axis in the main beam are shown in Figure 31. These are obtained from Equation (6)

$$AR = \frac{1+r}{1-r}$$

where r is the ratio of the right-handed and left-handed circularly polarized components of the radiation pattern given by

$$r = \frac{\tilde{I}(1-k)}{\tilde{I}(-1-k)}$$

The axial ratio is best (nearest unity) at the lowest operating frequency. These results are comparable with those obtained with the helical beam antenna.

The comparison of the measured patterns and the computed patterns, allowing for the differences in relative wire size, shows that the main beam radiation pattern is predicted by the calculations outlined in Chapter 5 based on the theory of Chapter 4. This theory is based upon an infinitely long antenna. The effect of the length of the structure accounts for the difference between measured and computed results as described in the next section.

6.3 Endfire Radiation from the Backfire Bifilar Helical Antenna

The endfire radiation from the backfire bifilar helical antenna is

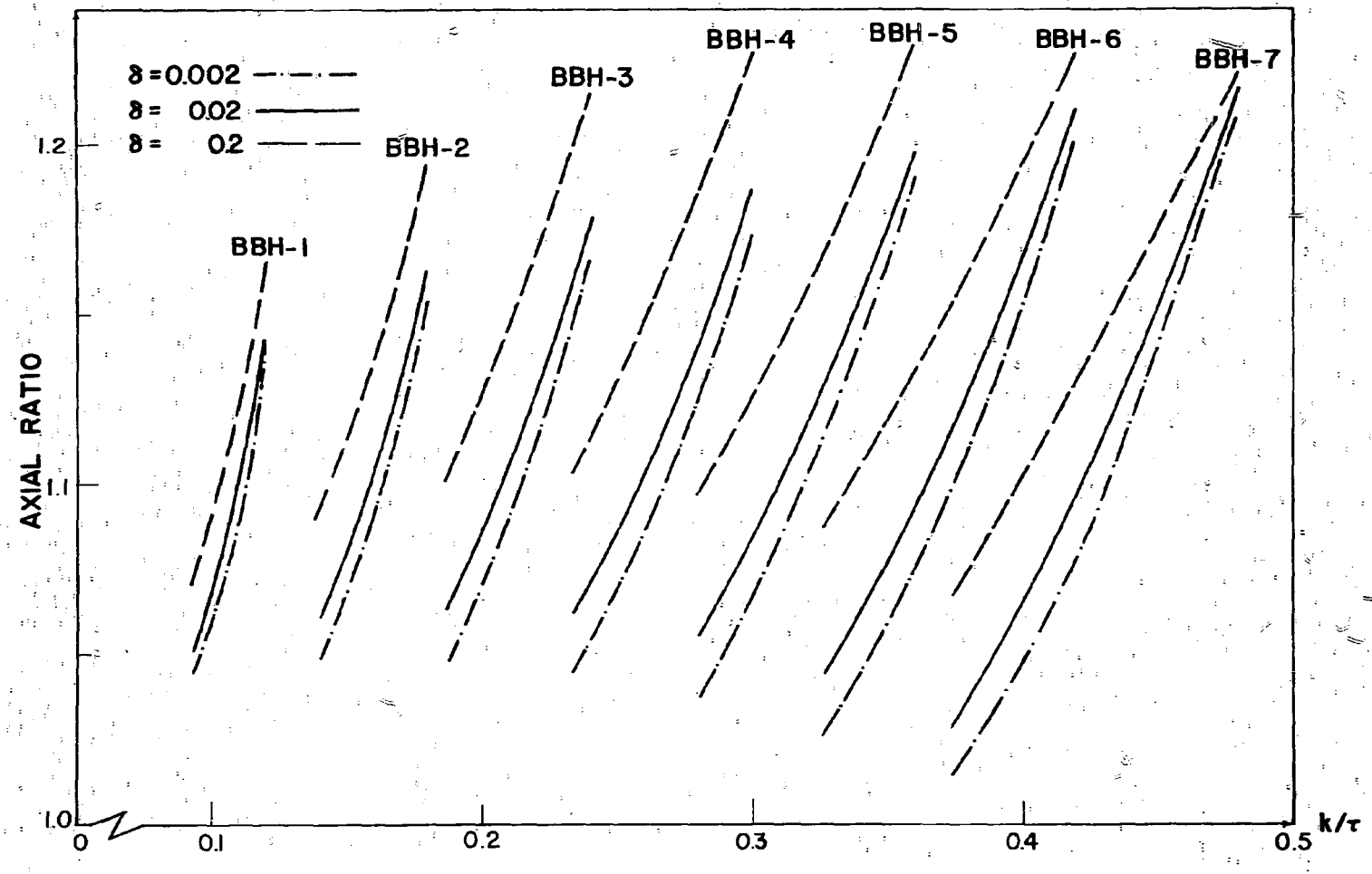

Figure 31. Axial Ratios for the Backfire Bifilar Helical Antenna

controlled by the root β_o of the determinantal equation. Values of this root for the parameters used in the pattern calculations are shown in Figure 32. In this figure the normalized values of the root $\frac{\beta_o'}{\tau} = \frac{\beta_o}{\tau} - 1$ have been shifted to the right one unit to account for the difference between the apparent phase constant as one travels along the wire and as one travels along the helical axis. Thus zero corresponds to a circularly polarized traveling wave of current traveling along the positive z-axis from the origin.

$$I = \begin{cases} I_o\, e^{-(j\beta_o' + \alpha)z} & z > 0 \\ & z < 0 \end{cases}$$

The pattern produced by this distribution is

$$P(\theta) = I_o \int_o^\infty e^{-[\beta_o' - k\cos\theta) + \alpha]z} dz$$

$$= \frac{-jI_o}{\beta_o' - k\cos\theta - j\alpha}$$

For vanishing α, the magnitude of $P(\theta)$ at $\theta = 0$ (the endfire direction) is

$$P_{(o)} = \frac{I_o}{\beta_o' - k}$$

In this equation I_o is proportional to the residue of $\tilde{I}_+(\beta)$ at $\beta = \beta_o$. This residue is inversely proportional to the slope of $\tilde{Z}(\beta)$ at $\beta = \beta_o$. Figure 10 shows that $\tilde{Z}(\beta)$ has a logarithmic singularity at $\beta = \tau + k$. When β_o is close to $\tau + k$, the case for k near k_c, the slope of $\tilde{Z}(\beta)$ at β_o is very large, and I_o is small. As k is increased the slope of $\tilde{Z}(\beta)$ at β_o decreases and I_o increases. At the same time, $(\beta_o' - k)^{-1}$ is very large when k is near k_c and decreases rapidly as k increases. The computed patterns for BBH-1 and BBH-2 show no radiation due to β_o because $(\beta_o' - k)$ is too large. At the other end of the range of parameters,

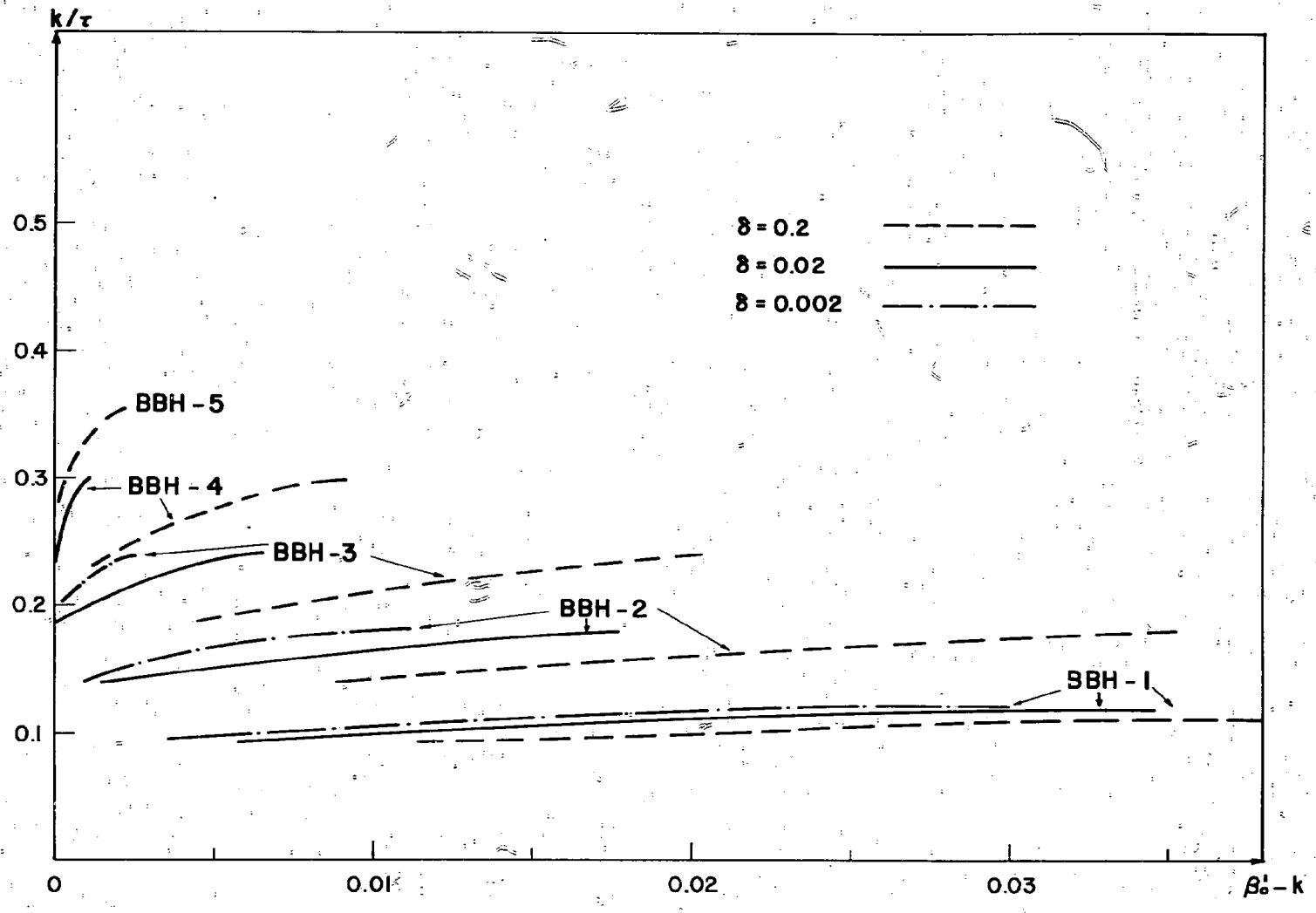

Figure 32. Calculated Values of the Propagation Constant of the Higher Order Waveguide Mode on the Bifilar Helix

BBH-7 shows little radiation due to β_o because I_o is small. The effect of relative wire size on this phenomenon is shown in the patterns for BBH-3, Figure 19. In this figure the curve for the largest wire size ($\delta = 0.2$) does not have radiation due to β_o while the smallest wire ($\delta = 0.002$) does. Endfire radiation due to β_o is also evident in the patterns for the other models.

If the bifilar helical antenna is long enough to support the feed region current, the shape of the main beam is not affected by truncation of the structure. The radiation due to β_o is, however, controlled by the length, L, of the antenna. Considering only the incident wave, Equation (50) must be modified for the finite antenna as follows

$$P_L(\theta) = I_o \int_o^L e^{-[j(\beta_o'-k\cos\theta)+\alpha]z} dz \qquad (51)$$

$$= I_o \frac{e^{-[j(\beta_o'-k\cos\theta)+\alpha]L} - 1}{-[j(\beta_o'-k\cos\theta)+\alpha]}$$

For vanishing α, the magnitude of $P_L(\theta)$ at $\theta = 0$ is

$$P_L(0) = 2\, I_o L/2 \frac{\sin(\beta_o'-k)}{\beta_o'-k}$$

Thus when $(\beta_o-k)\, L/2$ is small the radiation in the endfire direction is reduced by the factor $(\beta_o-k)L$.

$$P_L(0) = (\beta_o-k)L\, P(0) \qquad (52)$$

The magnitude of $P_L(\theta)$ at other angles is given by

$$P_L(\theta) = I_o L \frac{\sin x}{x} \qquad (53)$$

where

$$x = (\beta_o'-k\cos\theta)\, L/2$$

This term and a similar one due to the reflection of the higher order waveguide mode from the end of the antenna account for the back lobes in the measured patterns and "scallops" observed on the main beam at the higher frequencies. No attempt is made here to obtain an exact theoretical preduction of the effect of the length of the antenna since this requires a knowledge of the far field phase pattern of the feed region currents.

The effect of helix length on the performance of the bifilar helical antenna was studied experimentally. Figure 33 shows some typical patterns resulting from changing the length of the backfire bifilar helical antenna. The size of the back lobe decreases with length with little change in the main beam until the antenna becomes too short to support the feed region currents. Shortening the antenna beyond this point will generally broaden the main beam pattern. Front-to-back ratios obtained for different lengths are shown in Figure 34.

Figures 33 and 34 are for BBH-2 at a frequency of 1.4 Gc. A similar set of measurements was made, at the other end of the parameter range, for BBH-7. For this antenna there was no measurable endfire radiation for any of the lengths used in the measurements. This result is explainable when the calculated value of β_o is observed. For BBH-7 at k = 0.4

$$\beta_o - (1+k) < 1 \times 10^{-7}$$

it would take a very long antenna indeed to show endfire radiation. In general, a greater length of antenna is required at the lower frequencies than at the higher frequencies, because of the slower rate of current decay, observed in the near field amplitude measurements, near the critical frequency.

At frequencies well above the critical frequency, there is an optimum length for the bifilar helical antenna for each frequency. This optimum length is just that required to support the feed region currents. A longer

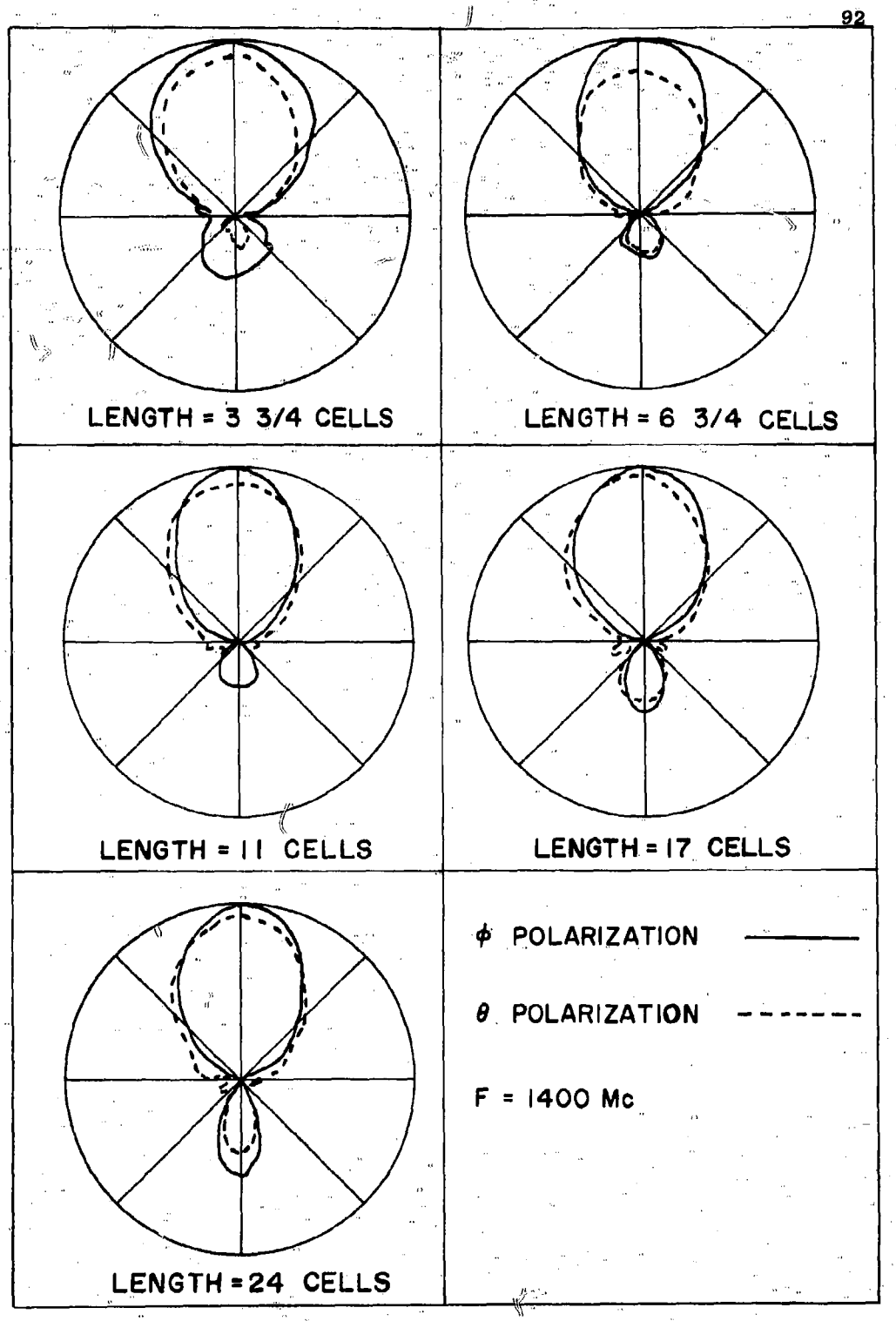

Figure 33. Radiation Patterns Showing the Effect of Changing the Length of the Antenna

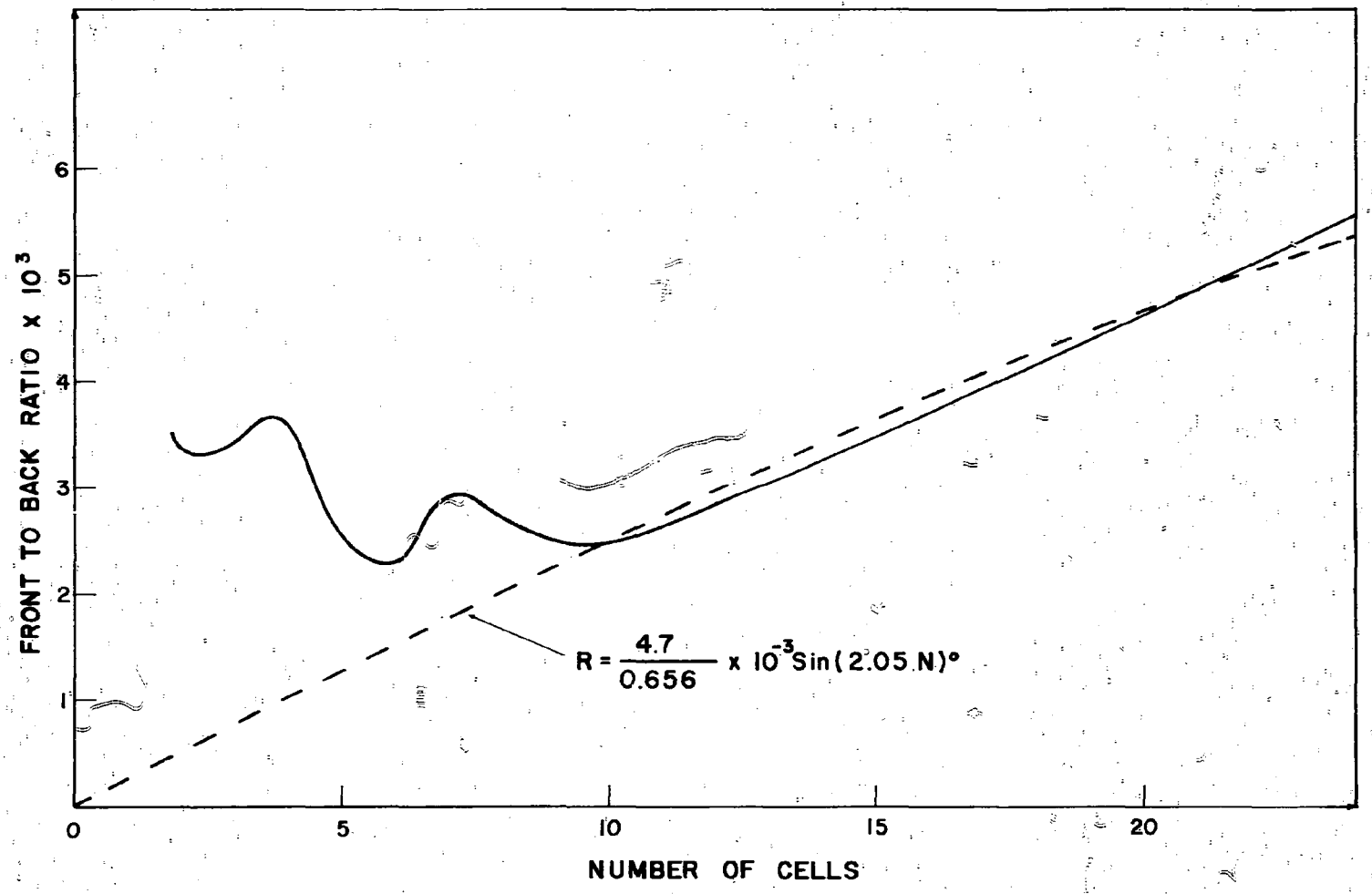

Figure 34. Front-to-Back Ratio as a Function of Antenna Length

length will decrease the front-to-back ratio by increasing the radiation due to β_o. At frequencies near the critical frequency the feed region current penetrates the structure to a much greater depth. The lowest frequency that can be used in the backfire mode on a particular model depends upon the length of the antenna. The required length changes very rapidly as the critical frequency is approached so that the cutoff frequency, determined from the pattern measurements on an antenna of a reasonable length (10-15 turns), is in error by less than one percent. An infinitely long antenna is required to support the feed region current at the cutoff frequency.

6.4 Other Experimental Results

Four investigations, supplemental to the main body of this study, are reported in this section. These investigations are by no means exhaustive and serve to suggest further work. The first of these is a study of the effect of placing a conducting core on the axis of the helical antenna. The second investigation is a study of high-grain backfire bifilar helical antennas. In the third experiment, a long slowly tapered helix is studied, and the last study shows that a monofilar can be made to operate in the backfire mode.

The backfire bifilar helical antenna, model BBH-4, has a diameter of 1.77 inches. The patterns obtained for this model, when a series of brass rods were placed inside the helix and coaxial with it, are shown in Figure 35. The core did not extend beyond the feed point. The core diameters ranged from 1/2 inch to 1 1/2 inch in diameter in 1/4-inch steps. The frequency, at which these patterns were taken, is one hundred megacycles below the frequency given by χ(1.5 Gc) for this model. When a 1 1/2-inch core is used, the thickness of the dielectric polystyrene foam between the core and the wires is 0.11 inches. This is 0.013 wavelengths at the frequency of 1.5 Gc.

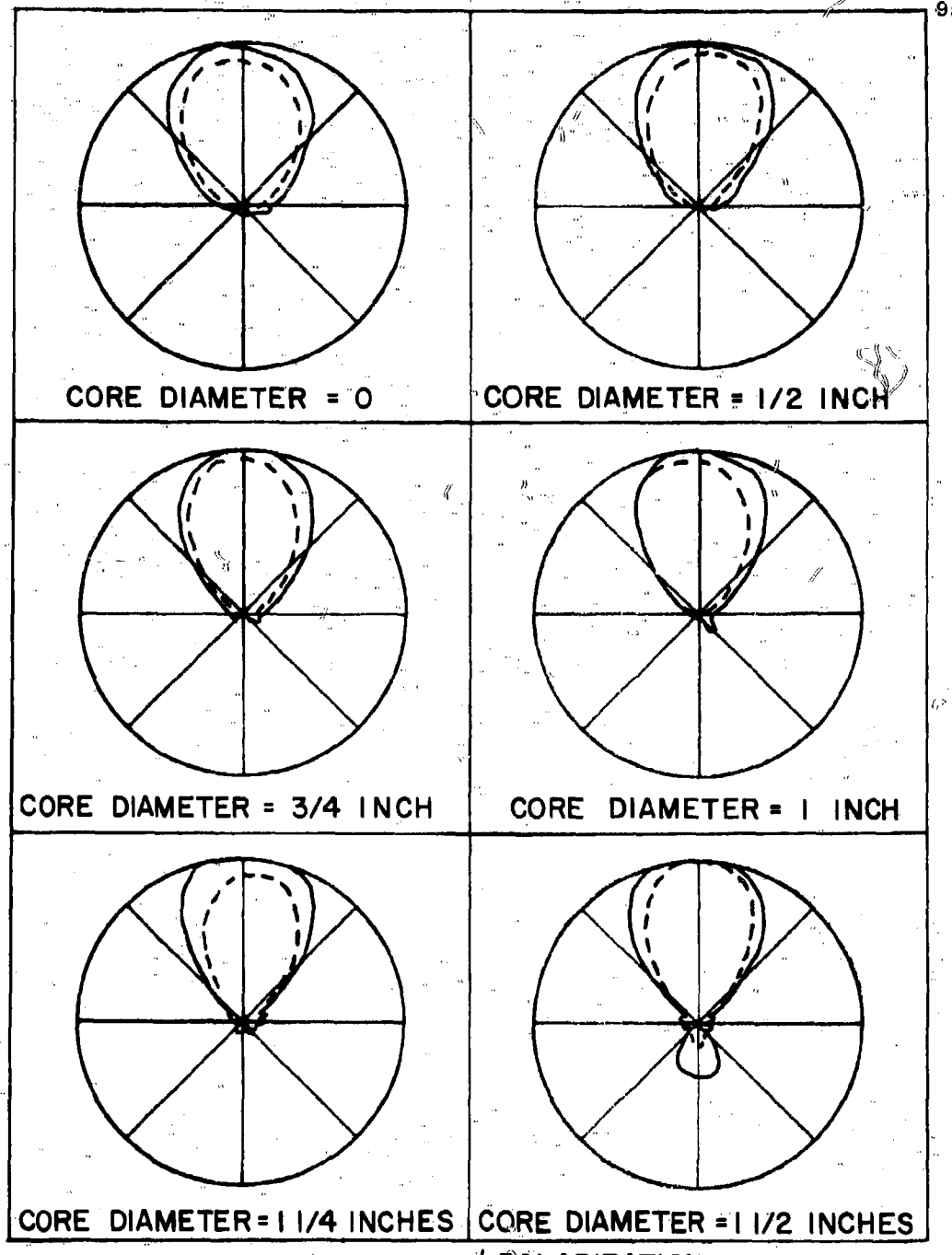

Figure 35. Patterns of BBH-4 With a Conducting Coaxial Core at f = 1.4 G_c

The main beam of the patterns shows little change with increasing core diameter except for some asymmetry due to misalignment of the core axis and some improvement in the circular polarization on axis. The principal effect of the core is to increase the excitation of the higher order waveguide mode. This is seen by the increase in endfire radiation. The increase in endfire radiation is significant only when the core nearly fills the center of the helix. It is expected that a further increase in core diameter would rapidly change the character of the radiation pattern, but, for the core diameters used in this investigation, surprisingly little effect was noted.

Backfire bifilar helical antennas with a large pitch angle tend to give the greatest directivity. To provide more information on this property, two antennas were built with a pitch angle of 45°. BBH-8a was constructed of number twenty-two wire wound on a 1-inch diameter plexiglass tube 48 inches long. BBH-8b was constructed of number thirty-four wire wound on a 0.475-inch diameter pyrex glass tube 48 inches long. The patterns obtained for these antennas are shown in Figure 36.

The pattern for BBH-8a at 1.315 Gc has a 28° beamwidth. The length of the antenna at this frequency is 5.35 wavelengths. Using the approximate relation between beamwidth and gain given by Kraus[20], the gain of the antenna at this frequency is 52.5 (17.2db). This gives a ratio of gain to length in wavelengths of 9.82. The pattern for BBH-8b at 2.575 Gc is 20°, and the length of the antenna at this frequency is 10.45 wavelengths. The gain of the antenna is 103.1 (21.1db), and the gain-to-length ratio is 9.9. This result can be compared with the expression given by Schelkunoff and Friis[21] for the gain of a long array of isotropic radiators in terms of its length.

$$g = 7.2\ L/\lambda$$

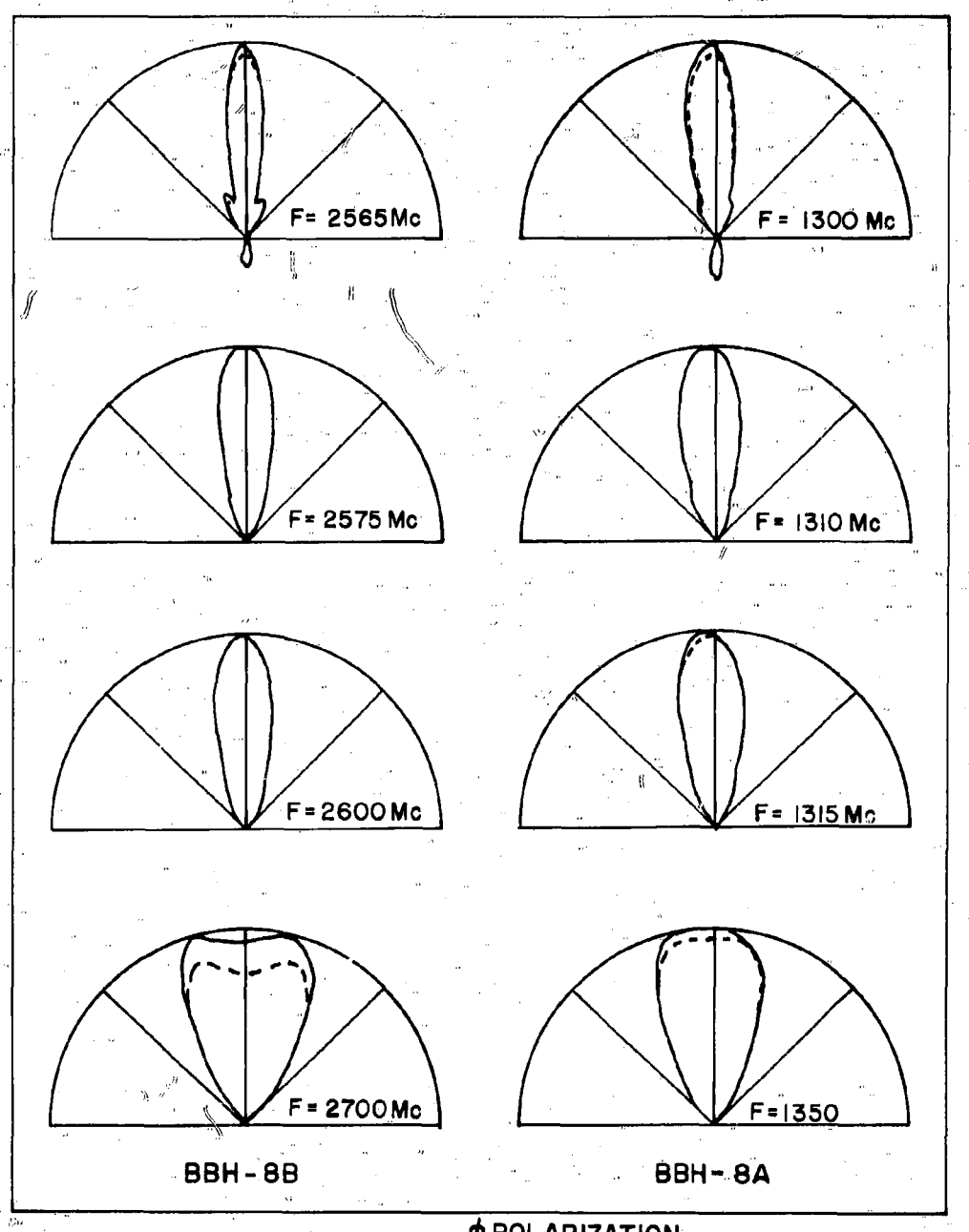

Figure 36. High-Gain Patterns Measured for BBH-8

This gain results when Hansen-Woodyard excess phase shift is used in the array. The backfire bifilar helix provided a gain about 1.375 times as great without side lobes. If side lobes were permitted as shown for the lower frequencies, the gain is increased 1.7 times. The backfire bifilar helices are obviously supergain antennas when operated near the critical frequency. The usual instability associated with supergain antennas takes the form of a very rapid widening of the beam with increasing frequency. One half percent increase in frequency increases the beam width 2^{o}.

In an attempt to retain some part of the high-gain performance of the antenna described above and at the same time increase the band width, a 8-foot long antenna was built, tapered from one-half inch diameter at one end to one-inch diameter at the other end. A Rexolite number 1422 core was used with number thirty-two wire wound at a pitch angle of 45^{o}. The patterns obtained for this antenna are shown in Figure 37. This antenna has an average gain of 36(15.5db) in a five percent band width. Thus tapering the helix slows the rate with which its patterns vary with frequency and at the same time reduces the maximum gain that can be achieved. This is the result expected since this antenna corresponds to a conical log-spiral antenna with a very small cone angle.

A backfire monofilar helix was constructed to show that the nomofilar helix will also operate in the backfire mode. This model used the parameters of BBH-2. The conductor in this case was a Microdot cable, which was also used to carry energy from the feedpoint to the receiver. At the feedpoint, the Microdot cable was brought radially from the parameter of the helix to the axis. The center conductor of the cable was connected to the center of a straight wire ten-centimeters long placed on the axis of the helix. The patterns obtained for the monofilar helix are shown in Figure 38. These patterns are very

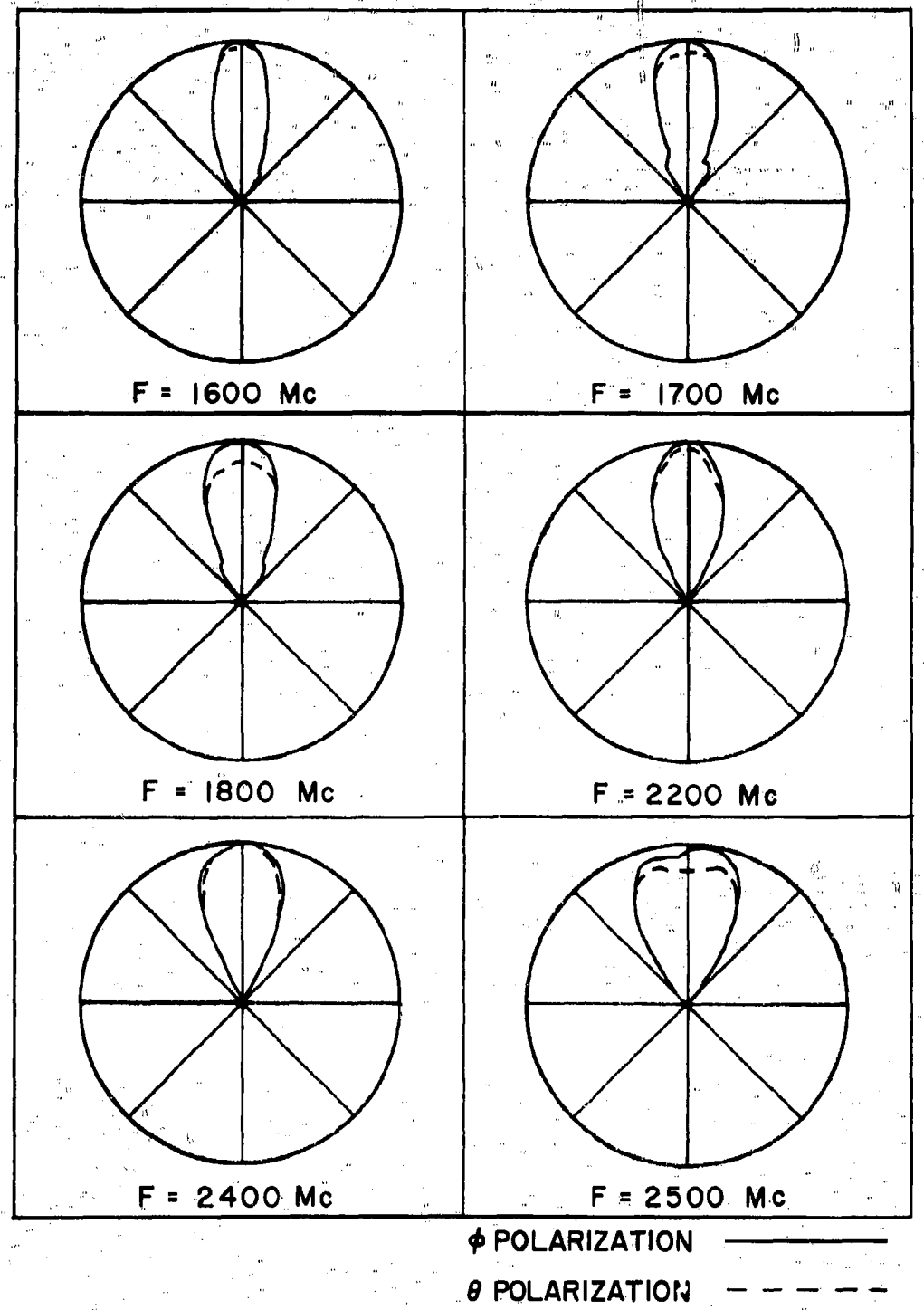

Figure 37. Measured Patterns for a Long Tapered Bifilar Helix

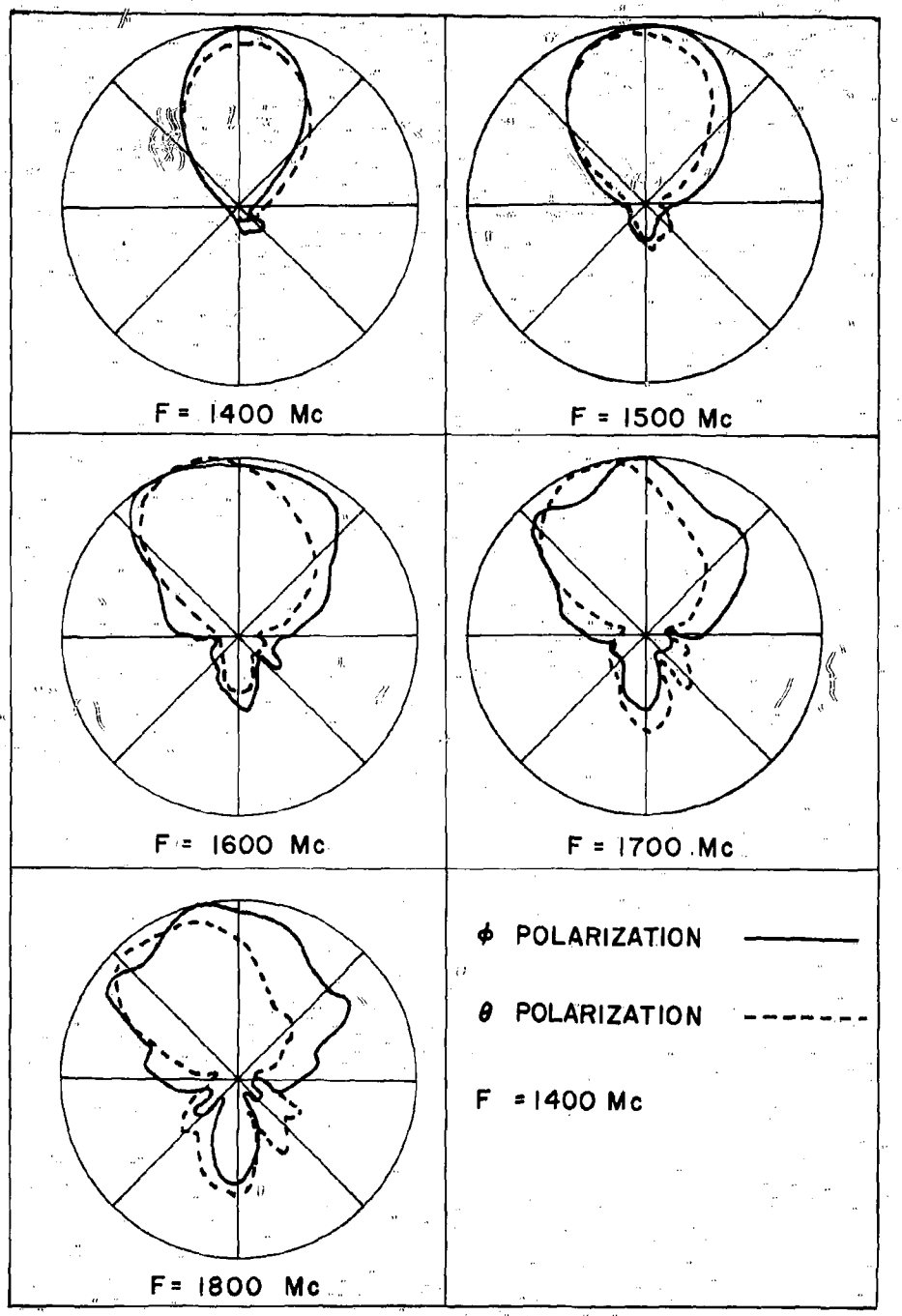

Figure 38. Radiation Patterns Measured for a Backfire Monofilar Helix

similar to those obtained for the bifilar antenna, BBH-2. This demonstrates that the monofilar helix will operate in the backfire mode, although it is more difficult to feed than the bifilar helix.

7. CONCLUSION

The object of this research was to provide a mathematical model of the backfire bifilar helical antenna that could be used to predict the radiation characteristics of this antenna. The model described here was shown to fulfill this objective. The study went beyond this objective in providing a detailed experimental study of the radiation patterns of the antenna.

In this research the radiation patterns were obtained using the known determinantal equation for the helical waveguide. This equation was factorized by the Wiener-Hopf technique to provide the Fourier transform of the current distribution on the semi-infinite helix. The radiation pattern was related to this Fourier spectrum.

Two regions in the frequency spectrum of the backfire bifilar helix were shown to be important. It was shown that at the lower frequencies the bifilar helix operates as a waveguide. Above the cutoff frequency of the principal waveguide mode, the bifilar helix operates as a circularly polarized backfire antenna.

The radiation characteristics of this antenna were shown to be determined by the feed region current. This current decays with distance along the structure. The near field has a phase progression directed toward the feedpoint. The distance to which the feed region current penetrates the structure was shown to decrease with frequency.

The phase pattern of the antenna was not obtained in the calculations because of the long numerical integration involved in its computation. This prevented a more accurate accounting of the endfire radiation from the antenna. The good agreement between measured and computed results reaffirmed the validity of the approximations used in the beginning of the analysis.

This study of the backfire bifilar helical antenna is important for several reasons. Not the least of these is the fact that the antenna is a useful, practical device in itself. It provides circularly polarized fields with a single lobed pattern of almost any desired gain. When pitch angles near 45° are used, the antenna can provide circularly polarized fields with a pattern that is omnidirectional in azimuth with high vertical directivity. If it is inconvenient to provide a balanced feed for this antenna, it can be fed from a coaxial line run inside one of the helical conductors to the feedpoint on the axis. The decay of the feed region current will keep antenna currents from flowing on the unbalanced feed line.

This study provides further insight into the operation of the conical log-spiral antenna, and it is the first simply periodic backward wave or backfire antenna for which a theoretical solution has been obtained. The study of other types of periodic antenna structures that operate in the backfire mode will aid in understanding the operation of known log-periodic antennas and will suggest new ones. These structures are important in themselves for their unidirectional single lobe patterns and their frequency scanning characteristics, as well as for the insight they give in the operation of log-periodic antennas.

The existence of a decaying backward wave current in the feed region suggests that the patterns of the backfire helix can be explained in terms of improper (decaying) helical waveguide modes. An investigation along these lines is now in progress by another investigator. The results of such an analysis may be simpler in interpretation than the present analysis.

Another line of inquiry suggested by this work concerns the effect of a conducting core on the axis of the helical antenna. In this study it was shown

that the helical conductors could be placed remarkably close to the conducting core with little degradation of performance. This study should be extended to other helix parameters. The effect of extending the conducting core beyond the feedpoint should be investigated. A backfire monofilar helix fed against a conducting central core should also be investigated.

The study of long slowly tapered bifilar helices should be extended. The results of this study combined with results obtained for the conical log-spiral antenna would establish the relation between gain, band width, and size over the entire spectrum of helical or conical log-spiral parameters. The conical log-spiral antenna is known to have practically constant characteristics over ten-to-one or greater band widths. This antenna in the usual range of parameters has considerably less gain than can be obtained by a slowly tapered helix, while the slowly tapered helix has a relatively smaller band width.

It is characteristic of a study of a new device that many diverging courses of investigation are suggested. A few of these, that were suggested during the study of the backfire bifilar helical antenna, are described above. However, the major effort in this investigation was concentrated on the study of the radiation pattern of the antenna. In this way it has been possible to provide information on this aspect of the problem over on extensive range of parameters.

BIBLIOGRAPHY

1. S. Sensiper, Electromagnetic Wave Propagation on Helical Conductors, Ph.D. Thesis, Massachusetts Institute of Technology, 1951.

2. S. K. Kogan, "The Propagation of Waves Along an Endless Helix," Compt. Rend. Acad. Sci. (USSR), Vol. 66, June 1949; p. 867.

3. S. Sensiper, "Electromagnetic Wave Propagation on Helical Structures," Proceedings of the IRE, Vol. 43, No. 2, February, 1955; pp. 149-161.

4. J. D. Kraus, "Helical Beam Antenna," Electronics, Vol. 20, April, 1947, pp. 109-111.

5. J. A. Marsh, "Measured Current Distributions on Helical Antennas," Proceedings of the IRE, Vol. 39, June, 1960, pp. 668-675.

6. A. G. Holtum, Jr., "Improving the Helical Beam Antenna," Electronics, Vol. 33, April 29, 1960; p. 99-101.

7. H. J. Bremermann and L. Durland, "On Analytic Continuation, Multiplication, and Fourier Transformations of Schwartz Distributions," Journal of Math. Physics., Vol. 2, No. 2, 1961; pp. 240-258.

8. G. N. Watson, Theory of Bessel Functions, Second Edition, Cambridge University Press, 1952; p. 429.

9. A. Erdelyi, et. al. Higher Transcendental Functions, Vol. 2, McGraw-Hill, New York, 1953; p. 86.

10. K. Knopp, Infinite Sequences and Series, Dover, 1956; p. 171.

11. B. L. Van der Waerden, "On the Method of Seddle Points," Appl. Sci. Res., Vol. B2; pp. 33-45.

12. B. Noble, "The Wiener-Hopf Technique, Pergamon Press, 1958.

13. S. A. Schelkunoff, Advanced Antenna Theory, John Wiley and Sons, New York, 1952, p. 102.

14. F. B. Hilderbrand, Introduction to Numerical Analysis, McGraw-Hill, New York, 1956.

15. Lowan, Davids, and Levenson, "Tables of the Zeros of the Legendre Polynomials of Order 1-16 and the Weight Coefficients for Gauss' Mechanical Quadrature Formula," Tables of Functions and Zeros of Functions, NBS, Applied Math. Series, No. 37, 1953.

16. D. E. Isbell, "Non-Planar Logarithmically Periodic Antenna Structures," Antenna Laboratory, University of Illinois, Urbana, Tech. Rept. No. 30, Contract AF33(616)-3220, February, 1958.

17. R. H. DuHamel and F. R. Ore, "Logarithmically Periodic Antenna Designs," IRE National Convention Record, pt. 1, 1958; pp. 139-151.

18. J. D. Dyson, "The Unidirectional Equiangular Spiral Antenna", IRE Trans. on Antennas and Propagation, Vol. AP-7, Oct. 1959, pp. 329-334.

19. P. E. Mayes, G. A. Deschamps, and W. T. Patton, "Backward-Wave Radiation from Periodic Structures and Application to the Design of Frequency-Independent Antennas," Proceedings of the IRE, Vol. 49, May, 1961; pp. 962-961.

20. J. D. Kraus, Antennas, McGraw-Hill, New York, 1951, p. 176.

21. S. A. Schelkunoff and H. T. Friis, "Antenna Theory and Practice, John Wiley and Sons, New York, 1952; p. 559.

22. W. Magnus and F. Oberhettinger, Formulas and Theorems for the Functions of Mathematical Physics, Chelsea, New York, 1954; p. 118.

23. R. S. Phillips, "The Electromagnetic Field Produced by a Helix," Quarterly of Appl. Math., Vol. 8, No. 3, October, 1950; pp. 229-246.

APPENDIX A

A FOURIER TRANSFORM

The Fourier transform of the free space Green's function specialized to the helix is important to the development of the analysis of the backfire bifilar helical antenna. This transform is easily related to the transform of the function

$$g_1(z) = \frac{\exp(jk[A^2-2AB\cos(\phi+\tau z)+B^2+(z-d)^2]^{1/2})}{[A^2-2AB\cos(\phi+\tau z)+B^2+(z-d)]^{1/2}} \qquad (A-1)$$

This function is periodic in $u = \phi+\tau z$ and can be expanded in the Fourier series

$$g_1(z) = \frac{1}{2\pi}\sum_{n=-\infty}^{\infty} e^{-jn(\phi+\tau z)} \int_o^{2\pi} \frac{\exp(jk[A^2-2AB\cos u+B^2+(z-d)^2]^{1/2})}{[A^2-2AB\cos u+B^2+(z-d)^2]^{1/2}} e^{jnu}du \qquad (A-2)$$

If we take the Fourier transform (Equation A-2) and change the order of integration, the resulting expression is

$$\tilde{g}_1(\beta) = \frac{1}{4\pi^2}\sum_{n=-\infty} e^{-jn\phi} \int_o^{2\pi} e^{jnu} \int_{-\infty}^{\infty} \frac{\exp(jk[A^2-2AB\cos u+B^2+(z-d)^2]^{1/2})}{[A^2-2AB\cos u+B^2+(z-d)^2]^{1/2}} e^{j(\beta-n\tau)z}dzdy$$

Using the result listed in Magnus and Oberhettinger 22 this expression becomes

$$\tilde{g}_1(\beta) = \frac{j}{8\pi}\sum_{n=-\infty}^{\infty} e^{-jn\phi} \int_o^{2\pi} e^{jnu} H_o^{(1)}([k^2-(\beta-n\tau)^2]^{1/2}[A^2-2AB\cos u+B^2]^{1/2})e^{j(\beta-n\tau)d}dy$$

The addition theorem for the Hankel function, applied to the expression, gives

$$\tilde{g}_1(\beta) = \frac{j}{8\pi}\sum_{n=-\infty}^{\infty} e^{j[(\beta-n)d-n\phi]} \int_o^{2\pi} \sum_{n=-\infty}^{\infty} J_m(B[k^2-(\beta-m\tau)^2]^{1/2}) H_m^{(1)}(A[k^2-(\beta-m\tau)^2]^{1/2}) e^{j(m+n)u}du$$

Interchanging the order of integration with summation and using the orthogonality of the exponential function allows the result to be written

$$\tilde{g}_1(\beta) = \frac{j}{4} \sum_{m=-\infty}^{\infty} J_m(\beta[k^2-(\beta-m\tau)^2]^{1/2}) H_m^{(1)}(A[k^2-(\beta-m\tau)^2]^{1/2})\ e^{j(\beta+m\tau)} d_e jm\phi \qquad \text{(A-3)}$$

This expression is valid wher B is less than A. If A is smaller it is necessary to interchange A and B. If A equals B the series does not converge. A similar result was obtained by Phillips[23] another way. He gives an extensive discussion of the convergence of this series.

If g_2 is deduced from g_1 in Equation (A-1) by changing the sign of the cosine term, g_2 can be deduced from $\tilde{g}_1$ by changing the sign of all odd numbered terms

$$\tilde{g}_2(\beta) = \frac{j}{4} \sum_{m=-\infty}^{\infty} (-1)^m J_m(B[k^2-(\beta-m\tau)^2]^{1/2}) H_m^{(1)}(A[k^2-(B-n\tau)^2]^{1/2}) \cdot e^{j(\beta+m\tau)} d_e jm\phi \qquad \text{(A-4)}$$

These transforms, then, have the sum

$$\tilde{g}_2(\beta)+\tilde{g}_1(\beta) = \frac{j}{2} \sum_{n=-\infty}^{\infty} J_m(B[k^2-(\beta-m\tau)^2]^{1/2}) H_m^{(1)}(A[k^2-(\beta^2-m\tau)^2]^{1/2}) \cdot e^{j(\beta+m\tau)} d_e jm\phi \qquad \text{(A-5)}$$

$$m=2n$$

and the difference

$$\tilde{g}_1(\beta)-\tilde{g}_2(\beta) = \frac{j}{2} \sum_{n=-\infty}^{\infty} J_p(B[k^2-(\beta-p\tau)^2]^{1/2}) H_p^{(1)}(A[k^2-(\beta-p\tau)^2]^{1/2}) \cdot e^{j(\beta+p\tau)} d_e jp\phi \qquad \text{(A-6)}$$

$$p=2n+1$$

Finally, the Fourier transform of the complex conjugate of g(z) is deduced from $\tilde{g}(\beta)$ by replacing the Hankel function of the first kind, $H_n^{(1)}$ with the Hankel function of the second kind, $H_n^{(2)}$.

APPENDIX B

THE RELATION BETWEEN THE FOURIER SPECTRUM OF A LINEAR CURRENT DISTRIBUTION AND ITS RADIATION PATTERN

The vector potential of a linear current distribution along the z-axis is given by

$$\vec{A}(r) = \hat{u} \int_{-\infty}^{\infty} g(r,\theta;z)\ I_{(z)}\ dz \qquad \text{(B-1)}$$

where $\hat{u}$ is the direction of the current elements and

$$g = \frac{\exp(-jk[(r \sin\theta)^2+(z-r\cos\theta)^2]^{1/2})}{4\pi[(r\sin\theta)^2+(z-r\cos\theta)^2]}$$

By Parseval's theorem this is equivalent to

$$\vec{A}(\vec{r}) = \hat{u}\ 2\pi \int_{-\infty}^{\infty} \tilde{G}^*\ (r,\theta;\beta)\ \tilde{I}(\beta)\ d\beta \qquad \text{(B-2)}$$

where

$$\tilde{I}(\beta) = \frac{1}{2\pi} \int_{-\infty}^{\infty} I(z)\ e^{j\beta z}\ dz$$

and

$$\tilde{G}(r,\theta;\beta) = \frac{1}{2\pi} \int_{-\infty}^{\infty} g^*(r,\theta;z)e^{j\beta z}dx$$

This is the same Fourier transform pair used in Appendix A. In this case,

$$\tilde{G}(r,\ ;\beta) = \frac{j}{8\pi} H_o^{(1)}(r \sin\theta[k^2-\beta^2]^{1/2})\ e^{j\beta r\cos\theta}$$

Thus Equation (B-2) is

$$\vec{A}(\vec{r}) = \frac{-j\hat{u}}{4} \int_{-\infty}^{\infty} H_o^{(2)}(r\sin\theta[k^2-\beta^2]^{1/2})\ I(\beta)\ e^{-j\beta r\cos\theta} d\beta \qquad \text{(B-3)}$$

To obtain the radiation pattern from this expression, it is necessary only to obtain an asymptotic estimation for the integral valid for large r. This is

accomplished by replacing the Hankel function with the first term of its asymptotic form and by introducing the change of variables defined by

$$\beta = k \cos \alpha \tag{B-4}$$

Equation (B-3) now becomes

$$u \cdot A(r) \approx \frac{-jke^{j\pi/4}}{4} \sqrt{\frac{2}{\pi}} \int_C \frac{e^{-jk\, r \cos(\alpha-\theta)}}{\sqrt{k\, r \sin\theta \sin\alpha}} \sin\alpha\, \tilde{I}(k \cos\alpha)\, d\alpha \tag{B-5}$$

This can be evaluated, using the method of Van der Waerden[11] by introducing the change of variables

$$u = j \cos(\alpha-\theta)$$

$$\lambda = kr$$

$$d\alpha = \frac{j\, du}{\sqrt{u^2+1}}$$

giving

$$A(\vec{r}) \approx \int_C P(u)\, e^{-\lambda u}\, du \tag{B-6}$$

where

$$P(u) = \frac{ke^{j\pi/4}}{4} \sqrt{\frac{2 \sin\alpha}{\pi kr \sin\theta}}\, \frac{I(k \cos\alpha)}{\sqrt{u^2+1}}$$

and C' is the path that extends to the right on both sides of the branch point at $u = j$. The contribution[11] on the branch point then is

$$A(r) \approx \frac{2\Gamma(1/2)e^{-j\lambda}}{\lambda^{1/2}} \lim_{u \to j} \sqrt{u-j}\; P(u)$$

$$\approx 2\sqrt{\frac{\pi}{kr}}\, \frac{k}{4} \sqrt{\frac{2}{\pi kr}}\, \frac{1}{\sqrt{2j}}\, e^{j\pi/4}\, \tilde{I}(k \cos\theta) e^{-jkr}$$

$$\approx \frac{e^{-jkr}}{2r}\, \tilde{I}(k \cos\theta)$$

We have deduced by a long and complicated argument the well known result that the current distribution of a line source and its radiation pattern are Fourier transform pairs. This result is more easily obtained by assuming that r is much larger than z in Equation (B-1) giving

$$A(r) \sim \frac{e^{-jkr}}{4\pi r} \int_{-\infty}^{\infty} e^{jk \cos \theta z} I(z)\, dz$$

This more direct approach, however, is valid only when the current has finite support. If the current has finite support and is square integrable there, Theorem X of Paley and Wiener* states that its Fourier spectrum is entire. The current spectrum then will contribute no singularities of its own to P(u) in Equation (B-6). If the current distribution is not finite, its spectrum may have singularities of its own that must be considered in the evaluation of Equation (B-6).

Mathematically, such additional singularities can be handled by the method of Van der Waerden[11]. Physically, they are usually interpreted as surface waves guided by the structure. The contribution of the branch point at u = j might be called the "space wave" of the distribution. It is this "square wave" that we have identified with the radiation patterns of a current distribution in this study.

AF33(657)-8460

DISTRIBUTION LIST

One copy each unless otherwise indicated

Armed Services Technical Information Agency
Attn: TIP-DR
Arlington Hall Station
Arlington 12, Virginia (10 copies)

Aeronuatical Systems Division
Attn: (ASRNRE-4)
Wright-Patterson Air Force Base
Ohio (3 copies)

Aeronautical Systems Division
Attn: ASDSED, Mr. Mulligan
Wright-Patterson Air Force Base
Ohio

Aeronautical Systems Division
Attn: AFCIN-4B1A
Wright-Patterson Air Force Base
Ohio

Air Force Cambridge Research Laboratory
Attn: CRRD
Laurence G. Hanscom Field
Bedford, Massachusetts

Commander
Air Force Missile Test Center
Patrick Air Force Base
Florida

Commander
Air Force Missile Development Center
Attn: Technical Library
Holloman Air Force Base
New Mexico

Air Force Ballistic Missile Division
Attn: Technical Library, Air Force Unit Post Office
Los Angeles, California

Director
Ballistics Research Laboratory
Attn: Ballistics Measurement Lab.
Aberdeen Proving Ground, Maryland

National Aeronautics & Space Adm.
Attn: Librarian
Langley Field, Virginia

Rome Air Development Center
Attn: RCLTM
Griffiss Air Force Base
New York

Research & Development Command
Hq. USAF (ARDRD-RE)
Washington 25, D. C.

Office of Chief Signal Officer
Engineering & Technical Division
Attn: SIGNET-5
Washington 25, D. C.

Commander
U. S. Army White Sands Signal Agency
Attn: SIGWS-FC-02
White Sands, New Mexico

Director
Surveillance Department
Evans Area
Attn: Technical Document Center
Belman, New Jersey

Commander
U. S. Naval Air Test Center
Attn: WST-54, Antenna Section
Patuxent River, Maryland

Material Laboratory, Code 932
New York Naval Shipyard
Brooklyn 1, New York

Commanding Officer
Diamond Ordnance Fuse Laboratories
Attn: 240
Washington 25, D. C.

Director
U. S. Navy Electronics Laboratory
Attn: Library
San Diego 52, California

Adams-Russell Company
200 Sixth Street
Attn: Library (Antenna Section)
Cambridge, Massachusetts

Aero Geo Astro
Attn: Security Officer
1200 Duke Street
Alexandria, Virginia

NASA Goddard Space Flight Center
Attn: Antenna Section, Code 523
Greenbelt, Maryland

Airborne Instruments Labs., Inc.
Attn: Librarian (Antenna Section)
Walt Whitman Road
Melville, L. I., New York

American Electronic Labs
Box 552 (Antenna Section)
Lansdale, Pennsylvania

Andrew Alfred Consulting Engineers
Attn: Librarian (Antenna Section)
299 Atlantic Ave.
Boston 10, Massachusetts

Ampheol-Borg Electronic Corporation
Attn: Librarian (Antenna Section)
2801 S. 25th Avenue
Broadview, Illinois

Bell Aircraft Corporation
Attn: Technical Library
(Antenna Section)
Buffalo 5, New York

Bendix Radio Division of
Bendix Aviation Corporation
Attn: Technical Library
(For Dept. 462-4)
Baltimore 4, Maryland

Boeing Airplane Company
Aero Space Division
Attn: Technical Library
M/F Antenna & Radomes Unit
Seattle, Washington

Boeing Airplane Company
Attn: Technical Library
M/F Antenna Systems Staff Unit
Wichita, Kansas

Chance Vought Aircraft Inc.
THRU: BU AER Representative
Attn: Technical Library
M/F Antenna Section
P. O. Box 5907
Dallas 22, Texas

Collins Radio Company
Attn: Technical Library (Antenna
Section)
Dallas, Texas

Convair
Ft. Worth Division
Attn: Technical Library (Antenna
Section)
Grants Lane
Fort Worth, Texas

Convair
Attn: Technical Library (Antenna
Section)
P. O. Box 1050
San Diego 12, California

Dalmo Victor Company
Attn: Technical Library (Antenna
Section)
1515 Industrial Way
Belmont, California

Dorne & Margolin, Inc.
Attn: Technical Library (Antenna
Section)
30 Sylvester Street
Westbury, L. I., New York

Dynatronics Inc.
Attn: Technical Library (Antenna
Section)
Orlando, Florida

Electronic Communications, Inc.
Research Division
Attn: Technical Library
1830 York Road
Timonium, Maryland

Fairchild Engine & Airplane Corporation
Fairchild Aircraft & Missiles Division
Attn: Technical Library (Antenna Section)
Hagerstown 10, Maryland

Georgia Institute of Technology
Engineering Experiment Station
Attn: Technical Library
M/F Electronics Division
Atlanta 13, Georgia

General Electric Company
Electronics Laboratory
Attn: Technical Library
Electronics Park
Syracuse, New York

General Electronic Labs., Inc.
Attn: Technical Library (Antenna Section)
18 Ames Street
Cambridge 42, Massachusetts

General Precision Lab., Division of General Precision Inc.
Attn: Technical Library (Antenna Section)
63 Bedford Road
Pleasantville, New York

Goodyear Aircraft Corporation
Attn: Technical Library
M/F Dept. 474
1210 Massilon Road
Akron 15, Ohio

Granger Associates
Attn: Technical Library (Antenna Section)
974 Commercial Street
Palo Alto, California

Grumman Aircraft Engineering Corp.
Attn: Technical Library
M/F Avionics Engineering
Bethpage, New York

The Hallicrafters Company
Attn: Technical Library (Antenna Section)
4401 W. Fifth Avenue
Chicago 24, Illinois

Hoffman Laboratories Inc.
Attn: Technical Library (Antenna Section)
Los Angeles 7, California

John Hopkins University
Applied Physics Laboratory
8621 Georgia Avenue
Silver Springs, Maryland

Hughes Aircraft Corporation
Attn: Technical Library (Antenna Section)
Florence & Teal Street
Culver City, California

ITT Laboratories
Attn: Technical Library (Antenna Section)
500 Washington Avenue
Nutley 10, New Jersey

U. S. Naval Ordnance Lab.
Attn: Technical Library
Corona, California

Lincoln Laboratories
Massachusetts Institute of Technology
Attn: Document Room
P. O. Box 73
Lexington 73, Massachusetts

Litton Industries
Attn: Technical Library (Antenna Section)
4900 Calvert Road
College Park, Maryland

Lockheed Missile & Space Division
Attn: Technical Library (M/F Dept-58-40, Plant 1, Bldg. 130)
Sunnyvale, California

The Martin Company
Attn: Technical Library (Antenna Section)
P. O. Box 179
Denver 1, Colorado

The Martin Company
Attn: Technical Library (Antenna Section)
Baltimore 3, Maryland

The Martin Company
Attn: Technical Library (M/F Microwave Laboratory)
Box 5837
Orlando, Florida

W. L. Maxson Corporation
Attn: Technical Library (Antenna Section)
460 West 34th Street
New York 1, New York

McDonnell Aircraft Corporation
Attn: Technical Library (Antenna Section)
Box 516
St. Louis 66, Missouri

Melpar, Inc.
Attn: Technical Library (Antenna Section)
3000 Arlington Blvd.
Falls Church, Virginia

University of Michigan
Radiation Laboratory
Willow Run
201 Catherine Street
Ann Arbor, Michigan

Mitre Corporation
Attn: Technical Library (M/F Electronic Warfare Dept. D-21)
Middlesex Turnpike
Bedford, Massachusetts

North American Aviation Inc.
Attn: Technical Library (M/F Engineering Dept.)
4300 E. Fifth Avenue
Columbus 16, Ohio

North American Aviation Inc.
Attn: Technical Library (M/F Dept. 56)
International Airport
Los Angeles, California

Northrop Corporation
NORAIR Division
1001 East Broadway
Attn: Technical Information (3924-3)
Hawthorne, California

Ohio State University Research Foundation
Attn: Technical Library (M/F Antenna Laboratory)
1314 Kinnear Road
Columbus 12, Ohio

Philco Corporation
Government & Industrial Division
Attn: Technical Library (M/F Antenna Section)
4700 Wissachickon Avenue
Philadelphia 44, Pennsylvania

Westinghouse Electric Corporation
Air Arms Division
Attn: Librarian (Antenna Lab)
P. O. Box 746
Baltimore 3, Maryland

Wheeler Laboratories
Attn: Librarian (Antenna Lab)
Box 561
Smithtown, New York

Electrical Engineering Research Laboratory
University of Texas
Box 8026, Univ. Station
Austin, Texas

University of Michigan Research Institute
Electronic Defense Group
Attn: Dr. J. A. M. Lyons
Ann Arbor, Michigan

Radio Corporation of America
RCA Laboratories Division
Attn: Technical Library
(M/F Antenna Section)
Princeton, New Jersey

Radiation, Inc.
Attn: Technical Library (M/F)
Antenna Section
Drawer 37
Melbourne, Florida

Radioplane Company
Attn: Librarian (M/F Aerospace Lab)
8000 Woodly Avenue
Van Nuys, California

Ramo-Wooldridge Corporation
Attn: Librarian (Antenna Lab)
Conoga Park, California

Rand Corporation
Attn: Librarian (Antenna Lab)
1700 Main Street
Santa Monica, California

Rantec Corporation
Attn: Librarian (Antenna Lab)
23999 Ventura Blvd.
Calabasas, California

Raytheon Electronics Corporation
Attn: Librarian (Antenna Lab)
1089 Washington Street
Newton, Massachusetts

Republic Aviation Corporation
Applied Research & Development
Division
Attn: Librarian (Antenna Lab)
Farmingdale, New York

Sanders Associates
Attn: Librarian (Antenna Lab)
95 Canal Street
Nashua, New Hampshire

Southwest Research Institute
Attn: Librarian (Antenna Lab)
8500 Culebra Road
San Antonio, Texas

H. R. B. Singer Corporation
Attn: Librarian (Antenna Lab)
State College, Pennsylvania

Sperry Microwave Electronics Company
Attn: Librarian (Antenna Lab)
P. O. Box 1828
Clearwater, Florida

Sperry Gyroscope Company
Attn: Librarian (Antenna Lab)
Great Neck, L. I., New York

Stanford Electronic Laboratory
Attn: Librarian (Antenna Lab)
Stanford, California

Stanford Research Institute
Attn: Librarian (Antenna Lab)
Menlo Park, California

Sylvania Electronic System
Attn: Librarian (M/F Antenna &
Microwave Lab)
100 First Street
Waltham 54, Massachusetts

Sylvania Electronic System
Attn: Librarian (Antenna Lab)
P. O. Box 188
Mountain View, California

Technical Research Group
Attn: Librarian (Antenna Section)
2 Aerial Way
Syosset, New York

Ling Temco Aircraft Corporation
Temco Aircraft Division
Attn: Librarian (Antenna Lab)
Garland, Texas

Texas Instruments, Inc.
Attn: Librarian (Antenna Lab)
6000 Lemmon Ave.
Dallas 9, Texas

A. S. Thomas, Inc.
Attn: Librarian (Antenna Lab)
355 Providence Highway
Westwood, Massachusetts

New Mexico State University
Head Antenna Department
Physical Science Laboratory
University Park, New Mexico

Bell Telephone Laboratories, Inc.
Whippany Laboratory
Whippany, New Jersey
Attn: Technical Reports Librarian
Room 2A-165

Robert C. Hansen
Aerospace Corporation
Box 95085
Los Angeles 45, California

Dr. Richard C. Becker
10829 Berkshire
Westchester, Illinois

Dr. Harry Letaw, Jr.
Raytheon Company
Surface Radar and Navigation
Operations
State Road West
Wayland, Massachusetts

Dr. Frank Fu Fang
IBM Research Laboratory
Poughkeepsie, New York

Mr. Dwight Isbell
1422 11th West
Seattle 99, Washington

Dr. Robert L. Carrel
Collins Radio Corporation
Antenna Section
Dallas, Texas

Dr. A. K. Chatterjee
Vice Principal & Head of the Department
of Research
Birla Institute of Technology
P. O. Mesra
District-Ranchi (Bihar) India

Aeronautical Systems Division
Attn: ASAD - Library
Wright-Patterson Air Force Base
Ohio

National Bureau of Standards
Department of Commerce
Attn: Dr. A. G. McNish
Washington 25, D. C.

ANTENNA LABORATORY
TECHNICAL REPORTS AND MEMORANDA ISSUED

Contract AF33(616)-310

"Synthesis of Aperture Antennas," Technical Report No. 1, C.T.A. Johnk, October, 1954.*

"A Synthesis Method for Broad-band Antenna Impedance Matching Networks," Technical Report No. 2, Nicholas Yaru, 1 February 1955.* AD 61049.

"The Assymmetrically Excited Spherical Antenna," Technical Report No. 3, Robert C. Hansen, 30 April 1955.*

"Analysis of an Airborne Homing System," Technical Report No. 4, Paul E. Mayes, 1 June 1955 (CONFIDENTIAL).

"Coupling of Antenna Elements to a Circular Surface Waveguide," Technical Report No. 5, H. E. King and R. H. DuHamel, 30 June 1955.*

"Axially Excited Surface Wave Antennas," Technical Report No. 7, D. E. Royal, 10 October 1955.*

"Homing Antennas for the F-86F Aircraft (450-2500 mc)," Technical Report No. 8, P. E. Mayes, R. F. Hyneman, and R. C. Becker, 20 February 1957, (CONFIDENTIAL).

"Ground Screen Pattern Range," Technical Memorandum No. 1, Roger R. Trapp, 10 July 1955.*

Contract AF33(616)-3220

"Effective Permeability of Spheroidal Shells," Technical Report No. 9, E. J. Scott and R. H. DuHamel, 16 April 1956.

"An Analytical Study of Spaced Loop ADF Antenna Systems," Technical Report No. 10, D. G. Berry and J. B. Kreer, 10 May 1956. AD 98615

"A Technique for Controlling the Radiation from Dielectric Rod Waveguides," Technical Report No. 11, J. W. Duncan and R. H. DuHamel, 15 July 1956.*

"Directional Characteristics of a U-Shaped Slot Antenna," Technical Report No. 12, Richard C. Becker, 30 September 1956.**

"Impedance of Ferrite Loop Antennas," Technical Report No. 13, V. H. Rumsey and W. L. Weeks, 15 October 1956. AD 119780

"Closely Spaced Transverse Slots in Rectangular Waveguide," Technical Report No. 14, Richard F. Hyneman, 20 December 1956.

"Distributed Coupling to Surface Wave Antennas," Technical Report No. 15, Ralph Richard Hodges, Jr., 5 January 1957.

"The Characteristic Impedance of the Fin Antenna of Infinite Length," Technical Report No. 16, Robert L. Carrel, 15 January 1957.*

"On the Estimation of Ferrite Loop Antenna Impedance," Technical Report No. 17, Walter L. Weeks, 10 April 1957.* AD 143989

"A Note Concerning a Mechanical Scanning System for a Flush Mounted Line Source Antenna," Technical Report No. 18, Walter L. Weeks, 20 April 1957.

"Broadband Logarithmically Periodic Antenna Structures," Technical Report No. 19, R. H. DuHamel and D. E. Isbell, 1 May 1957. AD 140734

"Frequency Independent Antennas," Technical Report No. 20, V. H. Rumsey, 25 October 1957

"The Equiangular Spiral Antenna," Technical Report No. 21, J. D. Dyson, 15 September 1957. AD 145019

"Experimental Investigation of the Conical Spiral Antenna," Technical Report No. 22, R. L. Carrel, 25 May 1957.** AD 144021

"Coupling between a Parallel Plate Waveguide and a Surface Waveguide," Technical Report No. 23, E. J. Scott, 10 August 1957.

"Launching Efficiency of Wires and Slots for a Dielectric Rod Waveguide," Technical Report No. 24, J. W. Duncan and R. H. DuHamel, August 1957.

"The Characteristic Impedance of an Infinite Biconical Antenna of Arbitrary Cross Section," Technical Report No. 25, Robert L. Carrel, August 1957.

"Cavity-Backed Slot Antennas," Technical Report No. 26, R. J. Tector, 30 October 1957

"Coupled Waveguide Excitation of Traveling Wave Slot Antennas," Technical Report No. 27, W. L. Weeks, 1 December 1957.

"Phase Velocities in Rectangular Waveguide Partially Filled with Dielectric," Technical Report No. 28, W. L. Weeks, 20 December 1957.

"Measuring the Capacitance per Unit Length of Biconical Structures of Arbitrary Cross Section," Technical Report No. 29, J. D. Dyson, 10 January 1958.

"Non-Planar Logarithmically Periodic Antenna Structure," Technical Report No. 30, D. E. Isbell, 20 February 1958. AD 156203

"Electromagnetic Fields in Rectangular Slots," Technical Report No. 31, N. J. Kuhn and P. E. Mast, 10 March 1958

"The Efficiency of Excitation of a Surface Wave on a Dielectric Cylinder," Technical Report No. 32, J. W. Duncan, 25 May 1958.

"A Unidirectional Equiangular Spiral Antenna," Technical Report No. 33, J. D. Dyson, 10 July 1958. AD 201138

"Dielectric Coated Spheriodal Radiators," Technical Report No. 34, W. L. Weeks, 12 September 1958. AD 204547

"A Theoretical Study of the Equiangular Spiral Antenna," Technical Report No. 35, P. E. Mast, 12 September 1958. AD 204548

Contract AF33(616)-6079

"Use of Coupled Waveguides in a Traveling Wave Scanning Antenna," Technical Report No. 36, R. H. MacPhie, 30 April 1959. AD 215558

"On the Solution of a Class of Wiener-Hopf Integral Equations in Finite and Infinite Ranges," Technical Report No. 37, Raj Mittra, 15 May 1959.

"Prolate Spheroidal Wave Functions for Electromagnetic Theory," Technical Report No. 38, W. L. Weeks, 5 June 1959.

"Log Periodic Dipole Arrays," Technical Report No. 39, D. E. Isbell, 1 June 1959. AD 220651

"A Study of the Coma-Corrected Zoned Mirror by Diffraction Theory," Technical Report No. 40, S. Dasgupta and Y. T. Lo, 17 July 1959.

"The Radiation Pattern of a Dipole on a Finite Dielectric Sheet," Technical Report No. 41, K. G. Balmain, 1 August 1959.

"The Finite Range Wiener-Hopf Integral Equation and a Boundary Value Problem in a Waveguide," Technical Report No. 42, Raj Mittra, 1 October 1959.

"Impedance Properties of Complementary Multiterminal Planar Structures," Technical Report No 43, G. A. Deschamps, 11 November 1959.

"On the Synthesis of Strip Sources," Technical Report No. 44, Raj Mittra, 4 December 1959.

"Numerical Analysis of the Eigenvalue Problem of Waves in Cylindrical Waveguides," Technical Report No. 45, C. H. Tang and Y. T. Lo, 11 March 1960.

"New Circularly Polarized Frequency Independent Antennas with Conical Beam or Omnidirectional Patterns," Technical Report No. 46, J. D. Dyson and P. E. Mayes, 20 June 1960. AD 241321

"Logarithmically Periodic Resonant-V Arrays," Technical Report No. 47, P. E. Mayes, and R. L. Carrel, 15 July 1960. AD 246302

"A Study of Chromatic Aberration of a Coma-Corrected Zoned Mirror," Technical Report No. 48, Y. T. Lo, June 1960

"Evaluation of Cross-Correlation Methods in the Utilization of Antenna Systems," Technical Report No. 49, R. H. MacPhie, 25 January 1961

"Synthesis of Antenna Product Patterns Obtained from a Single Array," Technical Report No. 50, R. H. MacPhie, 25 January 1961.

"On the Solution of a Class of Dual Integral Equations," Technical Report No. 51, R. Mittra, 1 October 1961. AD 264557

"Analysis and Design of the Log-Periodic Dipole Antenna," Technical Report No. 52, Robert L. Carrel, 1 October 1961.* AD 264558

"A Study of the Non-Uniform Convergence of the Inverse of a Doubly-Infinite Matrix Associated with a Boundary Value Problem in a Waveguide," Technical Report No. 53, R. Mittra, 1 October 1961. AD 264556

---

* Copies available for a three-week loan period.

** Copies no longer available.

ERRATA SHEET

"The Backfire Bifilar Helical Antenna" by Willard Thomas Patton

Should Read

Page 9, Equation (1) $\vec{E}xr = -jk\zeta\ \vec{A}x\hat{r}$

Page 9, Equation (2) $\vec{A}(\vec{r}) = \iiint G(\vec{r}, \vec{r}')\ \vec{I}(\vec{r}')\ dv$

Page 9, Last Equation on Page $G(\vec{r}, \vec{r}') = \dfrac{\exp[-jk|\vec{r}-\vec{r}'|]}{4\pi|\vec{r}-\vec{r}'|}$

Page 13, Equation (4) First Line

$$A_x(\vec{r}) \sim +j\pi \cos\psi \sum_{n\ \text{even}} G_o J_n(\rho)[\tilde{I}(k\cos\theta+(n-1)\tau) - \tilde{I}(k\cos\theta+(n+1)\tau)]e^{jn\phi}$$

Page 17, First Equation $p_1 = (b\cos\tau z\ ,\ b\sin\tau z\ ,\ z)$

Page 46, First Equation $R_e([(\beta-n\tau)^2-k^2]^{1/2}) = 0$

Page 53, Second Equation

$$E = \frac{2^{2m+1}(m!)^4}{(2m+1)[(2m)!]^3}\ (2m)\ f\ (\zeta)$$

Page 55, Equation (45) Line 3 $\dfrac{-k^2}{\tau^2}\ \cot^2\psi\ \cosh x\ [\ln(1-y^2e^{-2x}) + \dfrac{y4_e-4x}{y4} + y^2e^{-2x}]$

Page 90, Third Equation $P_L(0) = 2\ I_o\ \dfrac{\sin L/2\ (\beta'_o-k)}{\beta'_o-k}$